A THREE DIMENSIONAL MIXED FORMULATION NONLINEAR FRAME FINITE ELEMENT BASED ON HU-WASHIZU FUNCTIONAL

A THESIS SUBMITTED TO
THE GRADUATE SCHOOL OF NATURAL AND APPLIED SCIENCES
OF
MIDDLE EAST TECHNICAL UNIVERSITY

BY

OZAN SOYDAŞ

IN PARTIAL FULFILLMENT OF THE REQUIREMENTS
FOR
THE DEGREE OF DOCTOR OF PHILOSOPHY
IN
CIVIL ENGINEERING

DECEMBER 2013

Approval of the thesis:

A THREE DIMENSIONAL MIXED FORMULATION NONLINEAR FRAME FINITE ELEMENT BASED ON HU-WASHIZU FUNCTIONAL

submitted by **OZAN SOYDAŞ** in partial fulfillment of the requirements for the degree of **Doctor of Philosophy in Civil Engineering Department, Middle East Technical University** by,

Prof. Dr. Canan Özgen _____
Dean, Graduate School of **Natural and Applied Sciences**

Prof. Dr. Ahmet Cevdet Yalçıner _____
Head of Department, **Civil Engineering**

Assoc. Prof. Dr. Afşin Sarıtaş _____
Supervisor, **Civil Engineering Dept., METU**

Examining Committee Members:

Prof. Dr. Mehmet Utku _____
Civil Engineering Dept., METU

Assoc. Prof. Dr. Afşin Sarıtaş _____
Civil Engineering Dept., METU

Prof. Dr. Tekin Gültop _____
Civil Engineering Dept., Çankaya University

Assist. Prof. Dr. Serdar Göktepe _____
Civil Engineering Dept., METU

Assist. Prof. Dr. Ercan Gürses _____
Aerospace Engineering Dept., METU

Date: _____

I hereby declare that all information in this document has been obtained and presented in accordance with academic rules and ethical conduct. I also declare that, as required by these rules and conduct, I have fully cited and referenced all material and results that are not original to this work.

Name, Last Name : Ozan SOYDAŞ

Signature :

ABSTRACT

A THREE DIMENSIONAL MIXED FORMULATION NONLINEAR FRAME FINITE ELEMENT BASED ON HU-WASHIZU FUNCTIONAL

Soydaş, Ozan
Ph.D., Department of Civil Engineering
Supervisor: Assoc. Prof. Dr. Afşin Sarıtaş

December 2013, 172 pages

A three dimensional nonlinear frame finite element is presented in this analytical study by utilizing Hu-Washizu principle with three fields of displacement, strain and stress in the variational form. Timoshenko beam theory is extended to three dimensions in order to derive strains from the displacement field. The finite element approximation for the beam uses shape functions for section forces that satisfy equilibrium and discontinous section deformations along the beam. Nonlinear analyses are performed by considering aggregation of the stress-strain relations along certain control sections of the element. Fiber discretization of the sections accompanied by adequate material model ensures coupling of the stress resultants axial force, shear force, bending moment about both axes and torsion accurately. These attributes of the mixed element relax reliance on displacement approximations on the control sections of the beam element that are inevitable in displacement based elements. As a result, the element is free from shear-locking. Authentication and superiority of the proposed 3d element are displayed by comparing the ability of the mixed element to capture nonlinear coupling of axial, shear force, bending moments and torsion with the results of the similar 3d displacement based elements and exact solutions that are readily available in the literature. Moreover, linear elastic free

vibration analyses of the proposed mixed element are carried out by using the flexibility based consistent mass matrix that is also derived in this study and it is pointed out that 3d mixed element has the ability of determining not only the fundamental vibration frequency but also higher order frequencies with a considerable accuracy by using only a couple of elements per member span.

Keywords: Beam finite element, mixed formulation, Hu-Washizu variational, inelastic beam, axial-flexure-shear-torsion coupling, consistent mass matrix, vibration frequency

ÖZ

HU-WASHIZU FONKSİYONELİ TEMELLİ ÜÇ BOYUTLU KARMA FORMÜLASYON NONLİNEER ÇERÇEVE SONLU ELEMANI

Soydaş, Ozan
Doktora, İnşaat Mühendisliği Bölümü
Tez Yöneticisi: Doç. Dr. Afşin Sarıtaş

Aralık 2013, 172 sayfa

Bu analitik çalışmada, varyasyonel formunda deplasman, birim şekil değiştirme ve gerilme olmak üzere üç alanı kullanan Hu-Washizu prensibinin matematiksel teorisini temel alan üç boyutlu nonlineer bir kiriş sonlu elemanı sunulmaktadır. Birim şekil değiştirmelerini deplasmanlardan elde etmek için Timoshenko kiriş teorisi üçüncü boyuta uyarlanmıştır. Kiriş için varsayılan sonlu eleman yaklaşımı, eleman boyunca kiriş kesitlerinin dengesini ve süreksiz kesit deformasyonlarını göz önünde bulunduran kesit kuvvetleri için oluşturulmuş şekil fonksiyonlarını kullanır. Nonlineer analiz, belirli kesitlerin gerilme-birim şekil değiştirme ilişkilerinin eleman boyunca toplanmasıyla yapılır. Uygun bir malzeme modelinin eşlik ettiği kesit dilimlemesi, eksenel kuvvet, kesme kuvveti, iki eksen etrafındaki eğilme momentleri ve burulma olmak üzere gerilme bileşkelerinin doğru olarak etkileşimine olanak verir. Karma elemanın belirtilen bu özellikleri, deplasman temelli elemanların aksine eleman boyunca belirli kesitlerde deplasman değerlerine olan ihtiyacı ortadan kaldırır. Sonuç olarak, eleman kesme kilitlenmesi yaşamaz. Önerilmekte olan 3b elemanın doğrulaması ve üstünlüğü, karma formülasyon elemanın nonlineer eksenel, kesme kuvveti, burkulma momentleri ve burulma etkileşimini yakalamadaki yeteneğini benzer 3b deplasman temelli ve literatürde halihazırda bulunan kesin çözümlerle karşılaştırmak suretiyle gösterilmektedir. Bunun yanında, önerilmekte

olan karma elemanın lineer elastik serbest titreşim analizleri, türetimi bu çalışmada ayrıca yapılan esneklik temelli tutarlı kütle matrisi kullanılarak yapılmakta ve 3b karma formülasyon elemanın sadece temel titreşim frekansını değil yüksek dereceli titreşim frekanslarını da kiriş açıklığı boyunca sadece birkaç eleman kullanarak kayda değer bir doğrulukla tespit edebildiği gösterilmektedir.

Anahtar Kelimeler: Kiriş sonlu elemanı, karma formülasyon, Hu-Washizu varyasyoneli, elastik ötesi kiriş, eksenel-eğilme-kesme-burulma etkileşimi, tutarlı kütle matrisi, titreşim frekansı

To My Parents, A. & S. Soydaş

ACKNOWLEDGMENTS

I would like to express my sincere appreciation for the supervision of Assoc. Prof. Dr. Afşin Sarıtaş. This thesis would not have been realized without the encouragement, support and interest of him. I have learned a lot of things not only by means of academic study but also regarding being modest, kind and patient from him. I also want to thank a lot to his wife and children because of tolerating their patriarch's time spent with me during the study.

I would also like to thank Prof. Dr. Mehmet Utku and Prof. Dr. Tekin Gültop for their positive criticism, guidance and advice provided throughout the thesis progress committee meetings.

I am deeply indebted to my parents for the endless reliance, support and love they have given me throughout my life. My sister and her husband also helped me a lot for carrying out the study and I would like to thank them.

I would like to thank all of my friends from Zonguldak and Middle East Technical University and from Ministry of Energy and Natural Resources of Turkish Republic for helping and encouraging me on thesis study by providing both mental assistance and friendship without any complaint.

METU Library and librarians also deserve a special thank for providing me with the latest publications and books.

The financial support provided during Ph.D. study by "2211-Scholarship for Ph.D. Students" of Turkish Scientific and Technical Research Council (TÜBİTAK) is highly appreciated.

TABLE OF CONTENTS

ABSTRACT v
ÖZ vii
ACKNOWLEDGMENTS x
TABLE OF CONTENTS xi
LIST OF TABLES xiv
LIST OF FIGURES xv
CHAPTERS
1. INTRODUCTION 1
1.1. GENERAL 1
1.2. OBJECTIVE AND SCOPE 3
2. LITERATURE SURVEY 5
2.1. INTRODUCTION TO THE FINITE ELEMENTS 5
2.1.1. Finite Element Method 6
2.1.2. Displacement Based Finite Element Analysis 9
2.1.3. Mixed Formulation Finite Element Analysis 12
2.1.4. Comparison of Displacement Based and Mixed Finite Elements 13
2.2. STATIC NONLINEAR ANALYSIS OF MIXED FORMULATION BEAM FINITE ELEMENTS 14
2.3. VIBRATION CHARACTERISTICS OF BEAMS 20
3. FORMULATION OF THREE DIMENSIONAL MIXED ELEMENT 23
3.1. INTRODUCTION 23
3.2. COORDINATE SYSTEMS AND TRANSFORMATIONS 23
3.2.1. Basic System 23
3.2.2. Section Forces (Internal Forces) 26
3.2.3. Section Deformations 28

3.3. HU-WASHIZU FUNCTIONAL 32
3.4. KINEMATICS OF 3D TIMOSHENKO BEAM ELEMENT 33
3.5. VARIATION OF HU-WASHIZU FUNCTIONAL 36
3.6. FINITE ELEMENT APPROXIMATION 40
3.7. LINEARIZATION OF THE NONLINEAR EQUATION 55
3.8. FIBER DISCRETIZATION OF SECTION RESPONSE 61
3.9. THREE DIMENSIONAL MATERIAL MODEL 64
4. NUMERICAL VALIDATION OF 3D MIXED ELEMENT 67
4.1. INTRODUCTION 67
4.2. A 3D DISPLACEMENT BASED TIOMESHENKO FINITE ELEMENT . 67
4.3. VALIDATION OF MIXED ELEMENT IN 3D 71
4.3.1. Comparison of 3d Mixed and Displacement Based Elements 72
4.3.2. Nonlinear Performance of Mixed Element Under Torsion 79
4.3.2.1. Pure Torsion of a Uniform Cantilever Beam with Solid Circular Section 79
4.3.2.2. Combined Axial Load and Torque on a Uniform Cantilever Beam with Solid Circular Section 81
4.3.2.3. Comparison of Tapered MF and DB Elements Under Torsion 83
4.3.3. Nonlinear Analysis of Beams with Solid and Hollow Circular Sections 84
4.3.3.1. Nonlinear Analysis of Uniform MF for Solid Circular Section 85
4.3.3.2. Nonlinear Analysis of Uniform MF for Hollow Circular Section 92
4.3.4. Nonlinear Analysis of Uniform Fixed-Fixed Pipe 103
4.3.4.1. Combined Bending and Torsion of a Long Fixed-Fixed Pipe 105
4.3.4.2. Bending of a Short Fixed-Fixed Pipe 106
5. FREE VIBRATION OF MIXED ELEMENT 109
5.1. INTRODUCTION 109
5.2. DISPLACEMENT BASED MASS MATRIX 109
5.3. FLEXIBILITY BASED MASS MATRIX 113

5.3.1. Equilibrium of the Element 114
5.3.2. Element Displacements and Deformations 115
5.3.3. Response of the Element 115
5.3.4. Mass Matrix Based on Flexibility Method 118
6. VALIDATION OF VIBRATION OF MF ELEMENT 123
6.1. INTRODUCTION 123
6.2. UNIFORM MEMBER WITH CIRCULAR SECTION 124
6.3. TAPERED MEMBER WITH CIRCULAR SECTION 136
6.4. UNIFORM MEMBER WITH RECTANGULAR SECTION 142
6.5. TAPERED MEMBER WITH RECTANGULAR SECTION 151
7. CONCLUSIONS 159
7.1. SUMMARY 159
7.2. CONCLUSIONS 160
7.3. RECOMMENDATIONS FOR FUTURE STUDY 162
REFERENCES 163
CURRICULUM VITAE 171

LIST OF TABLES

TABLES

Table 2.1. Strong and weak satisfaction of parameters in variational principles 17

Table 4.1. Theoretical shear values calculated from moment at yield and plastic limit 94

Table 4.2. Features of elements used in comparison of nonlinear responses 104

Table 6.1. Mode shapes for various *L/d* ratios for uniform cantilever beam with solid circular section 131

LIST OF FIGURES

FIGURES

Figure 3.1. Free body diagram of element end forces 24
Figure 3.2. Demonstration of basic element forces 25
Figure 3.3. Transformation of element displacements to deformations 31
Figure 3.4. Beam deformations according to various beam theories 34
Figure 3.5. Assumed traction forces on beam element 40
Figure 3.6. Element forces for uniform axial traction 44
Figure 3.7. Element forces for uniform transverse traction in y direction 46
Figure 3.8. Element forces for uniform transverse traction in z direction 47
Figure 3.9. Nodal displacements for an element 50
Figure 4.1. Orientation of global and local axes and tip displacement 73
Figure 4.2. Discretization of circular section in radial and circumferential directions in local coordinates 75
Figure 4.3. Comparison of the variation of number of integration points on DB 76
Figure 4.4. Comparison of the variation of number of integration points on MF 77
Figure 4.5. Effect of different number of elements on MF 78
Figure 4.6. Comparison of the effect of number of elements on DB and MF 79
Figure 4.7. Exact solution vs. MF element under pure torsion for uniform cantilever member with solid circular section 81
Figure 4.8. Variation of axial load and torque with angle of twist for solid circular section by holding extension constant after yield 83
Figure 4.9. Comparison of the effect of number of elements for the analysis of tapered members with DB and MF frame elements 84
Figure 4.10. Force and displacement pseudo-time histories imposed on the element for Case A2 for $0.25N_y$ 86
Figure 4.11. Illustration of loading history for Case A2 for $0.25N_y$ 87

Figure 4.12. Base shear vs. tip displacement in global *X*-direction for Cases A1, A2, A3 and A4 for solid section. 88
Figure 4.13. Base shear vs. tip displacement in global *Z*-direction for Cases A1, A2, A3 and A4 for solid section. 89
Figure 4.14. Calculation of the shear stress for circular section. 90
Figure 4.15. Base shear vs. tip displacement in global *X*-direction for Cases B1, B2, B3 and B4 for solid section. 91
Figure 4.16. Base shear vs. tip displacement in global *Z*-direction for Cases B1, B2, B3 and B4 for solid section. 91
Figure 4.17. Loading of hollow circular section for Cases A and B 93
Figure 4.18. Cases A1 and B1 for *X* and *Z* directions for solid and hollow circular sections for different a/b ratio under cyclic loading. 95
Figure 4.19. Cases A2 and B2 for *X* and *Z* directions for solid and hollow circular sections for different a/b ratio under cyclic loading. 96
Figure 4.20. Cases A3 and B3 for *X* and *Z* directions for solid and hollow circular sections for different a/b ratio under cyclic loading. 97
Figure 4.21. Cases A4 and B4 for *X* and *Z* directions for solid and hollow circular sections for different a/b ratio under cyclic loading. 98
Figure 4.22. Base shear vs. tip displacement in global *X* and *Z* directions under cyclic loading for hollow circular sections for a/b ratio is equal to 0.90. 100
Figure 4.23. Base shear vs. tip displacement in global *X* and *Z* directions under cyclic loading for hollow circular sections for a/b ratio is equal to 0.95. 101
Figure 4.24. Base shear vs. tip displacement in global *X* and *Z* directions under cyclic loading for hollow circular sections for a/b ratio is equal to 0.99. 102
Figure 4.25. Comparison of load vs. transverse displacement at node 2 for long pipe. 106
Figure 4.26. Comparison of load vs. transverse displacement at node 2 for short pipe. 107
Figure 6.1. Free vibration modes obtained by Abaqus for *L/d*=1 126
Figure 6.2. Free vibration modes obtained by Abaqus for *L/d*=1.5 127
Figure 6.3. Free vibration modes obtained by Abaqus for *L/d*=2 128

Figure 6.4. Free vibration modes obtained by Abaqus for L/d=3 129
Figure 6.5. Free vibration modes obtained by Abaqus for L/d=5 130
Figure 6.6. Comparison of vibration frequencies between MF and LS for L/d=1 (Uniform cantilever beam with solid circular section) 132
Figure 6.7. Comparison of vibration frequencies between MF and LS for L/d=1.5 (Uniform cantilever beam with solid circular section) 132
Figure 6.8. Comparison of vibration frequencies between MF and LS for L/d=2 (Uniform cantilever beam with solid circular section) 133
Figure 6.9. Comparison of vibration frequencies between MF and LS for L/d=3 (Uniform cantilever beam with solid circular section) 133
Figure 6.10. Comparison of vibration frequencies between MF and LS for L/d=5 (Uniform cantilever beam with solid circular section) 134
Figure 6.11. Comparison of vibration frequencies between LS and Abaqus for various L/d 135
Figure 6.12. Tapered cantilever beam with circular cross section 137
Figure 6.13. Free vibration modes obtained by Abaqus for L/d_0=1 and d_1/d_0=0.5 . 138
Figure 6.14. Free vibration modes obtained by Abaqus for L/d_0=3 and d_1/d_0=0.5 . 139
Figure 6.15. Comparison of vibration frequencies between MF and Abaqus for L/d_0=1 and d_1/d_0=0.5 (Tapered cantilever beam with solid circular section) 140
Figure 6.16. Comparison of vibration frequencies between MF and Abaqus for L/d_0=3 and d_1/d_0=0.5 (Tapered cantilever beam with solid circular section) 141
Figure 6.17. Uniform cantilever beam with rectangular cross section 142
Figure 6.18. Free vibration modes obtained by Abaqus for a/c=1 144
Figure 6.19. Free vibration modes obtained by Abaqus for a/c=2 145
Figure 6.20. Free vibration modes obtained by Abaqus for a/c=5 146
Figure 6.21. Comparison of vibration frequencies between MF and LZ for a/c=1 (Uniform cantilever beam with solid rectangular section) 147
Figure 6.22. Comparison of vibration frequencies between MF and LZ for a/c=2 (Uniform cantilever beam with solid rectangular section) 148
Figure 6.23. Comparison of vibration frequencies between MF and Abaqus for a/c=5 (Uniform cantilever beam with solid rectangular section) 148

Figure 6.24. Comparison of vibration frequencies between LZ and Abaqus for various *a/c* 150
Figure 6.25. Tapered cantilever beam with rectangular cross section 151
Figure 6.26. Free vibration modes obtained by Abaqus for L/h_0=1 and h_1/h_0=0.5 . 153
Figure 6.27. Free vibration modes obtained by Abaqus for L/h_0=3 and h_1/h_0=0.5 . 154
Figure 6.28. Comparison of vibration frequencies between MF and Abaqus for L/h_0=1 and h_1/h_0=0.5 (Tapered cantilever beam with rectangular section)..... 155
Figure 6.29. Comparison of vibration frequencies between MF and Abaqus for L/h_0=3 and h_1/h_0=0.5 (Tapered cantilever beam with rectangular section)..... 156

CHAPTER 1

INTRODUCTION

1.1. GENERAL

There are numerous methods of analysis in the literature utilized in the field of structural analysis. These methods extend in a wide range and are named roughly as macroscopic and microscopic depending on the simplicity and accuracy of the method. Macroscopic methods are simpler than microscopic methods but do not offer the accuracy that the latter one provides.

The decision of method that will be used in the analysis of structures should be made carefully so as not to use more accurate and time consuming methods for the analysis of simple cases unnecessarily or vice versa. Briefly, the choice of the method of analysis is case-specific.

The finite element method is a microscopic method which is utilized mostly in the linear and nonlinear static and dynamic analysis of structures both in local (element) and global (structure) level. Since the method is microscopic, it has some complexity due to its nature. In this method, analyses are performed by dividing the geometry of the system analyzed into smaller elements.

There are countless finite elements developed for linear and nonlinear static and dynamic analysis of structures like truss, beam, plate, brick elements and etc. Type of

element that is used in the finite element analysis is also case-specific and selection of the proper element is important at least as the method of analysis.

For example, truss elements can only carry loads that are parallel to their axis and because of this reason they deform only axially. Therefore, they are solely suitable for modeling of structures where forces other than axial force are not the primary concern. However, it is also possible to model the structures that are composed of truss elements with three dimensional (3d) solid elements and obtain the same results that are obtained by using truss elements. But, with this choice, the duration for the finite element analysis and the capactiy needed to store the analysis data will increase in a considerable amount that will result in an unnecessary effort.

Therefore, suitable finite elements that combines the simplicity and accuracy needed from an analysis and still successful in capturing the true behavior of a structural system especially for nonlinear static and dynamic analysis should be developed.

Beams are good options for developing such kind of elements since a beam is a primitive structural member whose dimension parallel to its axis is such long that it is incomparable with its cross-sectional dimensions but yet capable of carrying transverse loads perpendicular to its axis and bending moments at the same time. Moreover, beam elements are frequently used in daily life in modeling structures or their components such as bridge supports, pipelines, crane booms, wind turbine or antenna towers.

Although there exists numerous 3d beam finite elements, there is a lack of adequate elements that has the ability of modeling coupling of forces and vibration characteristics in three dimensions truly in the literature. This ensures the motivation of developing a 3d beam element that is especially efficient in nonlinear static and

dynamic analysis and superior to other 3d beam elements in the literature both in accuracy and robustness.

1.2. OBJECTIVE AND SCOPE

The objective of this study is to present the work done to generate a three dimensional mixed formulation frame finite element that can be used confidently in linear and nonlinear static or dynamic analyses of frame systems and show that the proposed 3d mixed element is better by means of accuracy and robustness than other 3d elements available in the literature.

The proposed 3d mixed formulation beam element is developed by using the three field Hu-Washizu functional and can consider the 3d coupling between axial force, shear force, bending moments and torsion. Three fields utilized in the formulation are displacement, stress and strain. Force interpolation functions are used for section forces that satisfy equilibrium and discontinous section deformations along the beam. Nonlinear analyses are carried out by taking integral of stress-strain relations along limited number of preselected control sections. The formulation of the element cuts out the need for approximating displacements for each control sections along the beam. Displacement values at the nodes are enough for performing analysis. Resulting mixed element is free from shear locking. Superiority of the proposed element is highlighted by comparing it with other 3d elements in the literature and elements in a finite element program under nonlinear loading.

Another novelty presented in this study is the derivation of force based mass matrix which is compatible with the force based stiffness matrix. The advantage of using force based mass matrix in the free vibration analysis is displayed by comparing the

frequency values obtained by the proposed 3d mixed element with the frequency values obtained by explicit methods and as a result of modal analysis by a finite element analysis software for members that have different uniformity and various cross sections.

There are seven chapters in this thesis. The first chapter is an introductory chapter that summarizes the objective and scope of the thesis. Second chapter presents the literature survey on the finite element method, nonlinear analysis of mixed beam elements and vibration characteristics of beams. Derivation of the three dimensional mixed formulation frame finite element is carried out in the third chapter. The robustness and superiority of the proposed 3d mixed element are investigated for nonlinear loading in the fourth chapter through numerical comparisons. Derivation of the three dimensional consistent mass matrix obtained by both displacement and force based approaches are given in the fifth chapter emphasizing the advantages of the latter in the sixth chapter by numerical comparisons of the free vibration frequencies of various uniform and tapered cantilever beams with circular and rectangular cross sections. Conclusions are summarized in the last chapter which is the seventh chapter.

CHAPTER 2

LITERATURE SURVEY

2.1. INTRODUCTION TO THE FINITE ELEMENTS

Finite element analysis is used commonly in many fields of engineering analysis. The ability of the finite element method in offering approximate solutions for real systems even for the cases where differential equations of the physical system are difficult or impossible to establish made the method to be in great request. Developments in finite element procedures and computational mechanics have given rise to the popularity of the method. Although the development of the finite element method can be traced back to early 1940's, the name "finite element" was used firstly in the paper by Clough [1].

In the finite element method, mathematical model of the physical problem is generated with some assumptions on geometry, kinematics, material law, loading, boundary conditions and etc. The problem is solved approximately by dividing the mathematical model into numerous finite elements and using the assumptions. As a result the unknown state variables are obtained and can be used to determine the element response. Refinement of analysis can be usually made by increasing the number of finite elements if needed. Shortly, the method is a back and forth induction and deduction procedure.

Finite element method presents only a mathematical model and solution is correct as much as the correctness of the mathematical model. That means, one can not take much from the results of the finite element method than it is given for the

mathematical model. So it is important to form the mathematical model that is very close to the real case to obtain reasonable results.

It is impossible for a mathematical model to anticipate the actual physical situation exactly. Therefore, mathematical models should be reliable and capable of predicting the behavior as accurate as they can. As a result of this fact, there are two basic types of procedures that are used according to the needs of the performer, called "displacement based finite element method" and "mixed formulation finite element method". In the subsequent sections of this chapter the basic concepts related with these two methods are discussed.

2.1.1. Finite Element Method

There are two main types of mathematical models named as discrete system (also known as lumped parameter system) and continuous system. In a discrete system the response is anticipated by solution of the equilibrium equations directly for the unknown state variables. The actual system must be in such a state that the model can be generated easily with a finite number of state variables. A continuous-system mathematical model is the one that uses differential elements for obtaining differential equations that express the element equilibrium requirements, constitutive relations and element interconnectivity requirements [2]. Differentials of the state variables are used in the continuous system. Boundary conditions and initial conditions in case of dynamic analysis are met throughout the system. Direct and variational methods can be used in the solution of both discrete and continuous systems.

The variational method forms basis for the finite element method and is superior to the discrete method because the equilibrium equations can be generated in a more systematic manner by meeting the boundary conditions at the same time. However,

due to the automatic nature of the variational method, there is a possibility of oversight of the actual physical situation.

In the variational method the aim is to investigate the total potential, Π of the system. Π is a functional of differentials for which the stationarity is invoked with respect to the unknown state variables by taking the first variation of it ($\delta\Pi = 0$). Since the resulting expression includes integrals and derivatives, some manipulations are made on $\delta\Pi$ to find a weaker form rather than the "strong form" of the differential to carry out more easily the numerical calculations on the "weak form". Throughout the solution, the essential boundary condition (also known as Dirichlet or geometric boundary condition) and natural boundary condition (also known as Neumann or force boundary condition) are utilized.

Variational method has some advantages. Once the functional is formed, it can be used not only for a specific case but also for the similar problems. The functional contains scalar quantities rather than vectorial quantities which facilitate numerical calculations. In variational method, it is possible to obtain both exact and approximate solutions depending on the complexity of the problem. Additionally, shape functions can be used in functionals instead of the state variables to be determined. Weighted residual method and Ritz Method use these shape functions in approximate solution of the system.

In weighted residual method, a residual that is formed by approximate state variables of the differential is forced to be minimum in a weighted average sense by meeting the boundary conditions at the same time and a coefficient matrix of the constants of the approximate solution are obtained. Galerkin, least square, collocation and subdomain methods are all weighted residual methods that differ only in minimization of the residual and determination of the constants. However, the logic is the same for all. A symmetric coefficient matrix is always obtained in the least

squares method and a symmetric coefficient matrix is generally derived in the Galerkin method depending on the variational form whereas in the collocation and subdomain methods non-symmetric shape functions can be attained [2]. This is why Galerkin and least squares methods are used more frequently compared to others.

The difference of Ritz method from weighted methods is that it directly minimizes the functional, Π instead of the residual and should satisfy only the essential boundary conditions. Actually the Ritz method is a special case of the weighted residual method.

The common property of all the mentioned methods in the previous paragraphs is that they can all be used in both linear and nonlinear analysis. More detailed information and derivations related with the variational, weighted residual and the Ritz methods can be found in [3], [2], [4], [5] and [6].

Actually all the previously mentioned methods and analysis tools are different forms of virtual displacements and/or minimum total energy principle. They are general methods used for the analysis of solids and structures. Finite difference method is also an option for the analysis. In that case the derivatives in the functional of the variational method are approximated by the various finite divided differences and the solution is carried out accordingly.

In the subsequent sections, the application of the methods mentioned in this section is explained in two types of finite element analysis methods called “displacement based” and “force based” (also known as mixed formulation), respectively for linear static case by giving much importance to the latter since it comprises main scope of the thesis. The methods are also applicable to the dynamic and/or nonlinear case since they are an extension of the linear case.

2.1.2. Displacement Based Finite Element Analysis

As the name calls displacement based finite element analysis is the method of structural analysis that uses displacements as the state variables to be determined by utilizing the loading conditions, constitutive models (also known as material models), geometry, boundary conditions, and etc. The determined state variables are then used to designate other unknown properties of the system like internal forces and stresses. Since the procedure is straightforward and easy to computerize by just using the geometric coordinates and material properties of the structural system, displacement based finite element analysis has been adopted widely over the world for the analysis of solids and structures.

The theory behind the displacement based finite element analysis is the principle of virtual displacements (also known as the principal of virtual work). The theory states that if a virtual small displacement is applied to a system in equilibrium, the total internal virtual work done should be equal to the external virtual work done. Internal virtual work done is due to the strain energy whereas the external work done might be due to combination of body forces (f_B), traction forces (f_S) or the concentrated loads (F_C) on the surface.

$$\int_V \varepsilon'^{\mathrm{T}} \sigma dV = \int_V u'^{\mathrm{T}} f_B dV + \int_S u'^{\mathrm{T}} f_S dS + \sum_i u'_i{}^{\mathrm{T}} (F_C)_i \tag{2.1}$$

Where ε' corresponds to the virtual strains, u' are the virtual displacements and σ are the stresses that are in equilibrium with the external loads. The integrals are taken in the volume, V for the body forces; throughout the surface, S for tractions. According to Equation (2.1) if the principle of virtual displacements are satisfied for all

admissible virtual displacements, then three basic requirements of mechanics; equilibrium, compatibility and constitutive relations are also satisfied [2]. There are numerous references in the literature for the constitutive relations [7], [8] and etc.

Actually Equation (2.1) can be written for all the elements considered in the mathematical model of the actual system. In this case, instead of the integral the expression will necessitate summation symbols in order to assemble each element. Instead of the virtual displacements the nodal displacements of the elements and shape functions are utilized. As a result of the assembly procedure of the element equations the expression will take the well known form;

$$\mathbf{KU} = \mathbf{F} \tag{2.2}$$

and

$$\mathbf{F} = \boldsymbol{F_B} + \boldsymbol{F_S} + \boldsymbol{F_C} \tag{2.3}$$

Where **K** is the stiffness matrix, **U** is the unknown displacement vector comprised of nodal degrees of freedom, and $\boldsymbol{F_B}$, $\boldsymbol{F_S}$ and $\boldsymbol{F_C}$ are the body, surface and concentrated force vectors of the system, respectively.

The system of matrix equations in Equation (2.2) is solved and the unknown displacements are obtained. Then, other unknown quantities are determined by using the displacement values.

Above expressions are for the static case. The dynamic case can also easily be concerned by incorporation of the mass matrix to the Equation (2.2) and neglecting the damping as follows;

$$\mathbf{M\ddot{U} + KU = F} \tag{2.4}$$

Since the dynamic case is a combination of static cases, then the above expression can be solved similar to the static case though the expression includes time dependent matrices.

No matter the type of analysis is linear or nonlinear, nodal point and element equilibrium is always satisfied in displacement based finite element analysis although the differential equilibrium is not. Hence, the stress-strain relationship, the strain-displacement conditions and the displacement boundary conditions are satisfied exactly [2]. Besides, the element nodal forces and externally applied load vectors are in equilibrium at any time. Briefly displacement based finite element analysis concerns only with equilibrium conditions related with displacements. The shortcoming of violating the differential equilibrium is that the force boundary conditions are usually not satisfied and this results in the miscalculation of internal stresses. Because the continuity of the derivatives in differentials is not paid attention in generating the displacement based finite elements. Although this effect can be lessened by using a finer mesh or higher order shape functions in the analysis, it causes an increase in the analysis duration and necessitates a larger storage capacity.

Besides the stated deficiencies and as a result of them, displacement based finite element analysis is insufficient most of the time in plate/shell and incompressible media analysis. Therefore, attention was given to the research on new type of element formulation that will be used especially in the analysis of shells and incompressible media. This is the reason for why the research on mixed formulation finite element analysis has emerged.

2.1.3. Mixed Formulation Finite Element Analysis

Mixed formulation finite elements make use of not only the displacements as unknown state variables but also the strains and/or stresses in the formulation of the variational form of the principle of stationary of total potential energy. Mixed formulation finite element is also called as force based finite element in some of the literature due to the fact that not only displacements are independent but also the element forces or stresses, as well.

The general form of the solution for mixed formulation is known as the Hu-Washizu variational formulation [9] and it is nothing but the manipulation of the principle of virtual displacements that incorporates the strains, stresses and surface tractions into the variations. By this way a more general form is constituted for the analysis of solids and structures as follows;

$$\int_V \delta\varepsilon^{\mathrm{T}}\sigma dV - \int_V \delta u^{\mathrm{T}} f_B dV - \int_S \delta u^{\mathrm{T}} f_S dS - \int_V \delta\sigma^{\mathrm{T}}(\varepsilon - \partial_\varepsilon u)dV$$
$$- \int_V \sigma^{\mathrm{T}}(\delta\varepsilon - \partial_\varepsilon \delta u)dV - \int_S \delta {f_S}^{\mathrm{T}}(u - u_p)dS - \int_S {f_S}^{\mathrm{T}}\delta u dS = 0 \qquad (2.5)$$

Where the symbol δ designates the variational, ∂_ε stands for the differential operator on u and the vector u_p symbolizes the prescribed displacements. Other variables are the same as the ones in Equation (2.1).

With this expression, the constitutive relation, the compatibility and the equilibrium conditions are satisfied in a weak fashion for the volume of the body for each variational element and the applied surface tractions and reactions are equilibrated

with the stresses for the surface of the body. This nature of the mixed formulation makes it flexible to work with different finite elements and enables derivation of mixed formulation variationals that use combination of displacement, strain and stress. The variational is named two-field (displacement and stress) or three-field (displacement, stress and strain) according to the number of state variables used in the formulation.

The advantage of using mixed elements becomes perceptible when dealing with beams, shells or plates that are under the problem of locking due to shear. In a displacement based element the displacements found in the analysis may be smaller than the actual case due to locking. However, mixed based elements can eliminate that locking problem. Similar situation is observed in the incompressible media but in that case the erroneous variables are not the displacements but the pressures [2].

2.1.4. Comparison of Displacement Based and Mixed Finite Elements

Displacement based and mixed formulation finite elements have both advantages and disadvantages that necessitates the usage of them specifically to the type of analysis and the accuracy needed.

Displacement based method is easy to implement into the computer analysis. Because, the geometric coordinates of the domain that meshing is applied and the material properties of the system analyzed suffice to carry out the analysis. Besides, it is the preliminary type of finite element analysis and there are numerous studies related with both the theory and its implementation to computers. Therefore, most of the available commercial analysis programs are designed to perform analysis by displacement based elements which make them widely accessible. However, displacement based methods sometimes lack the accuracy needed for the analysis of

incompressible media and/or shells and plates. In that case, mixed finite elements are good options.

Mixed formulation finite elements are more robust and accurate for the elastic and inelastic analysis of beams. They provide more accurate results with fewer elements per member when material nonlinearities are considered. They are better than displacement based methods in the determination of internal stresses. Less number of elements is enough in mixed elements to determine internal stresses with sufficient accuracy. A disadvantage of mixed finite elements compared to displacements based elements may be the increased complexity of formulation and implementation.

No matter the type of formulation is displacement based or mixed formulation, both methods are subject to inaccuracies due to the nature of the finite element analysis. The errors may be because of appoximate discretization of the geometry, numerical integration of the expressions, evaluation of constitutive relations, solution of dynamic equilibrium equations, solution of equations by iteration and rounding off [2].

2.2. STATIC NONLINEAR ANALYSIS OF MIXED FORMULATION BEAM FINITE ELEMENTS

A beam element can be simply defined as a line on which all structural properties are condensed and this peculiarity of it facilitates analysis of systems composed of beam elements. However, the assumption of condensation of structural properties from three dimensions to one dimension may take away the accuracy needed for nonlinear analysis of important types of structural systems like pier of a deck or load carrying skeleton of a frame building under severe earthquake loading unless the properties in three dimensions are conserved. Therefore, beam finite elements that are capable of

embodying axial, bending, shear and torsion effects with a considerable accuracy are needed to be developed for nonlinear analyses.

Material nonlinearity of beams can be modeled by assuming concentrated or distributed inelasticity on the beam element. Concentrated inelasticity necessitates utilization of hinges that lump nonlinearity at each end of the beam whereas in order to capture distributed inelasticity, control sections composed of plenty of fibers that are necessary for defining material constitutive relations are used for the accumulation of distributed nonlinearity along the beam element. An important drawback of the utilization of strain components that are perpendicular to the control sections of the beam in distributed inelasticity is the inability to capture coupling of section forces unless a suitable element that eliminates this problem is not benefited from.

There are two main methods called displacement based (stiffness) and force based (flexibility) approaches in deriving frame elements, where the latter approach also falls into the category of mixed finite element method. Fields necessary for the determination of shape functions differ and help distinguishing two approaches from each other. However, fiber discretization of control sections and integration of sectional properties along the beam element is common for performing analysis with each approach.

Continuity of differential equations is violated in displacement based elements. Therefore, assumed shape functions utilized for the interpolation of displacement field along the beam element is only capable of ensuring the element equilibrium at the nodes. As a result of the violation of continuity requirement, in order to obtain reasonable values for section forces number of nodes per element (order of shape functions) or the number of elements should be increased which will result in increased computational effort. Moreover, this nature of the displacement based

elements may cause shear-locking in thin beam limit; although reduced integration methods can solve that phenomena to some extent, it cannot eliminate the accuracy problem completely. Hughes et al. [10] offered a reduced integration two-node element, for which integration of shear terms are performed with interpolation functions having order less than the order of shape functions for bending, required the use of at least two elements per span to obtain reasonable results. Yokoyama [11] presented a Timoshenko beam element with reduced integration, which has four nodes and two degrees of freedom (dofs) per node. Although Yokoyama's proposed element was able to eliminate shear locking, accuracy under linear elastic response was still in question with the use of single element discretization per span. A consistent interpolation element with three nodes in total was proposed by Reddy [3]. This element had two nodes at the ends with two dofs each and a middle node with only the transverse deflection as dof. Although this element solved the locking problem, it still necessitated the use of several elements per span under linear elastic conditions. Both locking and accuracy problems of displacement based elements were solved by the element proposed by Friedman and Kosmatka [12], where the element had two end nodes and was formulated in 2d by using Hamilton's principle and cubic and quadratic Lagrangian shape functions for transverse and rotational displacements. The shape functions in that study were made independent by requiring them to satisfy the two homogenous differential equations associated with Timoshenko's beam theory, and the shape functions thus contain sectional geometric properties unlike the standard finite element shape functions that are dimensionless. With this element, the response of a uniform prismatic beam under linear elastic conditions was accurately modeled through single element discretization per span. It should also be mentioned that the resulting element stiffness matrix with the use of these shape functions were earlier presented by Przemieniecki [13], where the stiffness matrix in the latter study was derived through integration of differential equilibrium equations under linear elastic material response. The beam finite element developed by Friedman and Kosmatka was later used by Mazars et al. [14] for the nonlinear analysis and capacity assessment of reinforced concrete columns and slender walls, where the effect of shear force and torsion was assumed to be

uncoupled. In a recent study, Triantafyllou and Koumousis [15] developed a locking-free 2d displacement based beam finite element, where the shape functions were derived under linear elastic material behavior similar to the effort presented by Friedman and Kosmatka [12]. The beam element proposed in that study was used to analyze structural members where shear effects were significant under nonlinear material response.

Last two decades witnessed the rise of mixed beam finite elements due to the computational issues faced with displacement based elements. In mixed finite elements, independent stress and strain fields are utilized in addition to the displacement field in the variational form of the element, thereby relaxing the strong satisfaction of the problem solution statements faced in the displacement based elements derived from minimum potential energy principle (Table 2.1, where meaning of the symbols are given in the derivation of the proposed beam element later in this thesis).

Table 2.1. Strong and weak satisfaction of parameters in variational principles

Varied Fields	**Functional Name**	**Strong Satisfaction**	**Weak Satisfaction**
$\mathbf{u}$	Potential Energy	$\boldsymbol{\varepsilon} = \nabla^s \mathbf{u}$ in Ω $\boldsymbol{\sigma} = \boldsymbol{\sigma}(\boldsymbol{\varepsilon})$ in Ω $\mathbf{u} = \mathbf{u}^*$ on Γ_u	div $\boldsymbol{\sigma} + \mathbf{b} = \mathbf{0}$ in Ω $\mathbf{t} = \mathbf{t}^*$ on Γ_t
$\mathbf{u}, \boldsymbol{\sigma}$	Hellinger-Reissner	$\boldsymbol{\varepsilon} = \nabla^s \mathbf{u}$ in Ω $\mathbf{u} = \mathbf{u}^*$ on Γ_u	div $\boldsymbol{\sigma} + \mathbf{b} = \mathbf{0}$ in Ω $\boldsymbol{\sigma} = \boldsymbol{\sigma}(\boldsymbol{\varepsilon})$ in Ω $\mathbf{t} = \mathbf{t}^*$ on Γ_t
$\mathbf{u}, \boldsymbol{\sigma}, \boldsymbol{\varepsilon}$	Hu-Washizu	-	div $\boldsymbol{\sigma} + \mathbf{b} = \mathbf{0}$ in Ω $\boldsymbol{\varepsilon} = \nabla^s \mathbf{u}$ in Ω $\boldsymbol{\sigma} = \boldsymbol{\sigma}(\boldsymbol{\varepsilon})$ in Ω $\mathbf{u} = \mathbf{u}^*$ on Γ_u $\mathbf{t} = \mathbf{t}^*$ on Γ_t

Mixed elements are advantageous compared to displacement based elements since they do not need to cope with shear or membrane locking, and they yield accurate results with lesser number of elements under nonlinear conditions [16]. In a recent study by Saritas and Soydas [17], the accuracy and robustness of the mixed finite elements compared to the displacement based elements were presented in detail with examples.

The keystone and highly cited study in the development and use of mixed beam finite elements under nonlinear conditions is the paper by Spacone et al. [18]. In that study, Hellinger-Reissner principle was used in the derivation of an Euler-Bernoulli beam finite element for the analysis and capacity assessment of reinforced concrete columns; thus only axial force and bending moment interaction was considered. Souza [19] presented a 3d Euler-Bernoulli beam element through the use of Hellinger-Reissner principle, where moderate displacements were taken into account along element length and large displacements and rotations at the nodes were considered through corotational formulation [20]. Nukala and White [21] developed a 3d Euler-Bernoulli beam finite element based on Hellinger-Reissner variational principle for nonlinear analysis of steel frames having open-walled cross-section by including finite rotations and warping of the cross-section due to torsion. In that study, nonlinear material behavior was obtained by a decoupled response of axial stress and shear stress through the use of a two-space Von Mises constitutive relation, where the element cross-section included the axial stress due to axial force, biaxial bending and bimoment, and the shear stress due to uniform torsion only, thus shear force effect was neglected.

A two dimensional Timoshenko mixed beam element free from shear-locking formed by the utilization of the three-field Hu-Washizu variational was proposed by Taylor et al. [16] by assuming the effect of shear is linear elastic and uncoupled from

axial force and bending moment. In a successor study, Saritas and Filippou [22] developed a 2d mixed element that considers the interaction of axial force, shear force and moment, where the reliability of the element with regards to experimental data was verified with steel shear link elements [23] and reinforced concrete members [24].

Recently, Papachristidis et al. [25] proposed a 3d Timoshenko mixed element for the capacity assessment of frame structures under high shear based on natural mode method [26] that incorporates axial force, shear force, bending moment and torsion to the element formulation. However, in that study the interaction between internal forces for the 3d beam element was not demonstrated. Furthermore, Wackerfuss and Gruttman [27] developed a three dimensional frame element by using Hu-Washizu variational for beams with arbitrary cross-section and nonlinear behavior was modeled by defining additional deformation modes for warping and deformations in the transverse direction of each node of the element. Verification studies in the latter paper comprised mostly of linear material and nonlinear geometric responses of members and thus did not provide verification of the nonlinear interaction between 3d sectional forces present in the element.

In this thesis, three field Hu-Washizu variational principle is used to develop a 3d Timoshenko mixed beam finite element that considers the interaction of axial force, shear force, biaxial bending moments and torsion through monitoring of responses over several control sections along element length and with the fiber discretization of the section. Shape functions that satisfy equilibrium and discontinuous strains are used for section resultants for the finite element approximation. This nature of the element eliminates the necessity of displacement interpolations along the element length except at the nodes. Nonlinear interaction between normal and shearing stresses is achieved with the use of an inelastic 3d material model. Nonlinear analyses of uniform or tapered members with solid and hollow circular sections are performed and the proposed 3d Timoshenko mixed element is compared with various

3d frame elements under nonlinear conditions, as well as with closed form solutions available in the literature. It is observed that the most significant advantage of the proposed beam element is its high accuracy through the use of single element discretization per span thereby reducing the computational burden of the extra fields necessary in the formulation of the mixed finite elements and furthermore the element can also accurately simulate the linear and nonlinear responses of tapered members without the need for the derivation of new shape functions.

As a part of the research study conducted in this thesis, Soydas and Saritas [28] recently published a paper that presented the 3d mixed formulation beam element based on Hu-Washizu functional.

2.3. VIBRATION CHARACTERISTICS OF BEAMS

Lumped or consistent mass matrices are used in dynamic analyses that are carried out by using finite element method. Although it is preferred to use lumped matrices for dynamic analyses of residential buildings under earthquake vibrations due to its practicality, it is important and necessary to use consistent mass matrices for special engineering structures like chimneys, towers of wind turbines, nuclear power plants, dams, etc. in order to obtain more accurate results.

There are countless studies regarding the determination of free vibration frequencies of structural elements and the development of methods to perform vibration analyses. As the abundance and variety of studies on aforementioned subjects are concerned, only the literature survey related with vibration characteristics of beam elements is presented in this section in order to be compatible with the objective and scope of this thesis.

Timoshenko indicated in two consecutive studies that the shear correction is more important than rotary inertia and both of them become unimportant if the wave-length of the transverse vibrations is large compared to the dimensions of the section. Additionally, the value of shear correction increases with a decrease in the wave-length [29, 30]. According to Cook et al. [31], the effects of inertia can be neglected if the frequency of the excitation the structure is exposed to is less than approximately one-third of the structure's lowest natural frequency of vibration. Besides, Chopra [32] stated that shear deformation and rotary inertia are important for higher vibration frequencies rather than fundamental natural frequency.

The study by Huang [33] showed the effect of shear deformation and rotary inertia on a cantilever beam by using a solution scheme for two complete differential equations in total deflection and slope. Huang and Kung [34] presented new tables of eigenfunctions that embody normal modes of vibration of Timoshenko beam for a cantilever beam. Cheng [35] also investigated the effect of rotary inertia and shear deformation on the eigenvalues of structural vibrations by comparing various Euler-Bernoulli and Timoshenko beams. Besides considering the same effects, Tessler and Dong [36] used consistent mass matrices in their study and presented vibration frequencies for uniform hinged beams.

Grant [37] studied the effect of rotary inertia and shear deformation on the frequency of uniform beams carrying a concentrated mass at an arbitrary location on the beam element. Swaminadham and Michael [38] derived the frequency equation for a cantilever beam with a heavy mass at the free end. In another study by To [39], natural frequencies of a cantilever beam with a tip mass attached to the free node and exposed to base excitation were calculated by reckoning the gap between the centre of gravity of the mass and the point where it was attached. The study that considered

the variation of thickness of the cross section of a cantilever member which had a concentrated mass at the free end belonged to Rossi et al. [40].

Leissa and So [41] developed a method of 3d analysis for the free vibration analysis of solid circular cylinders of elastic material and obtained accurate frequencies even for higher vibration modes for beams that had different boundary conditions. They also compared the frequencies with the frequencies obtained from known elementary and improved 1d theories.

There are numerous studies that include 2d and 3d consistent mass matrices for elements with uniform cross-sections obtained by displacement based approaches [12, 13, 42, 43]. As explained in the study of Molins et al. [44], it is also possible to use flexibility-based approach and come up with the same consistent mass matrix for a straight beam with uniform cross section obtained by displacement based approach.

In this thesis, not only a 3d mixed beam element but also a consistent mass matrix is derived by using flexibility based approach and the flexibility based consistent mass matrix is used for the determination of higher order free vibration frequencies of the proposed 3d mixed element in the following chapters.

CHAPTER 3

FORMULATION OF THREE DIMENSIONAL MIXED ELEMENT

3.1. INTRODUCTION

In this chapter the derivation of a three dimensional mixed formulation beam finite element is presented by using three-field variational form. Shape functions are used for the finite element approximation of the beam section forces that satisfy equilibrium in the undeformed configuration. The presented formulation eliminates the necessity of displacement variables for sections along element length except the nodal displacements.

3.2. COORDINATE SYSTEMS AND TRANSFORMATIONS

3.2.1. Basic System

The coordinate system is a right-handed coordinate system both on local and global level. The global coordinate system has orthogonal axes as X, Y and Z and the local coordinate system has orthogonal axes as x, y and z.

The member has two nodes that the local *x*-axis is oriented from the node i at the beginning of the member to node j at the end of the member such that *y*-axis is in the same plane with the *x*-axis and *z*-axis is perpendicular to the planes formed by *x* and y axes and *z*-axis points out of the *x*-*y* plane. Forces, moments, displacements and

rotations in the direction of positive axes are considered to be positive. An accent "¯" sign is used for variables in local axis to distinguish them from variables in global axis. Single headed arrows are used to symbolize forces and axial displacements whereas double headed arrows are utilized to represent moments and rotations about orthogonal axes hereafter.

It is possible to reduce the number of element end forces that are shown with the letter p followed by a subscript in Figure 3.1 by replacing them with interdependent element end forces which are called "Basic Element Forces" by utilizing equilibrium equations. For each node in a member, number of degrees of freedom is 6 summing up to 12 for two end nodes. Therefore, in a 3d system number of element end forces is 12 and it is reduced to 6 by separating 6 rigid body modes and 6 deformation modes of displacement.

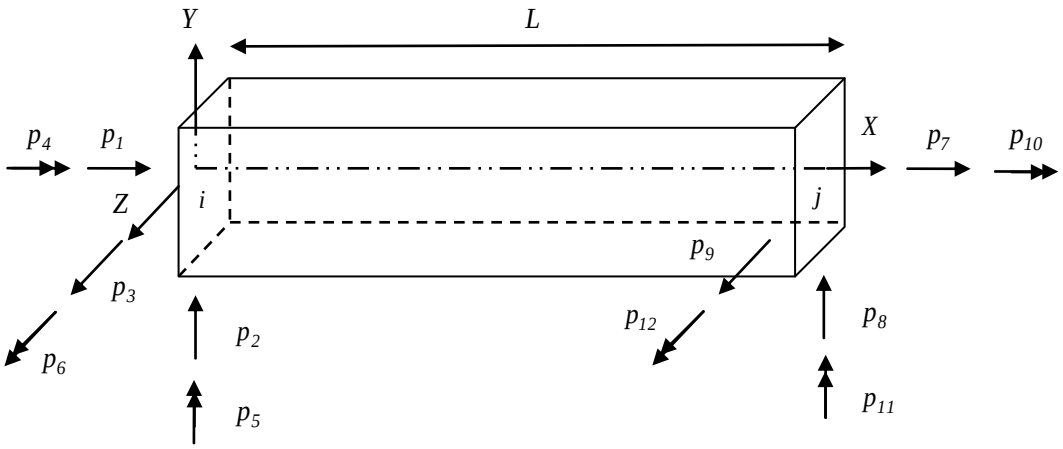

Figure 3.1. Free body diagram of element end forces

Using force and moment equilibrium equations, following equalities can be derived according to the Figure 3.1;

$$
\begin{aligned}
p_1 &= -p_7 \\
p_8 L &= -p_6 - p_{12} \\
p_2 L &= p_6 + p_{12} \\
p_9 L &= p_5 + p_{11} \\
p_3 L &= -p_5 - p_{11} \\
p_4 &= -p_{10}
\end{aligned}
\tag{3.1}
$$

If following equalities are assumed;

$$p_7 = q_1 \qquad p_6 = q_2 \qquad p_{12} = q_3 \qquad p_5 = q_5 \qquad p_{11} = q_6 \qquad p_{10} = q_4 \tag{3.2}$$

Where q designates basic element forces, then the relationship between element end forces and basic element forces are obtained as depicted in Figure 3.2.

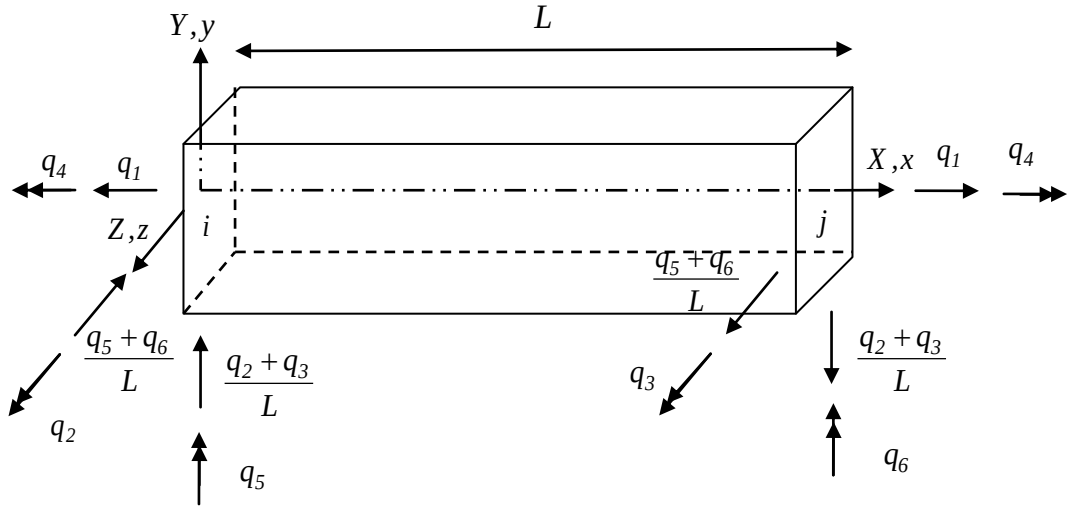

Figure 3.2. Demonstration of basic element forces

The relationship between element end forces and basic element forces in matrix form can be denoted as follows;

$$\boldsymbol{p} = \boldsymbol{a}^{\mathbf{T}}\boldsymbol{q} \tag{3.3}$$

$$\begin{pmatrix} p_1 \\ p_2 \\ p_3 \\ p_4 \\ p_5 \\ p_6 \\ p_7 \\ p_8 \\ p_9 \\ p_{10} \\ p_{11} \\ p_{12} \end{pmatrix} = \begin{bmatrix} -1 & 0 & 0 & 0 & 0 & 0 \\ 0 & 1/L & 1/L & 0 & 0 & 0 \\ 0 & 0 & 0 & 0 & -1/L & -1/L \\ 0 & 0 & 0 & -1 & 0 & 0 \\ 0 & 0 & 0 & 0 & 1 & 0 \\ 0 & 1 & 0 & 0 & 0 & 0 \\ 1 & 0 & 0 & 0 & 0 & 0 \\ 0 & -1/L & -1/L & 0 & 0 & 0 \\ 0 & 0 & 0 & 0 & 1/L & 1/L \\ 0 & 0 & 0 & 1 & 0 & 0 \\ 0 & 0 & 0 & 0 & 0 & 1 \\ 0 & 0 & 1 & 0 & 0 & 0 \end{bmatrix} \begin{pmatrix} q_1 \\ q_2 \\ q_3 \\ q_4 \\ q_5 \\ q_6 \end{pmatrix}$$

Where *L* is length of the member and $\boldsymbol{a}$ is the transformation matrix.

3.2.2. Section Forces (Internal Forces)

It is possible to establish the relationship between basic element forces and section forces (internal forces of the element) by utilizing element equilibrium equations neglecting any traction along the member as follows;

$$\boldsymbol{s}(x) = \boldsymbol{b}(x)\boldsymbol{q} \tag{3.4}$$

$$\boldsymbol{s}(x) = [N(x) \quad M_z(x) \quad M_y(x) \quad V_y(x) \quad V_z(x) \quad T(x)]^{\mathrm{T}} \tag{3.5}$$

$$\boldsymbol{q} = [q_1 \quad q_2 \quad q_3 \quad q_4 \quad q_5 \quad q_6]^{\mathrm{T}} \tag{3.6}$$

$$\boldsymbol{b}(x) = \begin{bmatrix} 1 & 0 & 0 & 0 & 0 & 0 \\ 0 & \frac{x}{L} - 1 & x/L & 0 & 0 & 0 \\ 0 & 0 & 0 & -\frac{x}{L} + 1 & -x/L & 0 \\ 0 & -1/L & -1/L & 0 & 0 & 0 \\ 0 & 0 & 0 & 0 & 1/L & 1/L \\ 0 & 0 & 0 & 1 & 0 & 0 \end{bmatrix} \tag{3.7}$$

Where

$\boldsymbol{s}(x)$: Internal or section force vector

$\boldsymbol{b}(x)$: Matrix of force interpolation functions

$\boldsymbol{q}$: Basic element force vector

$N(x)$: Axial force in the section

$M_z(x)$: Moment about the z-axis

$M_y(x)$: Moment about the y-axis

$V_y(x)$: Shear force in the y direction

$V_z(x)$: Shear force in the z direction

$T(x)$: Torsion about longitudinal axis

L : Length of the member

Where the section forces are computed by integration of the stress values over the cross-section as follows;

$$N = \int_A \sigma_{xx} dA \qquad M_y = \int_A z\sigma_{xx} dA \qquad M_z = \int_A -y\sigma_{xx} dA$$

$$V_y = \int_A \sigma_{xy} dA \qquad V_z = \int_A \sigma_{xz} dA \qquad T = \int_A \left(-z\sigma_{xy} + y\sigma_{xz}\right) dA \tag{3.8}$$

Where A is the area of the section.

3.2.3. Section Deformations

Element deformations can be obtained by integration of the section deformations along the element length and given as follows;

$$\mathbf{v} = \int_0^L \boldsymbol{b}^T(x)\boldsymbol{e}(x)\, dx \tag{3.9}$$

$$\mathbf{v} = [\mathrm{v}_1 \quad \mathrm{v}_2 \quad \mathrm{v}_3 \quad \mathrm{v}_4 \quad \mathrm{v}_5 \quad \mathrm{v}_6]^{\mathrm{T}} \tag{3.10}$$

$$\boldsymbol{e}(x) = [\varepsilon_a(x) \quad \kappa_z(x) \quad \kappa_y(x) \quad \gamma_y(x) \quad \gamma_z(x) \quad \varphi(x)]^{\mathrm{T}} \tag{3.11}$$

Where

$\boldsymbol{e}(x)$: Section deformation vector

$\mathbf{v}$: Basic element deformation vector

$\varepsilon_a(x)$: Axial deformation of reference axis

$\kappa_y(x)$: Curvature about y-axis

$\kappa_z(x)$: Curvature about z-axis

$\gamma_y(x)$: Shear deformation (distortion angle) about y-axis

$\gamma_z(x)$: Shear deformation (distortion angle) about z-axis

$\varphi(x)$: Twist angle around longitudinal axis

$\mathbf{v}$ is related to displacement degrees of freedom in local coordinates, $\bar{\boldsymbol{u}}$ as follows;

$$\mathbf{v} = \boldsymbol{a}\bar{\boldsymbol{u}} \tag{3.12}$$

Where $\boldsymbol{a}$ is the transformation matrix as explained presviously and $\bar{\boldsymbol{u}}$ is defined as follows;

$$\bar{\boldsymbol{u}} = [\bar{u}_1 \quad \bar{u}_2 \quad \bar{u}_3 \quad \bar{u}_4 \quad \bar{u}_5 \quad \bar{u}_6 \quad \bar{u}_7 \quad \bar{u}_8 \quad \bar{u}_9 \quad \bar{u}_{10} \quad \bar{u}_{11} \quad \bar{u}_{12}]^{\mathrm{T}} \tag{3.13}$$

Displacement degrees of freedom in local coordinates, $\bar{\boldsymbol{u}}$ are related to the global degrees of freedom linearly as follows;

$$\bar{\boldsymbol{u}} = \boldsymbol{a}_r \boldsymbol{u}_{el} \tag{3.14}$$

Where $\boldsymbol{u}_{el}$ demonstrates displacement degrees of freedom in global coordinates such that;

$$\boldsymbol{u_{el}} = [u_1 \quad u_2 \quad u_3 \quad u_4 \quad u_5 \quad u_6 \quad u_7 \quad u_8 \quad u_9 \quad u_{10} \quad u_{11} \quad u_{12}]^{\mathrm{T}} \tag{3.15}$$

and $\boldsymbol{a_r}$ is rotation matrix from global to local reference system given by;

$$\boldsymbol{a_r} = \begin{bmatrix} \boldsymbol{M_{rot}} & \mathbf{0} & \mathbf{0} & \mathbf{0} \\ \mathbf{0} & \boldsymbol{M_{rot}} & \mathbf{0} & \mathbf{0} \\ \mathbf{0} & \mathbf{0} & \boldsymbol{M_{rot}} & \mathbf{0} \\ \mathbf{0} & \mathbf{0} & \mathbf{0} & \boldsymbol{M_{rot}} \end{bmatrix} \tag{3.16}$$

Where

$$\boldsymbol{M_{rot}} = (\boldsymbol{\eta_x} \quad \boldsymbol{\eta_y} \quad \boldsymbol{\eta_z})^{\mathrm{T}} \tag{3.17}$$

Where $\boldsymbol{\eta_x}$ denotes the unit vector in the direction of the X axis formed by the difference between global coordinates (X, Y, Z) of nodes i and j and found as;

$$\boldsymbol{\eta_x} = \frac{1}{L}\begin{pmatrix} X_j - X_i \\ Y_j - Y_i \\ Z_j - Z_i \end{pmatrix}^{\mathrm{T}} \tag{3.18}$$

Since the element is in a 3d coordinate system, the unit vector (or the coordinate of a point not existing on the line connecting nodes i and j) in the direction of Y axis, $\boldsymbol{\eta_y}$ should be given as an input in order to determine the unit vector in the direction of Z axis, $\boldsymbol{\eta_z}$ from the cross product $\boldsymbol{\eta_z} = \boldsymbol{\eta_x} \times \boldsymbol{\eta_y}$. It should be noted that $\boldsymbol{\eta_z}$ can be interchanged with $\boldsymbol{\eta_y}$ in the cross product, i.e. at least one unit vector in addition to the unit vector in the direction of the beam axis is needed to define the third unit vector in the 3d coordinate system.

If Equation (3.14) is substituted into Equation (3.12), basic element deformation vector can be related to displacements as follows;

$$\mathbf{v} = \boldsymbol{a}\boldsymbol{a}_r\boldsymbol{u}_{el}=\boldsymbol{a}_g\boldsymbol{u}_{el} \tag{3.19}$$

Transformation of element displacements to deformations can be visualized as displayed in Figure 3.3.

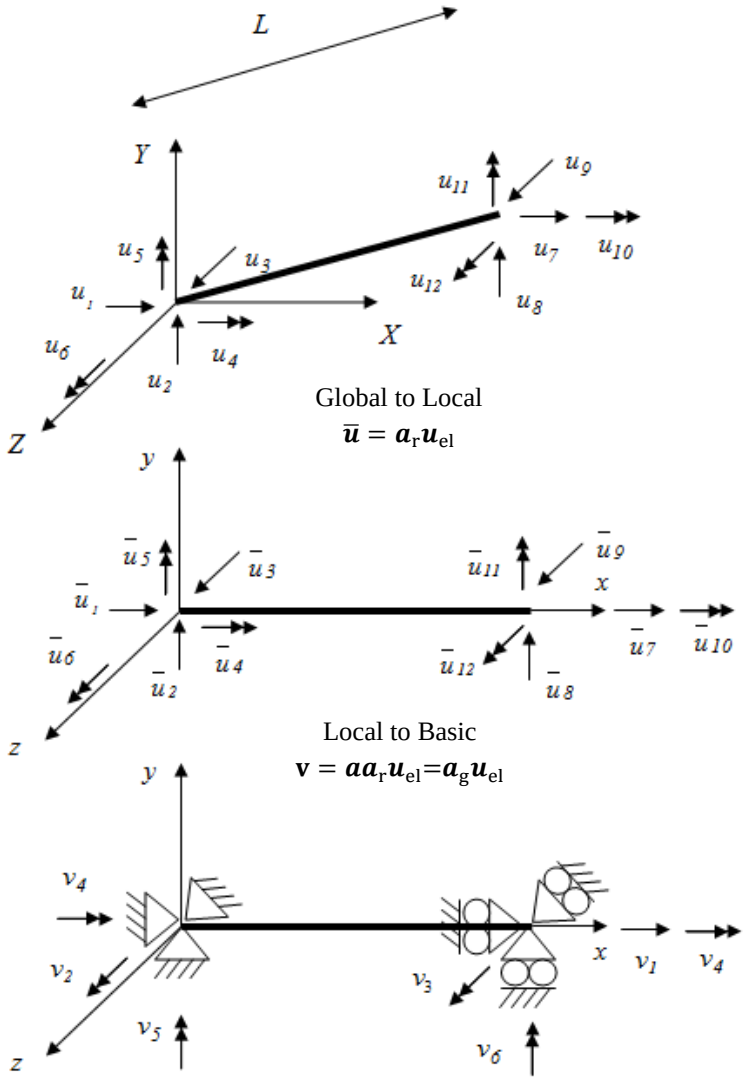

Figure 3.3. Transformation of element displacements to deformations

The basic system is chosen as the simply supported beam as shown in Figure 3.3 in the derivation presented in this chapter. The alternative choice for the basic system is the cantilever basic system, as done in Chapter 5 in the derivation of consistent mass matrix. Carrying out the formulation of the element with these alternative choices actually results in the same response in the complete system for the finite element model. The important physical aspect of the use of a basic system is the elimination of the rigid body modes of displacements, thus the element is left with only the deformation modes in the basic system. Formulation in the basic system enables the possibility of deriving flexibility matrix, which would have been impossible to obtain in the complete system due to the singularity caused by rigid body modes.

3.3. HU-WASHIZU FUNCTIONAL

The mathematical theory of the proposed 3d beam finite element is based on the Hu-Washizu [9] functional with three independent fields. These fields are stress field $\boldsymbol{\sigma}$, strain field $\boldsymbol{\varepsilon}$, and displacement field $\mathbf{u}$.

$$\Pi_{\mathrm{HW}}(\boldsymbol{\sigma}, \boldsymbol{\varepsilon}, \mathbf{u}) = \int_{\Omega} \mathrm{W}(\boldsymbol{\varepsilon})\mathrm{d}\Omega + \int_{\Omega} \boldsymbol{\sigma}^{\mathrm{T}} [\boldsymbol{\varepsilon}^{\mathbf{u}} - \boldsymbol{\varepsilon}]\mathrm{d}\Omega + \Pi_{\mathrm{ext}} \tag{3.20}$$

$\mathrm{W}(\boldsymbol{\varepsilon})$ is the strain energy function from which stresses are derived as;

$$\widehat{\boldsymbol{\sigma}}(\boldsymbol{\varepsilon}) = \frac{\partial \mathrm{W}(\boldsymbol{\varepsilon})}{\partial \boldsymbol{\varepsilon}} \tag{3.21}$$

$\boldsymbol{\varepsilon}^{\mathbf{u}}$ is the strain vector that is compatible with the displacements $\mathbf{u}$.

Π_{ext} denotes the potential energy of the external loading due to body forces and displacement and traction boundary conditions such that;

$$\Pi_{ext} = -\int_{\Omega} \mathbf{u}^{\mathbf{T}}\mathbf{b}d\Omega - \int_{\Gamma_t} \mathbf{u}^{\mathbf{T}}\mathbf{t}^{*}d\Gamma - \int_{\Gamma_u} \mathbf{t}^{\mathbf{T}}[\mathbf{u} - \mathbf{u}^{*}]\, d\Gamma \tag{3.22}$$

In Equation (3.22), $\mathbf{b}$ denotes body forces and $\mathbf{t} = \boldsymbol{\sigma}.\mathbf{n}$ is the dot product of the stress tensor with the outward normal $\mathbf{n}$ to the boundary, designating forces caused by tractions. The imposed values of tractions and displacements are indicated by superscript asterisks. It is assumed that the external loading is conservative so that the work depends only on the final displacement values of $\mathbf{u}$. Domain of the body and traction and displacement boundaries are Ω , Γ_t and Γ_u , respectively.

3.4. KINEMATICS OF 3D TIMOSHENKO BEAM ELEMENT

There are two basic beam theories called Euler-Bernoulli (EBT) and Timoshenko beam theories (TBT) where the latter has some improvements compared to the former. As the name calls, the equation of the elastic curve was formulated by James Bernoulli and Leonhard Euler extended its application [45] in EBT. The assumption that section plane remains normal to the beam tangential axis after the deformation of section brings along the negligence of shear effects in the section in EBT whereas the theory considers still the axial and flexural effects. However, TBT counts in shear deformations by presuming there exists constant shear deformation in the section.

Consequently, section plane does not have to be normal to the axis of the beam after deformation as compared to the assumption in EBT although the plane remains plane after deformation. But, in TBT, a shear correction factor need to be used in order to calculate shear force in the section properly [46] because of the assumption of constant shear deformation on the section. It is possible to employ higher order shape functions for section deformations for surmounting that issue [47] in higher order beam theories (HOBT). However, additional computational effort will be required in that circumstance. This fact induced utilization of kinematic relations of TBT in the derivation of the 3d mixed beam element in this thesis. Figure 3.4 epitomizes the deformation of a beam element according to, EBT, TBT and HOBT, respectively.

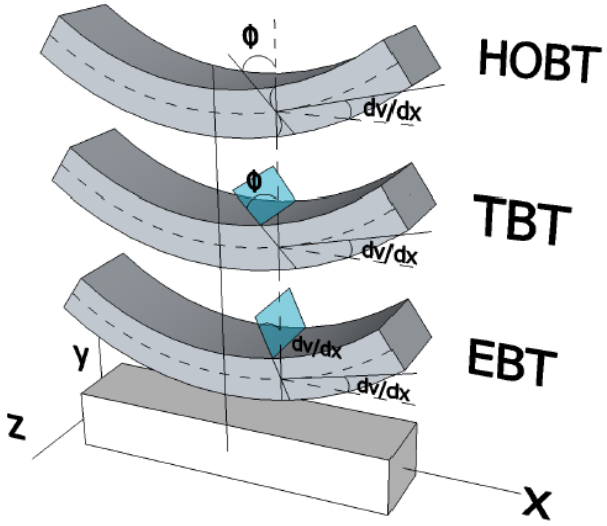

Figure 3.4. Beam deformations according to various beam theories

Three field variational principle that is used in Equation (3.20) and (3.22) enables the specification of $\boldsymbol{\varepsilon}$ and $\mathbf{u}$ independently which also allows selection of section kinematic relations that are independent from beam kinematics. If kinematic relations of the Timoshenko beam theory is used for a three dimensional geometry as follows;

$$\mathbf{u} = \begin{Bmatrix} u_x(x,y,z) \\ u_y(x,y,z) \\ u_z(x,y,z) \end{Bmatrix} = \begin{Bmatrix} u(x) - y\theta_z(x) + z\theta_y(x) \\ v(x) - z\theta_x(x) \\ w(x) + y\theta_x(x) \end{Bmatrix} \tag{3.23}$$

Where $u_x(x,y,z)$, $u_y(x,y,z)$ and $u_z(x,y,z)$ are the displacements of any point on the section in *x*, *y* and *z* directions, respectively. $u(x)$ is the displacement of the point $(x,0,0)$ along *x*-axis and $v(x)$ and $w(x)$ are the transverse deflections of the point $(x,0,0)$ from *x*-axis in *y* and *z* directions, respectively. $\theta_x(x)$, $\theta_y(x)$ and $\theta_z(x)$ are the small rotations of the beam cross section around three orthogonal axes *x*, *y* and *z*, respectively. Hence the vector of displacements at a section of the beam can be given as;

$$\mathbf{u_s} = [u(x) \quad v(x) \quad w(x) \quad \theta_x(x) \quad \theta_y(x) \quad \theta_z(x)]^{\mathrm{T}} \tag{3.24}$$

Strains that are compatible with the displacement field **u** can be derived from Equation (3.23) under small strain assumption as follows;

$$\begin{aligned} \varepsilon_{xx}^u &= \frac{du_x(x,y,z)}{dx} = u'(x) - y\theta_z{}'(x) + z\theta_y{}'(x) \\ \gamma_{xy}^u &= \frac{du_x(x,y,z)}{dy} + \frac{du_y(x,y,z)}{dx} = -\theta_z(x) + v'(x) - z\theta_x{}'(x) \\ \gamma_{xz}^u &= \frac{du_x(x,y,z)}{dz} + \frac{du_z(x,y,z)}{dx} = \theta_y(x) + w'(x) + y\theta_x{}'(x) \end{aligned} \tag{3.25}$$

It should be noted that ε_{yy}^u , ε_{zz}^u and γ_{yz}^u are equal to zero as a result of the derivation.

The strain fields for the beam are selected independently from those in Equation (3.25) as follows;

$$\boldsymbol{\varepsilon} = \begin{Bmatrix} \varepsilon_{xx} \\ \gamma_{xy} \\ \gamma_{xz} \end{Bmatrix} = \begin{Bmatrix} \varepsilon_a(x) - y\kappa_z(x) + z\kappa_y(x) \\ \gamma_y(x) - z\varphi(x) \\ \gamma_z(x) + y\varphi(x) \end{Bmatrix} \tag{3.26}$$

Where $\varepsilon_a(x)$, $\kappa_y(x)$ and $\kappa_z(x)$ are the axial deformation and curvature around *y* and *z* axes, respectively. $\gamma_y(x)$ and $\gamma_z(x)$ are the shear deformations (distortions) of the section in *y* and *z* directions, respectively. $\varphi(x)$ is the angle of twist of the cross section. Hence section deformations, $\boldsymbol{e}(x)$ are given by Equation (3.11).

3.5. VARIATION OF HU-WASHIZU FUNCTIONAL

The variation of the Equation (3.20) gives;

$$\delta\Pi_{\mathrm{HW}} = \int_{\Omega} \widehat{\boldsymbol{\sigma}}(\boldsymbol{\varepsilon})\boldsymbol{\delta\varepsilon} d\Omega + \int_{\Omega} \delta\boldsymbol{\sigma}^{\mathrm{T}} [\boldsymbol{\varepsilon^{u}} - \boldsymbol{\varepsilon}] d\Omega + \int_{\Omega} \boldsymbol{\sigma}^{\mathrm{T}} [\delta\boldsymbol{\varepsilon^{u}} - \delta\boldsymbol{\varepsilon}] d\Omega + \delta\Pi_{\mathrm{ext}} \tag{3.27}$$

The functional in Equation (3.27) can be generalized for an inelastic material by assuming that $\widehat{\boldsymbol{\sigma}}(\boldsymbol{\varepsilon})$ describes an inelastic material although the variation in Equation (3.21) is based on a strain-energy function that is in accordance with Cauchy elastic

material model. If Equations (3.25) and (3.26) are substituted into Equation (3.27) by noting that for the 3d beam element $\sigma_{yy} = \sigma_{zz} = \hat{\sigma}_{yy} = \hat{\sigma}_{zz} = \hat{\sigma}_{yz} = \gamma_{yz} = 0$ and implementing integration along the length of the beam element;

$$
\begin{aligned}
\delta\Pi_{\mathrm{HW}} \quad &= \int_{\Omega} \{\hat{\sigma}_{xx}\big(\delta\varepsilon_a(x) - y\delta\kappa_z(x) + z\delta\kappa_y(x)\big)\}d\Omega \\
&+ \int_{\Omega} \left\{\hat{\sigma}_{xy}\left(\delta\gamma_y(x) - z\delta\varphi(x)\right) + \hat{\sigma}_{xz}\big(\delta\gamma_z(x) + y\delta\varphi(x)\big)\right\} d\Omega \\
&+ \int_{\Omega} \{\delta\sigma_{xx}\big[\big(u'(x) - \varepsilon_a(x)\big) - y\big(\theta_z{}'(x) - \kappa_z(x)\big) + z\big(\theta_y{}'(x) - \kappa_y(x)\big)\big]\}d\Omega \\
&+ \int_{\Omega} \{\delta\sigma_{xy}\big[v'(x) - \theta_z(x) - \gamma_y(x)\big] + \delta\sigma_{xz}\big[w'(x) + \theta_y(x) - \gamma_z(x)\big]\}d\Omega \\
&+ \int_{\Omega} \{\big(-z\delta\sigma_{xy} + y\delta\sigma_{xz}\big)(\theta_x{}'(x) - \varphi(x))\}d\Omega \\
&+ \int_{\Omega} \{\sigma_{xx}\big[\big(\delta u'(x) - \delta\varepsilon_a(x)\big) - y\big(\delta\theta_z{}'(x) - \delta\kappa_z(x)\big) + z\big(\delta\theta_y{}'(x) - \delta\kappa_y(x)\big)\big]\}d\Omega \\
&+ \int_{\Omega} \{\sigma_{xy}\big[\delta v'(x) - \delta\theta_z(x) - \delta\gamma_y(x)\big] + \sigma_{xz}\big[\delta w'(x) + \delta\theta_y(x) - \delta\gamma_z(x)\big]\}d\Omega \\
&+ \int_{\Omega} \{\big(-z\sigma_{xy} + y\sigma_{xz}\big)(\delta\theta_x{}'(x) - \delta\varphi(x))\}d\Omega \\
&+ \delta\Pi_{\mathrm{ext}}
\end{aligned}
\tag{3.28}
$$

The section stress resultants for a 3d beam element are defined as in Equation (3.5) and section stress resultants can be computed by taking integration over the section area, A as in Equation (3.8). If Equation (3.8) is substituted into Equation (3.28) and

the integration is carried out along the length, L of the beam, following expression is obtained;

$$
\begin{aligned}
\delta\Pi_{\mathrm{HW}} = & \int_0^L \{\delta\varepsilon_a(x)(\widehat{N}-N) + \delta\kappa_z(x)(\widehat{M}_z - M_z) \\
& \qquad + \delta\kappa_y(x)(\widehat{M}_y - M_y)\}d\mathrm{x} \\
& + \int_0^L \{\delta\gamma_y(x)(\widehat{V}_y - V_y) + \delta\gamma_z(x)(\widehat{V}_z - V_z) + \delta\varphi(x)(\widehat{T}-T)\}d\mathrm{x} \\
& + \int_0^L \{\delta N(u'(x) - \varepsilon_a(x)) + \delta M_z(\theta_z{}'(x) - \kappa_z(x)) \\
& \qquad + \delta M_y(\theta_y{}'(x) - \kappa_y(x))\}d\mathrm{x} \\
& + \int_0^L \{\delta V_y(v'(x) - \theta_z(x) - \gamma_y(x)) \\
& \qquad + \delta V_z(w'(x) + \theta_y(x) - \gamma_z(x)) \\
& \qquad + \delta T(\theta_x{}'(x) - \varphi(x))\}\,d\mathrm{x} \\
& + \int_0^L \{\delta u'(x)N + \delta\theta_z{}'(x)M_z + \delta\theta_y{}'(x)M_y\}d\mathrm{x} \\
& + \int_0^L \{(\delta v'(x) - \delta\theta_z(x))V_y + (\delta w'(x) + \delta\theta_y(x))V_z \\
& \qquad + \delta\theta_x{}'(x)T\}\,d\mathrm{x} \\
& + \delta\Pi_{\mathrm{ext}}
\end{aligned}
\tag{3.29}
$$

Where $\widehat{N}$, $\widehat{M}_y$, $\widehat{M}_z$, $\widehat{T}$, $\widehat{V}_y$ and $\widehat{V}_z$ are given below as Equation (3.30) and they are the section stress resultants such that the stress terms in Equation (3.8) are interchanged with the stresses, $\widehat{\sigma}_{xx}$, $\widehat{\sigma}_{xy}$ and $\widehat{\sigma}_{xz}$ that are satisfying the material constitutive relations.

$$\widehat{N} = \int_{A} \widehat{\sigma}_{xx} dA \qquad \widehat{M}_y = \int_{A} z\widehat{\sigma}_{xx} dA \qquad \widehat{M}_z = \int_{A} -y\widehat{\sigma}_{xx} dA$$

$$\widehat{V}_y = \int_{A} \widehat{\sigma}_{xy} dA \qquad \widehat{V}_z = \int_{A} \widehat{\sigma}_{xz} dA \qquad \widehat{T} = \int_{A} \left(-z\widehat{\sigma}_{xy} + y\widehat{\sigma}_{xz}\right) dA \tag{3.30}$$

The formulation enables the utilization of constitutive relation $\widehat{\boldsymbol{\sigma}} \equiv \widehat{\boldsymbol{\sigma}}(\boldsymbol{\varepsilon})$ in Equation (3.27) for various types of materials.

Π_{ext} in Equtation (3.29) can be defined as the variation of the work-conjugate of the displacement and stress resultant fields since it is the variation of external potential energy. If it is assumed that the body forces are zero so that they are eliminated from the variation of external potential, then;

$$\begin{aligned} \delta\Pi_{ext} \quad &= -\int_{0}^{L} \left\{\bar{n}(x)\delta u(x) + \bar{q}_y(x)\delta v(x) + \bar{q}_z(x)\delta w(x)\right\} dx \\ &- \int_{0}^{L} \left\{\bar{m}_x(x)\delta\theta_x(x) + \bar{m}_y(x)\delta\theta_y(x) + \bar{m}_z(x)\delta\theta_z(x)\right\} dx \\ &- \delta\Pi_{bc} \end{aligned} \tag{3.31}$$

Where $\bar{n}(x)$ and $\bar{q}_y(x)$, $\bar{q}_z(x)$, are distributions of longitudinal tractions and transverse tractions along *x*, *y* and *z* axes, respectively. $\bar{m}_x(x)$, $\bar{m}_y(x)$ and $\bar{m}_z(x)$ are moment tractions around *x*, *y* and *z* axes, respectively. Since in real structural engineering problems moment tractions around *y* and *z* axes are negligible, then $\bar{m}_y(x) = \bar{m}_z(x) = 0$ (See Figure 3.5) and Equation (3.31) becomes;

$$\delta\Pi_{\text{ext}} = -\int_0^L \{\bar{n}(x)\delta u(x) + \bar{q}_y(x)\delta v(x) + \bar{q}_z(x)\delta w(x) + \bar{m}_x(x)\delta\theta_x(x)\}dx \qquad (3.32)$$

$$-\delta\Pi_{\text{bc}}$$

Where $\delta\Pi_{\text{bc}}$ is the variation of the energy due to boundary conditions.

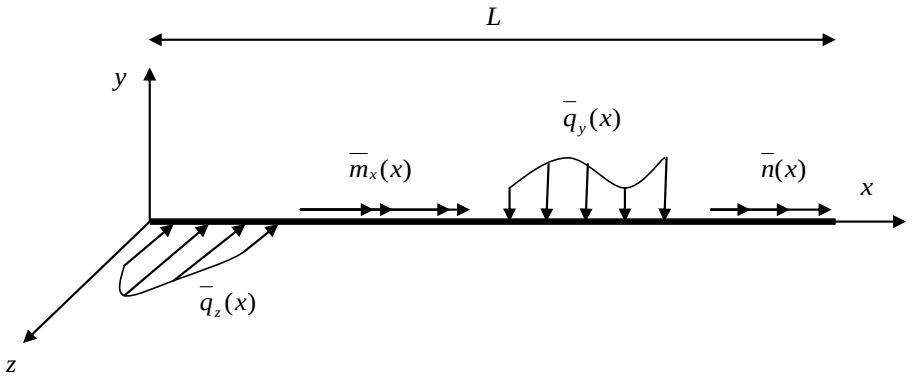

Figure 3.5. Assumed traction forces on beam element

3.6. FINITE ELEMENT APPROXIMATION

If Equation (3.32) is substituted into Equation (3.29) and a typical element of length *L* is considered for the finite element approximation, integration by parts of all terms with derivatives on the displacement fields in Equation (3.29) gives;

$$\int_0^L \{\delta N u'(x) + \delta u'(x) N - \delta u(x)\bar{n}(x)\}dx = \{\delta N u(x) + \delta u(x) N\}\Big|_0^L - \int_0^L \{\delta N' u(x) + \delta u(x)\big(N' + \bar{n}(x)\big)\}dx \tag{3.33}$$

$$\int_0^L \{\delta M_z \theta_z{}'(x) + \delta \theta_z{}'(x) M_z - \delta V_y \theta_z(x) - \delta \theta_z(x) V_y\}dx = \{\delta M_z \theta_z(x) + \delta \theta_z(x) M_z\}\Big|_0^L - \int_0^L \{\big(\delta M_z' + \delta V_y\big)\theta_z(x) + \delta \theta_z(x)\big(M_z' + V_y\big)\}dx \tag{3.34}$$

$$\int_0^L \{\delta M_y \theta_y{}'(x) + \delta \theta_y{}'(x) M_y + \delta V_z \theta_y(x) + \delta \theta_y(x) V_z\}dx = \{\delta M_y \theta_y(x) + \delta \theta_y(x) M_y\}\Big|_0^L - \int_0^L \{\big(\delta M_y' - \delta V_z\big)\theta_y(x) + \delta \theta_y(x)\big(M_y' - V_z\big)\}dx \tag{3.35}$$

$$\int_0^L \{\delta V_z w'(x) + \delta w'(x) V_z - \bar{q}_z(x)\delta w(x)\}dx = \{\delta V_z w(x) + \delta w(x) V_z\}\Big|_0^L - \int_0^L \{\delta V_z' w(x) + \delta w(x)\big(V_z' + \bar{q}_z(x)\big)\}dx \tag{3.36}$$

$$\int_0^L \{\delta V_y v'(x) + \delta v'(x) V_y - \bar{q}_y(x)\delta v(x)\}dx = \{\delta V_y w(x) + \delta v(x) V_y\}\Big|_0^L - \int_0^L \left\{\delta V_y' v(x) + \delta v(x)\left(V_y' + \bar{q}_y(x)\right)\right\} dx \tag{3.37}$$

$$\int_0^L \{\delta T\theta_x{}'(x) + \delta\theta_x'(x)T - \bar{m}_x(x)\delta\theta_x(x)\}dx = \{\delta T\theta_x(x) + \delta\theta_x(x)T\}\Big|_0^L - \int_0^L \{\delta T'\theta_x(x) + \delta\theta_x(x)(T' + \bar{m}_x(x))\}dx \tag{3.38}$$

A detailed review of Equation (3.33) to (3.38) arises the question whether it is possible to simplify the expressions in those equations. The answer to that question is positive if there can be found appropriate shape functions for section forces and their variations. If the approximation of the section forces and their variation satisfy the following conditions at the same time;

$$\begin{array}{lll} N'(x) + \bar{n}(x) = 0 & V_y'(x) + \bar{q}_y(x) = 0 & M_z'(x) + V_y(x) = 0 \\ T'(x) + \bar{m}_x(x) = 0 & V_z'(x) + \bar{q}_z(x) = 0 & M_y'(x) - V_z(x) = 0 \end{array} \tag{3.39}$$

and

$$\begin{array}{lll} \delta N'(x) = 0 & \delta V_y'(x) = 0 & \delta M_z'(x) + \delta V_y(x) = 0 \\ \delta T'(x) = 0 & \delta V_z'(x) = 0 & \delta M_y'(x) - \delta V_z(x) = 0 \end{array} \tag{3.40}$$

Then the integral terms on the right hand sides of Equations (3.33) to (3.38) vanish and it becomes unnecessary to approximate the displacements u, v, w, θ_x , θ_y and θ_z

along the beam. Displacement values at the end nodes are enough for carrying out definite integrals in those equations. Derivation of approximation functions for section forces and their variation are summarized in the following part.

For $N'(x) + \bar{n}(x) = 0$

Assuming uniform axial traction, $\bar{n}(x) = w_x$ is constant along the whole beam length;

$$N'(x) + w_x = 0 \Longrightarrow N(x) = -w_x x + C$$

Where C is the integration constant.

$N(0) = -w_x.0 + C \Longrightarrow\ C = N(0) = q_1 + w_x L$ (See Figure 3.6)

$N(x) + w_x x - (q_1 + w_x L) = 0$

$$N(x) = q_1 + w_x(L - x) \tag{3.41}$$

and

$$\delta N(x) = \delta q_1 \tag{3.42}$$

a.

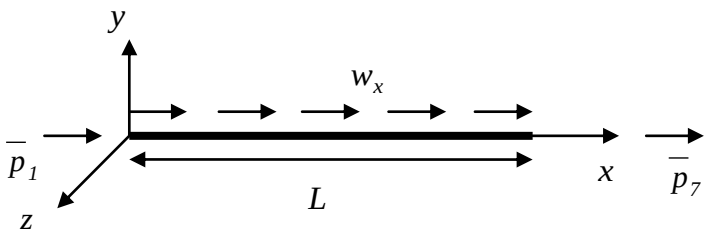

Complete System

b.

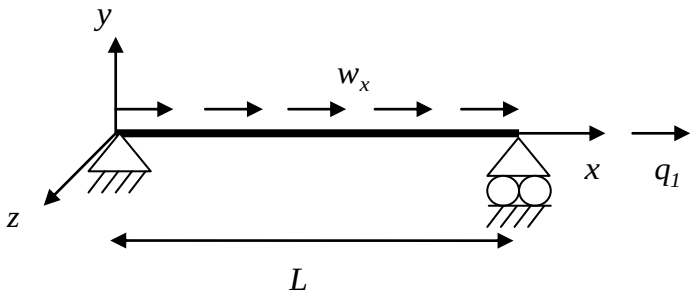

Basic System

c.

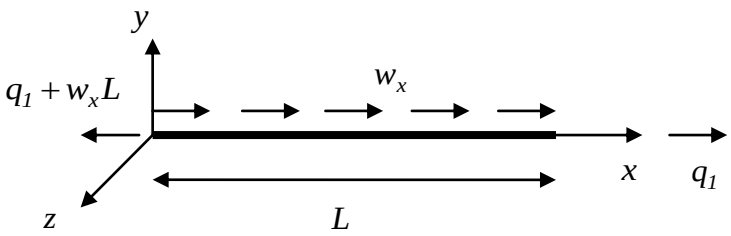

Free Body of Basic System

d.

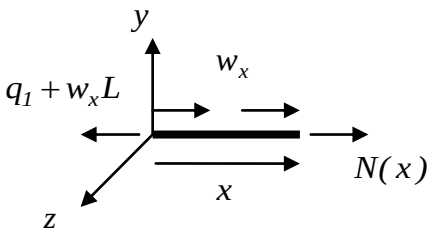

Section Cut from Free Body of Basic System

Figure 3.6. Element forces for uniform axial traction

For $M_z'(x) + V_y(x) = 0$ and $V_y'(x) + \bar{q}_y(x) = 0$

Assuming uniform transverse traction, $\bar{q}_y(x) = w_y$ is constant along the whole beam length;

$$V_y'(x) + w_y = 0 \Longrightarrow V_y(x) = -w_y x + C_1$$

$$M_z'(x) - w_y x + C_1 = 0 \Longrightarrow M_z(x) = \frac{1}{2} w_y x^2 - C_1 x + C_2$$

Where C_1 and C_2 are integration constants.

According to the Figure 3.7.d;

$$\Sigma M_{right} = 0$$

$$M_z(x) + q_2 - w_y \frac{x^2}{2} + w_y \frac{L}{2} x - \frac{q_2 + q_3}{L} x = 0$$

$$M_z(x) = \left(\frac{x}{L} - 1\right) q_2 + \frac{x}{L} q_3 + \frac{L^2}{2}\left[\left(\frac{x}{L}\right)^2 - \frac{x}{L}\right] w_y \tag{3.43}$$

and

$$\delta M_z(x) = \left(\frac{x}{L} - 1\right) \delta q_2 + \frac{x}{L} \delta q_3 \tag{3.44}$$

$$\Sigma F_y = 0$$

$$V_y(x) + w_y x - w_y \frac{L}{2} + \frac{q_2 + q_3}{L} = 0$$

$$V_y(x) = -\frac{1}{L} q_2 - \frac{1}{L} q_3 + \frac{L}{2}\left[1 - \frac{2x}{L}\right] w_y \tag{3.45}$$

and

$$\delta V_y(x) = -\frac{1}{L} \delta q_2 - \frac{1}{L} \delta q_3 \tag{3.46}$$

a.

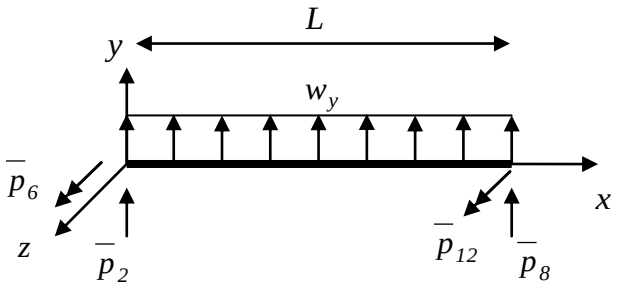

Complete System

b.

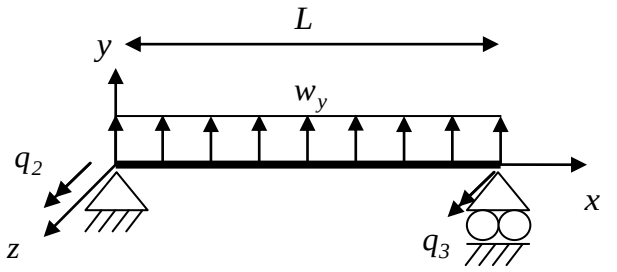

Basic System

c.

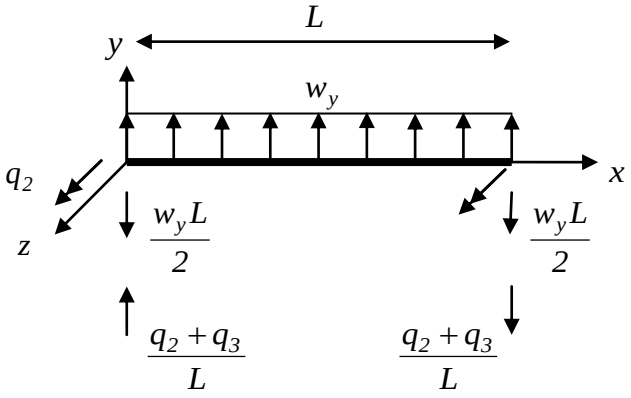

Free Body of Basic System

d.

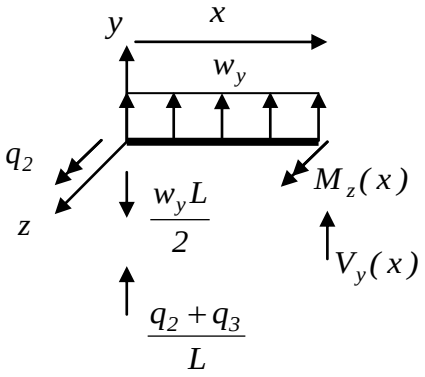

Section Cut from Free Body of Basic System

Figure 3.7. Element forces for uniform transverse traction in y direction

For $M_y'(x) - V_z(x) = 0$ and $V_z'(x) + \bar{q}_z(x) = 0$

Assuming uniform transverse traction, $\bar{q}_z(x) = w_z$ is constant along the whole beam length;

a.

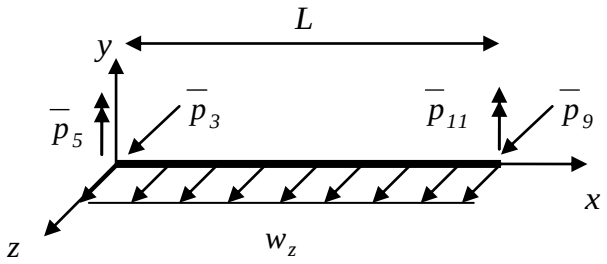

Complete System

b.

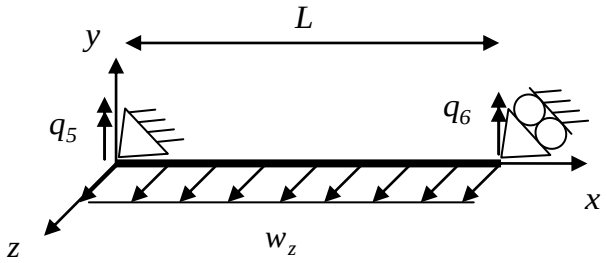

Basic System

c.

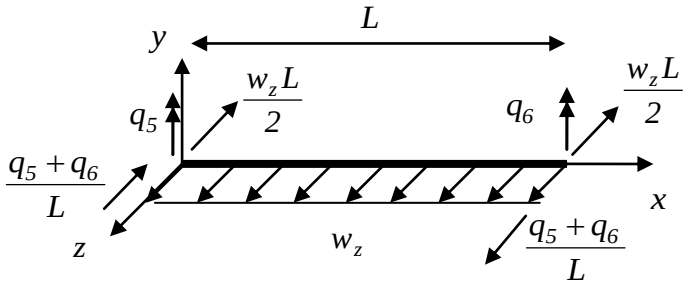

Free Body of Basic System

d.

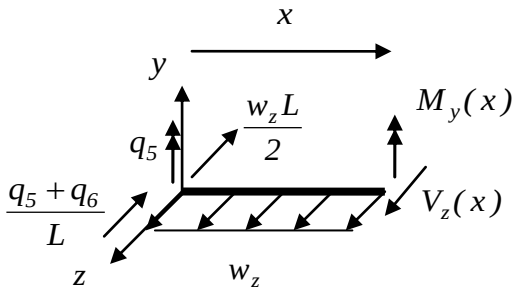

Section Cut from Free Body of Basic System

Figure 3.8. Element forces for uniform transverse traction in z direction

According to the Figure 3.8.d;

$$\Sigma M_{right} = 0$$

$$M_y(x) + q_5 - w_z \frac{L}{2} x - \frac{q_5 + q_6}{L} x + w_z \frac{x^2}{2} = 0$$

$$M_y(x) = \left(\frac{x}{L} - 1\right) q_5 + \frac{x}{L} q_6 + \frac{L^2}{2}\left[-\left(\frac{x}{L}\right)^2 + \frac{x}{L}\right] w_z \tag{3.47}$$

and

$$\delta M_y(x) = \left(\frac{x}{L} - 1\right) \delta q_5 + \frac{x}{L} \delta q_6 \tag{3.48}$$

$$\Sigma F_z = 0$$

$$V_z(x) + w_z x - \frac{q_5 + q_6}{L} - w_z \frac{L}{2} = 0$$

$$V_z(x) = \frac{1}{L} q_5 + \frac{1}{L} q_6 + \frac{L}{2}\left[1 - \frac{2x}{L}\right] w_z \tag{3.49}$$

and

$$\delta V_z(x) = \frac{1}{L} \delta q_5 + \frac{1}{L} \delta q_6 \tag{3.50}$$

For $T'(x) + \bar{m}_x(x) = 0$, the situation is similar to the case for the uniform axial traction. Therefore, assuming $\bar{m}_x(x) = m_x$ is constant along the beam length and switching q_1 with q_4;

$$T(x) = q_4 + m_x(L - x) \tag{3.51}$$

and

$$\delta T(x) = \delta q_4 \tag{3.52}$$

By using Equations (3.41) to (3.52), Equation sets (3.39) and (3.40) can be validated. If constant axial and transverse tractions are assumed along the beam element and Equations (3.41) to (3.52) are used, Equation (3.4) becomes;

$$\boldsymbol{s}(x) = \boldsymbol{b}(x)\boldsymbol{q} + \boldsymbol{s_p}(x) \tag{3.53}$$

Where $\boldsymbol{q}$ and $\boldsymbol{b}(x)$ are already given in Equations (3.6) and (3.7), respectively. $\boldsymbol{s_p}(x)$ is the section stress resultants due to element loading, $\boldsymbol{w}$ found as,

$$\boldsymbol{s_p}(x) = \begin{bmatrix} L\left(1-\frac{x}{L}\right) & 0 & 0 & 0 \\ 0 & \frac{L^2}{2}\left(\left(\frac{x}{L}\right)^2 - \frac{x}{L}\right) & 0 & 0 \\ 0 & 0 & \frac{L^2}{2}\left(\left(-\frac{x}{L}\right)^2 + \frac{x}{L}\right) & 0 \\ 0 & \frac{L}{2}\left(1-\frac{2x}{L}\right) & 0 & 0 \\ 0 & 0 & L\left(1-\frac{2x}{L}\right) & 0 \\ 0 & 0 & 0 & L\left(1-\frac{x}{L}\right) \end{bmatrix} \begin{Bmatrix} w_x \\ w_y \\ w_z \\ m_x \end{Bmatrix} \tag{3.54}$$

The variation of section stress resultants is;

$$\delta\boldsymbol{s}(x) = \boldsymbol{b}(x)\delta\boldsymbol{q} \tag{3.55}$$

Boundary Terms

If the first expression on the right hand side of Equation (3.33) is evaluated as follows;

$$\{\delta N u(x) + \delta u(x) N\}\Big|_0^L = \delta N(L)u(L) - \delta N(0)u(0) + N(L)\delta u(L) - N(0)\delta u(0) \qquad (3.56)$$

According to Equations (3.41) and (3.42) and Figure 3.9;

$$\begin{array}{llll} \delta N(0) = \delta q_1 & \delta N(L) = \delta q_1 & N(0) = q_1 + w_x L & N(L) = q_1 \\ u(0) = \bar{u}_1 & u(L) = \bar{u}_7 & \delta u(0) = \delta \bar{u}_1 & \delta u(L) = \delta \bar{u}_7 \end{array} \qquad (3.57)$$

Then Equation (3.56) becomes;

$$\{\delta N u(x) + \delta u(x) N\}\Big|_0^L = \delta q_1(\bar{u}_7 - \bar{u}_1) + q_1(\delta \bar{u}_7 - \delta \bar{u}_1) - w_x L \delta \bar{u}_1 \qquad (3.58)$$

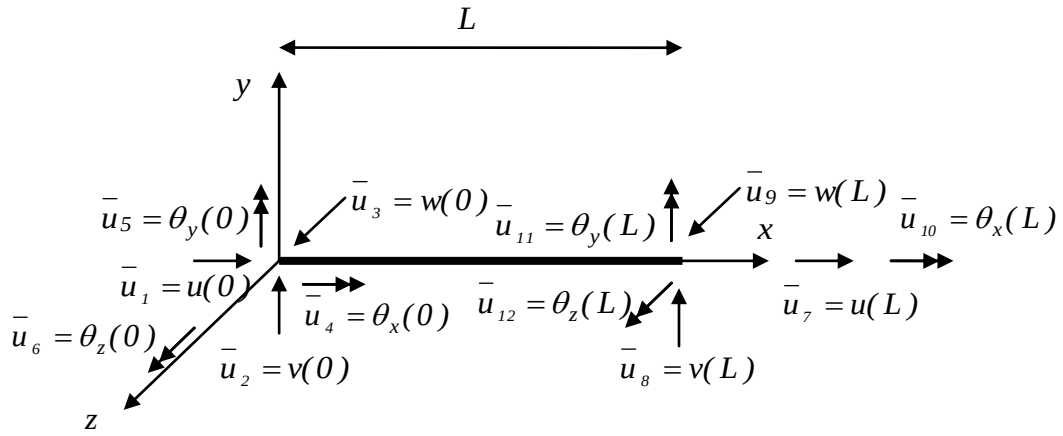

Figure 3.9. Nodal displacements for an element

If the first expression on the right hand side of Equation (3.34) is evaluated as follows;

$$\{\delta M_z\theta_z(x) + \delta\theta_z(x)M_z\}\Big|_0^L = \begin{array}{l}\delta M_z(L)\theta_z(L) - \delta M_z(0)\theta_z(0) \\ +M_z(L)\delta\theta_z(L) - M_z(0)\delta\theta_z(0)\end{array} \tag{3.59}$$

According to Equations (3.43) and (3.44) and Figure 3.9;

$$\begin{array}{llll}\delta M_z(0) = -\delta q_2 & \delta M_z(L) = \delta q_3 & M_z(0) = -q_2 & M_z(L) = q_3 \\ \theta_z(0) = \bar{u}_6 & \theta_z(L) = \bar{u}_{12} & \delta\theta_z(0) = \delta\bar{u}_6 & \delta\theta_z(L) = \delta\bar{u}_{12}\end{array} \tag{3.60}$$

then Equation (3.59) becomes;

$$\{\delta M_z\theta_z(x) + \delta\theta_z(x)M_z\}\Big|_0^L = \delta q_3\bar{u}_{12} + \ \delta q_2\bar{u}_6 + q_3\delta\bar{u}_{12} + q_2\delta\bar{u}_6 \tag{3.61}$$

If the first expression on the right hand side of Equation (3.35) is evaluated as follows;

$$\{\delta M_y\theta_y(x) + \delta\theta_y(x)M_y\}\Big|_0^L = \begin{array}{l}\delta M_y(L)\theta_y(L) - \delta M_y(0)\theta_y(0) \\ +M_y(L)\delta\theta_y(L) - M_y(0)\delta\theta_y(0)\end{array} \tag{3.62}$$

According to Equations (3.47) and (3.48) and Figure 3.9;

$$\begin{array}{llll}\delta M_y(0) = -\delta q_5 & \delta M_y(L) = \delta q_6 & M_y(0) = -q_5 & M_y(L) = q_6 \\ \theta_y(0) = \bar{u}_5 & \theta_y(L) = \bar{u}_{11} & \delta\theta_y(0) = \delta\bar{u}_5 & \delta\theta_y(L) = \delta\bar{u}_{11}\end{array} \tag{3.63}$$

then Equation (3.62) becomes;

$$\{\delta M_y \theta_y(x) + \delta\theta_y(x) M_y\}\Big|_0^L = \delta q_6 \bar{u}_{11} + \delta q_5 \bar{u}_5 + q_6 \delta \bar{u}_{11} + q_5 \delta \bar{u}_5 \tag{3.64}$$

If the first expression on the right hand side of Equation (3.36) is evaluated as follows;

$$\begin{aligned}\{\delta V_z w(x) + \delta w(x) V_z\}\Big|_0^L = \quad & \delta V_z(L) w(L) - \delta V_z(0) w(0) \\ & + V_z(L)\delta w(L) \quad - V_z(0)\delta w(0)\end{aligned} \tag{3.65}$$

According to Equations (3.49) and (3.50) and Figure 3.9;

$$\begin{aligned}&\delta V_z(0) = \frac{1}{L}(\delta q_5 + \delta q_6) && \delta V_z(L) = \frac{1}{L}(\delta q_5 + \delta q_6) \\ &V_z(0) = \frac{1}{L}(q_5 + q_6) + w_z\frac{L}{2} && V_z(L) = \frac{1}{L}(q_5 + q_6) - w_z\frac{L}{2} \\ &w(0) = \bar{u}_3 \qquad w(L) = \bar{u}_9 && \delta w(0) = \delta\bar{u}_3 \qquad \delta w(L) = \delta\bar{u}_9\end{aligned} \tag{3.66}$$

Then Equation (3.65) becomes;

$$\begin{aligned}\{\delta V_z w(x) + \delta w(x) V_z\}\Big|_0^L = \quad & \frac{1}{L}(\delta q_5 + \delta q_6)(\bar{u}_9 - \bar{u}_3) \\ & + \frac{1}{L}(q_5 + q_6)(\delta\bar{u}_9 - \delta\bar{u}_3) \\ & - w_z\frac{L}{2}(\delta\bar{u}_3 + \delta\bar{u}_9)\end{aligned} \tag{3.67}$$

If the first expression on the right hand side of Equation (3.37) is evaluated as follows;

$$\{\delta V_y v(x) + \delta v(x) V_y\}\Big|_0^L = \quad \delta V_y(L)v(L) - \delta V_y(0)v(0) + V_y(L)\delta v(L) - V_y(0)\delta w(0) \tag{3.68}$$

According to Equations (3.45) and (3.46) and Figure 3.9;

$$\begin{aligned} &\delta V_y(0) = -\frac{1}{L}(\delta q_2 + \delta q_3) && \delta V_y(L) = -\frac{1}{L}(\delta q_2 + \delta q_3) \\ &V_y(0) = -\frac{1}{L}(q_2 + q_3) + w_y\frac{L}{2} && V_y(L) = -\frac{1}{L}(q_5 + q_6) - w_y\frac{L}{2} \\ &v(0) = \bar{u}_2 \qquad v(L) = \bar{u}_8 && \delta v(0) = \delta\bar{u}_2 \qquad \delta v(L) = \delta\bar{u}_8 \end{aligned} \tag{3.69}$$

then Equation (3.68) becomes;

$$\begin{aligned} \{\delta V_y v(x) + \delta v(x) V_y\}\Big|_0^L = &\frac{1}{L}(\delta q_2 + \delta q_3)(\bar{u}_2 - \bar{u}_8) \\ &+ \frac{1}{L}(q_2 + q_3)(\delta\bar{u}_2 - \delta\bar{u}_8) - w_y\frac{L}{2}(\delta\bar{u}_2 + \delta\bar{u}_8) \end{aligned} \tag{3.70}$$

The case for the torsion component is similar to the case for the axial component. Therefore the first expression on the right hand side of Equation (3.38) is as follows;

$$\{\delta T\theta_x(x) + \delta\theta_x(x)T\}\Big|_0^L = \delta q_4(\bar{u}_{10} - \bar{u}_4) + q_4(\delta\bar{u}_{10} - \delta\bar{u}_4) - m_x L\delta\bar{u}_4 \tag{3.71}$$

Equations (3.58), (3.61), (3.64), (3.67), (3.70) and (3.71) can be grouped as follows;

$$
\begin{aligned}
&\{\delta N u(x) + \delta u(x) N\}\Big|_0^L + \\
&\{\delta M_z \theta_z(x) + \delta \theta_z(x) M_z\}\Big|_0^L + \\
&\{\delta M_y \theta_y(x) + \delta \theta_y(x) M_y\}\Big|_0^L + \\
&\{\delta V_z w(x) + \delta w(x) V_z\}\Big|_0^L + \\
&\{\delta V_y v(x) + \delta v(x) V_y\}\Big|_0^L + \\
&\{\delta T \theta_x(x) + \delta \theta_x(x) T\}\Big|_0^L
\end{aligned}
= \delta \boldsymbol{q}^{\mathrm{T}} \boldsymbol{a} \bar{\boldsymbol{u}} + \delta \bar{\boldsymbol{u}}^{\mathrm{T}} \boldsymbol{a}^{\mathrm{T}} \boldsymbol{q} - \delta \bar{\boldsymbol{u}}^{\mathrm{T}} \boldsymbol{p}_w \tag{3.72}
$$

Where $\boldsymbol{p_w}$ is the rigid mode of applied tractions at the nodes and defined as;

$$
\boldsymbol{p_w} = \begin{pmatrix} w_x L & w_y \frac{L}{2} & w_z \frac{L}{2} & m_x L & 0 & 0 & 0 & w_y \frac{L}{2} & w_z \frac{L}{2} & 0 & 0 & 0 \end{pmatrix} \tag{3.73}
$$

Equation (3.29) can be rearranged by utilizing Equations (3.6), (3.7), (3.53), (3.54), (3.72) and (3.73) as follows;

$$
\begin{aligned}
\delta \Pi_{\mathrm{HW}} = & \int_0^L \delta \boldsymbol{e}(x)^{\mathrm{T}} \big(\hat{\boldsymbol{s}}(x) - \boldsymbol{b}(x) \boldsymbol{q} - \boldsymbol{s_p}(x)\big) dx - \\
& \delta \boldsymbol{q}^{\mathrm{T}} \int_0^L \boldsymbol{b}(x)^{\mathrm{T}} \boldsymbol{e}(x)\, dx + \delta \boldsymbol{q}^{\mathrm{T}} \boldsymbol{a} \bar{\boldsymbol{u}} + \delta \bar{\boldsymbol{u}}^{\mathrm{T}} \boldsymbol{a}^{\mathrm{T}} \boldsymbol{q} - \delta \bar{\boldsymbol{u}}^{\mathrm{T}} \boldsymbol{p_w} - \delta \Pi_{\mathrm{bc}}
\end{aligned} \tag{3.74}
$$

$\delta \Pi_{\mathrm{bc}}$ can be ignored until the assembly of the elements and the Equation (3.74) can be written in terms of global displacements by using Equations (3.14) and (3.19) for the element as follows;

$$\delta\Pi_{\mathrm{HW}} = \int_0^L \delta \boldsymbol{e}(x)^{\mathrm{T}}\left(\hat{\boldsymbol{s}}(x) - \boldsymbol{b}(x)\boldsymbol{q} - \boldsymbol{s_p}(x)\right)dx - \delta \boldsymbol{q}^T \int_0^L \boldsymbol{b}(x)^{\mathrm{T}}\boldsymbol{e}(x)\,dx + \delta \boldsymbol{q}^{\mathrm{T}}\boldsymbol{a}_{\mathrm{g}}\boldsymbol{u_{el}} + \delta \boldsymbol{u_{el}}^{\mathrm{T}}\boldsymbol{a}_{\mathrm{g}}{}^{\mathrm{T}}\boldsymbol{q} - \delta \boldsymbol{u_{el}}^{\mathrm{T}}\boldsymbol{a_r}{}^{\mathrm{T}}\boldsymbol{p_w} \tag{3.75}$$

3.7. LINEARIZATION OF THE NONLINEAR EQUATION

Equation (3.75) can be minimized by equating the expression to zero. That form of the equation will be generally nonlinear and can be linearly approximated to find the root of solution by using first order Taylor Series expansion as follows;

$$\begin{aligned} 0 \cong \delta\Pi_{\mathrm{HW}}\left(\boldsymbol{u_{el}}, \boldsymbol{q}, \boldsymbol{e}(x)\right) = \quad & \delta\Pi_{\mathrm{HW}}\left(\boldsymbol{u_{el}}^i, \boldsymbol{q}^i, \boldsymbol{e}(x)^i\right) \\ & + \frac{\partial \delta\Pi_{\mathrm{HW}}\left(\boldsymbol{u_{el}}^i, \boldsymbol{q}^i, \boldsymbol{e}(x)^i\right)}{\partial \boldsymbol{u_{el}}}\Big|_i \Delta \boldsymbol{u_{el}} \\ & + \frac{\partial \delta\Pi_{\mathrm{HW}}\left(\boldsymbol{u_{el}}^i, \boldsymbol{q}^i, \boldsymbol{e}(x)^i\right)}{\partial \boldsymbol{q}}\Big|_i \Delta \boldsymbol{q} \\ & + \frac{\partial \delta\Pi_{\mathrm{HW}}\left(\boldsymbol{u_{el}}^i, \boldsymbol{q}^i, \boldsymbol{e}(x)^i\right)}{\partial \boldsymbol{e}(x)}\Big|_i \Delta \boldsymbol{e}(x) \end{aligned} \tag{3.76}$$

Where i denotes the last converged values of the variables.

According to Equation (3.75);

$$\frac{\partial \delta \Pi_{\mathrm{HW}}\left(\boldsymbol{u_{el}}, \boldsymbol{q}, \boldsymbol{e}(x)\right)}{\partial \boldsymbol{u_{el}}} = \delta \boldsymbol{q}^{\mathrm{T}} \boldsymbol{a}_{\mathrm{g}} \tag{3.77}$$

$$\frac{\partial \delta \Pi_{\mathrm{HW}}\left(\boldsymbol{u_{el}}, \boldsymbol{q}, \boldsymbol{e}(x)\right)}{\partial \boldsymbol{q}} = -\int_0^L \delta \boldsymbol{e}(x)^{\mathrm{T}} \boldsymbol{b}(x) dx + \delta \boldsymbol{u_{el}}^{\mathrm{T}} \boldsymbol{a_{\mathrm{g}}}^{\mathrm{T}} \tag{3.78}$$

$$\frac{\partial \delta \Pi_{\mathrm{HW}}\left(\boldsymbol{u_{el}}, \boldsymbol{q}, \boldsymbol{e}(x)\right)}{\partial \boldsymbol{e}(x)} = \int_0^L \delta \boldsymbol{e}(x)^{\mathrm{T}} \boldsymbol{k_{\mathrm{s}}}(x) dx - \delta \boldsymbol{q}^{\mathrm{T}} \int_0^L \boldsymbol{b}(x)^{\mathrm{T}} dx \tag{3.79}$$

And tangent stiffness of the section is given as;

$$\boldsymbol{k_s}(x) = \frac{\partial \hat{\boldsymbol{s}}(x)}{\partial \boldsymbol{e}(x)} \tag{3.80}$$

If Equations (3.77), (3.78) and (3.79) are substituted into Equation (3.76) and similar terms are grouped together following expression is obtained;

$$\begin{aligned} 0 = & \int_0^L \delta \boldsymbol{e}(x)^{\mathrm{T}} \left[\hat{\boldsymbol{s}}(x) - \boldsymbol{b}(x)(\boldsymbol{q} + \Delta \boldsymbol{q}) - \boldsymbol{s_p}(x) + \boldsymbol{k_s}(x) \Delta \boldsymbol{e}(x)\right] dx \\ & + \delta \boldsymbol{q}^T \left[\int_0^L -\boldsymbol{b}(x)^{\mathrm{T}} \left(\boldsymbol{e}(x) + \Delta \boldsymbol{e}(x)\right) dx + \boldsymbol{a}_{\mathrm{g}}(\boldsymbol{u_{el}} + \Delta \boldsymbol{u_{el}})\right] \\ & + \delta \boldsymbol{u_{el}}^{\mathrm{T}} \left[\boldsymbol{a_{\mathrm{g}}}^{\mathrm{T}}(\boldsymbol{q} + \Delta \boldsymbol{q}) - \boldsymbol{a_r}^{\mathrm{T}} \boldsymbol{p_{\mathrm{w}}}\right] \end{aligned} \tag{3.81}$$

It should be noted that three fields of the formulation are disassembled in Equation (3.81). Basic element forces and section deformations are internal variables which do not need to fulfill inter-element continuity requirements. Additionally, displacement field does not have to satisfy continuity requirements along member span except at the inter-element nodes. In order to ensure that Equation (3.81) is satisfied for all arbitrary values of $\delta \boldsymbol{u_{el}}$, $\delta \boldsymbol{q}$, and $\delta \boldsymbol{e}(x)$, all values that are multiplied with these terms should vanish for all equation to be equal to zero at all times as follows;

$$\boldsymbol{a}_{\mathrm{g}}{}^{\mathrm{T}}(\boldsymbol{q}+\Delta\boldsymbol{q}) - \boldsymbol{a_r}{}^{\mathrm{T}}\boldsymbol{p}_{\mathbf{w}} = 0 \tag{3.82}$$

$$\int_0^L -\boldsymbol{b}(x)^{\mathrm{T}}\big(\boldsymbol{e}(x)+\Delta\boldsymbol{e}(x)\big)\,dx + \boldsymbol{a}_{\mathrm{g}}(\boldsymbol{u_{el}}+\Delta\boldsymbol{u_{el}}) = 0 \tag{3.83}$$

$$\int_0^L \big[\hat{\boldsymbol{s}}(x) - \boldsymbol{b}(x)(\boldsymbol{q}+\Delta\boldsymbol{q}) - \boldsymbol{s_p}(x) + \boldsymbol{k_s}(x)\Delta\boldsymbol{e}(x)\big]dx = 0 \tag{3.84}$$

Equations (3.83) and (3.84) can be rearranged as follows;

$$\int_0^L -\boldsymbol{b}(x)^{\mathrm{T}}\boldsymbol{e}(x)dx - \int_0^L \boldsymbol{b}(x)^{\mathrm{T}}\boldsymbol{k_s}{}^{-1}(x)\boldsymbol{k_s}(x)\Delta\boldsymbol{e}(x)dx + \boldsymbol{a}_{\mathrm{g}}(\boldsymbol{u_{el}}+\Delta\boldsymbol{u_{el}}) = 0 \tag{3.85}$$

$$\int_0^L \boldsymbol{k_s}(x)\Delta\boldsymbol{e}(x)dx = \int_0^L \big[\boldsymbol{b}(x)(\boldsymbol{q}+\Delta\boldsymbol{q}) + \boldsymbol{s_p}(x) - \hat{\boldsymbol{s}}(x)\big]dx \tag{3.86}$$

Equation (3.86) can be substituted into Equation (3.85) as follows;

$$\begin{aligned} 0 = \quad & \int_0^L -\boldsymbol{b}(x)^{\mathrm{T}}\boldsymbol{e}(x)dx - \int_0^L \boldsymbol{b}(x)^{\mathrm{T}}\boldsymbol{k_s}{}^{-1}(x)\big[\boldsymbol{b}(x)(\boldsymbol{q}+\Delta\boldsymbol{q}) + \boldsymbol{s_p}(x) - \hat{\boldsymbol{s}}(x)\big]dx \\ & + \boldsymbol{a}_{\mathrm{g}}(\boldsymbol{u_{el}}+\Delta\boldsymbol{u_{el}}) \end{aligned} \tag{3.87}$$

Equation (3.87) can be further rearranged as follows;

$$0 = \int_0^L -\boldsymbol{b}(x)^{\mathrm{T}}\boldsymbol{e}(x)dx - \int_0^L \boldsymbol{b}(x)^{\mathrm{T}}\boldsymbol{k_s}^{-1}(x)\boldsymbol{b}(x)\Delta\boldsymbol{q}dx - \int_0^L \boldsymbol{b}(x)^{\mathrm{T}}\boldsymbol{k_s}^{-1}(x)\left(\boldsymbol{b}(x)\boldsymbol{q} + \boldsymbol{s_p}(x) - \hat{\boldsymbol{s}}(x)\right)dx + \boldsymbol{a}_{\mathrm{g}}(\boldsymbol{u_{el}} + \Delta\boldsymbol{u_{el}}) \tag{3.88}$$

Where $\boldsymbol{k_s}^{-1}(x) = \boldsymbol{f_s}(x)$ is section flexibility matrix, and element flexibility matrix in basic system, $\boldsymbol{f}$ can be found as follows;

$$\boldsymbol{f} = \int_0^L \boldsymbol{b}(x)^{\mathrm{T}}\boldsymbol{k_s}^{-1}(x)\boldsymbol{b}(x)dx \tag{3.89}$$

Equation (3.88) can be rearranged by using Equations (3.53) and (3.89) as follows;

$$0 = -\boldsymbol{f}\Delta\boldsymbol{q} - \int_0^L \boldsymbol{b}(x)^{\mathrm{T}}\boldsymbol{e}(x)dx - \int_0^L \boldsymbol{b}(x)^{\mathrm{T}}\boldsymbol{k_s}^{-1}(x)\big(\boldsymbol{s}(x) - \hat{\boldsymbol{s}}(x)\big)dx + \boldsymbol{a}_{\mathrm{g}}(\boldsymbol{u_{el}} + \Delta\boldsymbol{u_{el}}) \tag{3.90}$$

Section force residual, $\boldsymbol{s}_{\mathrm{r}}(x)$ can be defined as follows;

$$\boldsymbol{s_r}(x) = \big(\boldsymbol{s}(x) - \hat{\boldsymbol{s}}(x)\big) \tag{3.91}$$

And section deformation residual, $\boldsymbol{e}_{\mathrm{r}}(x)$ can be defined as follows;

$$\boldsymbol{e_r}(x) = \boldsymbol{k_s}^{-1}(x)\boldsymbol{s_r}(x) \tag{3.92}$$

Equation (3.90) can be rearranged by using Equation (3.92) as follows;

$$\boldsymbol{f}\Delta\boldsymbol{q} = \boldsymbol{a}_{\mathrm{g}}\Delta\boldsymbol{u_{el}} + \boldsymbol{a}_{\mathrm{g}}\boldsymbol{u_{el}} - \int_0^L \boldsymbol{b}(x)^{\mathrm{T}}\big(\boldsymbol{e}(x) + \boldsymbol{e_r}(x)\big)dx \tag{3.93}$$

Resisting element deformation, $\hat{\mathbf{v}}$ can be defined as follows;

$$\hat{\mathbf{v}} = \int_0^L \boldsymbol{b}(x)^{\mathrm{T}}\big(\boldsymbol{e}(x) + \boldsymbol{e_r}(x)\big)dx \tag{3.94}$$

Equations (3.19) and (3.94) can be substituted into Equation (3.93) and the expression can be rearranged as follows;

$$\Delta\boldsymbol{q} = \boldsymbol{f}^{-1}\big(\boldsymbol{a}_{\mathrm{g}}\Delta\boldsymbol{u_{el}} + \mathbf{v} - \hat{\mathbf{v}}\big) \tag{3.95}$$

Residual element deformation, $\mathbf{v_r}$ can be defined as follows;

$$\mathbf{v_r} = -\mathbf{v} + \hat{\mathbf{v}} \tag{3.96}$$

If Equation (3.96) is substituted into Equation (3.95) and the resulting expression is substituted into Equation (3.82);

$$\boldsymbol{a}_{\mathrm{g}}{}^{\mathrm{T}}\boldsymbol{f}^{-1}\boldsymbol{a}_{\mathrm{g}}\Delta\boldsymbol{u_{el}} = \boldsymbol{a_r}{}^{\mathrm{T}}\boldsymbol{p_w} - \boldsymbol{a}_{\mathrm{g}}{}^{\mathrm{T}}(\boldsymbol{q} - \boldsymbol{f}^{-1}\mathbf{v_r}) \tag{3.97}$$

Where element stiffness in global coordinates, $\boldsymbol{k_{el}}$ is given by;

$$\boldsymbol{k_{el}} = \boldsymbol{a}_{\mathrm{g}}{}^{\mathrm{T}} \boldsymbol{f}^{-1} \boldsymbol{a}_{\mathrm{g}} \tag{3.98}$$

If Equation (3.98) is substituted into Equation (3.97);

$$\boldsymbol{k_{el}} \Delta \boldsymbol{u_{el}} = \boldsymbol{a_r}{}^{\mathrm{T}} \boldsymbol{p_w} - \boldsymbol{a}_{\mathrm{g}}{}^{\mathrm{T}} (\boldsymbol{q} - \boldsymbol{f}^{-1} \mathbf{v}_r) \tag{3.99}$$

The procedure presented up to now tries to condense out all internal variables other than nodal displacements by keeping them as internal parameters to the element only. By this way, it is possible to implement the condensed reponse of the element to a standard finite element software that uses nodal displacement values in the solution of structural systems. Since the procedure includes condensation, it becomes easier to compute the structure stiffness matrix which in turn results in increased computational efficiency. Therefore, this solution scheme is opted for numerical validation studies presented in the following parts. There are studies that explain the condensation procedure of the element variables in matrix form and the corresponding solution algorithms in detail [17, 48]. Anyhow, the resulting form of the equation for the whole structural system is the renowned expression given as follows;

$$\mathbf{K} \Delta \mathbf{U} = \mathbf{P} - \mathbf{P_R} \tag{3.100}$$

In Equation (3.100), **K** is the stiffness matrix, **U** is the displacement vector, **P** is the applied force vector and $\mathbf{P_R}$ is the resisting force vector of the structure and those parameters are computed by assemblage of the responses of each elements per member span. Nonlinear analysis of this configuration of the expression necessitates an iterative process.

3.8. FIBER DISCRETIZATION OF SECTION RESPONSE

The proposed 3d mixed beam element, derivation of which is given in the previous sections possesses a general form in terms of accommodating linear or nonlinear material response. Therefore, the proposed mixed element is eligible for the nonlinear analysis of 3d structural systems composed of beam type elements having any sort of cross-section. Nevertheless, the section geometry of the members utilized in the nonlinear analysis presented in the subsequent parts are solid and hollow circular sections. Because, that kind of sections has a wide range of application area both at micro and macro levels from past to present such as historical pillars, nanotubes, machinery parts, pier of a deck, towers of wind turbines and antenna towers, pile foundations, pipelines, tunnels, etc. Moreover, it is easier to compare the results obtained by nonlinear analysis of the member composed of 3d mixed element that have circular cross section with closed form solutions that are readily available in the literature. Therefore, section modeling of the 3d mixed beam element is performed by using following expressions.

The relationship between the strains at a fiber point on the beam cross-section and the section deformations is given in Equation (3.26). This equation can be written in an alternative way by defining section compatibility matrix, $\boldsymbol{a_s}$ as follows;

$$\boldsymbol{a_s} = \begin{bmatrix} 1 & -y & z & 0 & 0 & 0 \\ 0 & 0 & 0 & \sqrt{k_y} & 0 & -z \\ 0 & 0 & 0 & 0 & \sqrt{k_z} & y \end{bmatrix} \tag{3.101}$$

$$\boldsymbol{\varepsilon} = (\varepsilon_{xx} \quad \gamma_{xy} \quad \gamma_{xz})^{\mathrm{T}} = \boldsymbol{a_s e}(x) \tag{3.102}$$

In Equation (3.102), $\boldsymbol{e}(x)$ is the same with the one given in Equation (3.11). In Equation (3.101), k_y and k_z are the shear correction factors in y and z directions, respectively and shear correction factors depend on section geometry and material. These are introduced in the section compatibility matrix in order to estimate the shear strain energy accurately for the linear elastic portion of element response. Shear correction factor for solid and hollow circular cross sections is the same about both axes in the plane of the section (denoted as k) and there are a lot of studies regarding proper estimation of that coefficient [46, 49, 50]. However, in this thesis, the shear correction factor is calculated from the general and more recent expression that is stated in the study of Hutchinson [51] for a hollow circular section as given below in Equation (3.103) for outer radius, b, inner radius, a and Poisson ratio, υ.

$$k = \frac{6(a^2+b^2)^2(1+\upsilon^2)^2}{7a^4+34a^2b^2+7b^4+\upsilon(12a^4+48a^2b^2+12b^4)+\upsilon^2(4a^4+16a^2b^2+4b^4)} \quad (3.103)$$

It is important to note that the value of k simplifies to $6(1+\upsilon)^2/(7+12\upsilon+4\upsilon^2)$ if $a = 0$, i.e. if the member has solid circular section. According to the Stephen [52], that value of the shear correction factor is not only suitable for the static case but also for the dynamic case provided that $\upsilon \geq 0.2$, a broad range that encloses most of the materials including steel which is the preferred material that is used in nonlinear analysis in the subsequent parts. However, it was also stated in the same study that caution is necessary in case of dynamic analysis of a stubby cantilevered beam.

It should also be emphasized that some kind of higher-order elements do not need to cope with shear correction factor. The element that is derived recently by Zhang and Fu [53] is that kind of element which makes use of Laurent series expansion form for the displacement field to remove the need of shear correction factor for solid and hollow circular sections. Additionally, it is also possible to presume the distribution

of shear strain a priori in the mixed element formulation and eliminate the necessity of shear correction factor as preferred in the study of Saritas and Filippou [22].

Equation (3.5) can be rearranged by using the Equation (3.101) to perform integration of stresses that satisfy the material constitutive relations $\hat{\boldsymbol{\sigma}} = \hat{\boldsymbol{\sigma}}(\boldsymbol{\varepsilon})$ as follows;

$$\hat{\boldsymbol{s}} = \begin{pmatrix} \hat{N} & \hat{M}_z & \hat{M}_y & \hat{V}_y & \hat{V}_z & \hat{T} \end{pmatrix}^{\mathrm{T}} = \int_A \boldsymbol{a_s}^{\mathrm{T}} \begin{pmatrix} \hat{\sigma}_{xx} \\ \hat{\sigma}_{xy} \\ \hat{\sigma}_{xz} \end{pmatrix} dA \tag{3.104}$$

If derivative of Equation (3.104) with respect to section deformations is taken, tangent stiffness of section, $\boldsymbol{k_s}(x)$ that is employed to compute the expression in Equation (3.81) can be obtained as follows,

$$\boldsymbol{k_s}(x) = \frac{\partial \hat{\boldsymbol{s}}(x)}{\partial \boldsymbol{e}(x)} = \int_A \boldsymbol{a_s}^{\mathrm{T}} \frac{\partial \hat{\boldsymbol{\sigma}}(\boldsymbol{\varepsilon})}{\partial \boldsymbol{e}} dA = \int_A \boldsymbol{a_s}^{\mathrm{T}} \boldsymbol{k_m} \boldsymbol{a_s} dA \tag{3.105}$$

In Equation (3.105), $\boldsymbol{k_m}$ is the material tangent modulus that is calculated as follows;

$$\boldsymbol{k_m} = \frac{\partial \hat{\boldsymbol{\sigma}}(\boldsymbol{\varepsilon})}{\partial \boldsymbol{e}} \tag{3.106}$$

Gauss-quadrature, midpoint or trapezoidal rule are the numerical integration methods that can be implemented on a section for the numerical integration of Equations

(3.104) and (3.105). Gauss-quadrature is preferred in numerical analysis due to its some advantages as explained where necessary in the subsequent chapters.

3.9. THREE DIMENSIONAL MATERIAL MODEL

There are three stress components at a material point of the cross-section of the proposed mixed beam element which are not equal to zero. These are normal and shear stresses (σ_{xx}, σ_{xy} and σ_{xz}) and the rest of the stress components are equal to zero on the cross-section. However, there are six stress components in the material model. The transverse stress components can be equated to zero ($\sigma_{yy} = 0$ and $\sigma_{zz} = 0$) in order to linearize the residuals that will appear in the expression stated in Equation (3.81) with respect to an initial strain which results in an update scheme for the unknown transverse strain fields given as follows;

$$\begin{bmatrix} C_{2222} & C_{2233} \\ C_{3322} & C_{3333} \end{bmatrix} \begin{Bmatrix} \Delta\varepsilon_{yy} \\ \Delta\varepsilon_{zz} \end{Bmatrix} = -\begin{Bmatrix} \sigma_{yy} \\ \sigma_{zz} \end{Bmatrix} - \begin{bmatrix} C_{2211} & C_{2212} & C_{2213} \\ C_{3311} & C_{3312} & C_{3313} \end{bmatrix} \begin{Bmatrix} \Delta\varepsilon_{xx} \\ \Delta\gamma_{xy} \\ \Delta\gamma_{xz} \end{Bmatrix} \tag{3.107}$$

$C_{ijkl} = \partial\sigma_{ij}/\partial\varepsilon_{kl}$ designates the tensor form of the consistent tangent matrix for a 3d material in Equation (3.107). For notational ease, the indices are shown by the letters i, j, k and l that have values 1, 2 and 3 and these numbers correspond to x, y and z, respectively. Transverse strain fields on the left hand side of the equation are updated until the norm of the residuals is smaller than a specified tolerance by the help of the strain values on the right hand side of the equation, increments of which are obtained from the finite element analysis. Since the material model is isotropic, the shear stress components can be set equal to zero ($\sigma_{yz} = \sigma_{xz} = 0$) by imposing zero shear strains in those directions ($\gamma_{yz} = 0$) in a straightforward fashion.

The material stiffness for the beam formulation given in Equation (3.106) is determined by condensing out the stress and strain components that do not arise in a structural mechanics application such as a beam element formulation. For three active stress components (σ_{xx}, σ_{xy} and σ_{xz}) this condensation should result in the following material stiffness matrix.

$$\boldsymbol{k}_{\mathrm{m}} = \begin{bmatrix} \dfrac{\Delta\sigma_{xx}}{\Delta\varepsilon_{xx}} & \dfrac{\Delta\sigma_{xx}}{\Delta\gamma_{xy}} & \dfrac{\Delta\sigma_{xx}}{\Delta\gamma_{xz}} \\ \dfrac{\Delta\sigma_{xy}}{\Delta\varepsilon_{xx}} & \dfrac{\Delta\sigma_{xy}}{\Delta\gamma_{xy}} & \dfrac{\Delta\sigma_{xy}}{\Delta\gamma_{xz}} \\ \dfrac{\Delta\sigma_{xz}}{\Delta\varepsilon_{xx}} & \dfrac{\Delta\sigma_{xz}}{\Delta\gamma_{xy}} & \dfrac{\Delta\sigma_{xz}}{\Delta\gamma_{xz}} \end{bmatrix} \tag{3.108}$$

It is possible to write the incremental stress-strain relation initially in terms of all six components of stress and strain as $\Delta\sigma_{ij} = C_{ijkl}\Delta\varepsilon_{ij}$ and separate the normal strains in the transverse direction from others as follows;

$$\begin{Bmatrix} \Delta\sigma_{xx} \\ \Delta\sigma_{xy} \\ \Delta\sigma_{xz} \end{Bmatrix} = \begin{bmatrix} C_{1111} & C_{1112} & C_{1113} \\ C_{1211} & C_{1212} & C_{1213} \\ C_{1311} & C_{1312} & C_{1313} \end{bmatrix} \begin{Bmatrix} \Delta\varepsilon_{xx} \\ \Delta\gamma_{xy} \\ \Delta\gamma_{xz} \end{Bmatrix} + \begin{bmatrix} C_{1122} & C_{1133} \\ C_{1222} & C_{1233} \\ C_{1322} & C_{1333} \end{bmatrix} \begin{Bmatrix} \Delta\varepsilon_{yy} \\ \Delta\varepsilon_{zz} \end{Bmatrix} \tag{3.109}$$

Normal strain increments on the left side of Equation (3.107) are substituted into Equation (3.109) for the converged state of the transverse stresses $\sigma_{yy} = \sigma_{zz} = 0$ and the resulting expression is the condensed material stiffness matrix given as follows;

$$\boldsymbol{k}_{\mathrm{m}} = \begin{bmatrix} C_{1111} & C_{1112} & C_{1113} \\ C_{1211} & C_{1212} & C_{1213} \\ C_{1311} & C_{1312} & C_{1313} \end{bmatrix} - \begin{bmatrix} C_{1122} & C_{1133} \\ C_{1222} & C_{1233} \\ C_{1322} & C_{1333} \end{bmatrix} \begin{bmatrix} C_{2222} & C_{2233} \\ C_{3322} & C_{3333} \end{bmatrix}^{-1} \begin{bmatrix} C_{2211} & C_{2212} & C_{2213} \\ C_{3311} & C_{3312} & C_{3313} \end{bmatrix} \tag{3.110}$$

CHAPTER 4

NUMERICAL VALIDATION OF 3D MIXED ELEMENT

4.1. INTRODUCTION

Numerical validation of the the 3d mixed finite element, the formulation of which is given in the previous parts is presented in this chapter for nonlinear static case. In order to be able to use in comparison of the 3d proposed mixed element, a 3d displacement based Timoshenko beam element is introduced initially. Then, this element and other 3d displacement based elements are used together with the exact solutions that exist the literature in comparsion of the nonlinear response of the proposed mixed element that has various circular and hollow cross-sections in the last part of this chapter.

4.2. A 3D DISPLACEMENT BASED TIOMESHENKO FINITE ELEMENT

A 2d two node displacement based Timoshenko beam finite element was developed by Friedman and Kosmatka [12] by using Hamilton's principle and cubic and quadratic Lagrangian shape functions for transverse and rotational displacements that are made independent by requiring them to satisfy the two homogenous differential equations associated with Timoshenko's beam theory. This requirement makes element free from shear-locking. Mazars et al. [14] adapted those shape functions to displacement based 3d Timoshenko beam element that considers uncoupled effect of shear and torsion by referring to its predecessor study. In a recent study, Triantafyllou and Koumousis [15] developed a locking-free 2d displacement based

beam finite element, where the shape functions were derived under linear elastic material behavior as done by Friedman and Kosmatka [12]. The proposed beam element in that study was used to analyze structural members where shear effects are significant under nonlinear material response.

The derivation of shape functions included in the study of Przemieniecki [13] was demonstrated by Friedman and Kosmatka [12] for 2d and they can be extended to 3d as in the study of Luo [54] and rearranged by making slight changes in accordance with the coordinate system in this thesis as follows;

$$
\begin{aligned}
N_1 &= 1 - \xi \\
N_2 &= \xi \\
N_3 &= \left[2\xi^3 - 3\xi^2 - \phi_y\xi + \left(1 + \phi_y\right)\right]/\left(1 + \phi_y\right) \\
N_4 &= \left[\xi^3 - \left(2 + \phi_y/2\right)\xi^2 + \left(1 + \phi_y/2\right)\xi\right]L/\left(1 + \phi_y\right) \\
N_5 &= -\left[2\xi^3 - 3\xi^2 - \phi_y\xi\right]/\left(1 + \phi_y\right) \\
N_6 &= \left[\xi^3 - \left(1 - \phi_y/2\right)\xi^2 - \left(\phi_y/2\right)\xi\right]L/\left(1 + \phi_y\right) \\
N_7 &= [2\xi^3 - 3\xi^2 - \phi_z\xi + (1 + \phi_z)]/(1 + \phi_z) \\
N_8 &= -[\xi^3 - (2 + \phi_z/2)\xi^2 + (1 + \phi_z/2)\xi]L/(1 + \phi_z) \\
N_9 &= -[2\xi^3 - 3\xi^2 - \phi_z\xi]/(1 + \phi_z) \\
N_{10} &= -[\xi^3 - (1 - \phi_z/2)\xi^2 - (\phi_z/2)\xi]L/(1 + \phi_z) \\
N_{11} &= -6[\xi^2 - \xi]/L/(1 + \phi_z) \\
N_{12} &= [3\xi^2 - (4 + \phi_z)\xi + (1 + \phi_z)]/(1 + \phi_z)
\end{aligned}
\tag{4.1}
$$

$$N_{13} = 6[\xi^2 - \xi]/L/(1 + \phi_z)$$

$$N_{14} = [3\xi^2 - (2 - \phi_z)\xi]/(1 + \phi_z)$$

$$N_{15} = 6[\xi^2 - \xi]/L/(1 + \phi_y)$$

$$N_{16} = [3\xi^2 - (4 + \phi_y)\xi + (1 + \phi_y)]/(1 + \phi_y)$$

$$N_{17} = -6[\xi^2 - \xi]/L/(1 + \phi_y)$$

$$N_{18} = [3\xi^2 - (2 - \phi_y)\xi]/(1 + \phi_y)$$

In Equation set (4.1), $\xi = x/L$ and ϕ is the ratio of the bending stiffness to the shear stiffness of the beam calculated in the y and z directions, respectively as follows;

$$\phi_y = \frac{12}{L^2}\left(\frac{EI_y}{k_y GA}\right) \quad \phi_z = \frac{12}{L^2}\left(\frac{EI_z}{k_z GA}\right) \tag{4.2}$$

In Equation set (4.2), L is the length of the member and A is the area of the section as defined previously. E and G are the Young and shear moduli, respectively, I_y and I_z are moment of inertia in the x and y directions, respectively.

End node displacements, $\bar{\boldsymbol{u}}$ in Equation (3.13) and the shape functions in Equation set (4.1) are used to calculate the displacements along the x axis of the beam, $\mathbf{u_s}$ as follows;

$$\mathbf{u_s} = \mathbf{N}\bar{\boldsymbol{u}} \tag{4.3}$$

$$\mathbf{N} = \begin{bmatrix} N_1 & 0 & 0 & 0 & 0 & 0 & N_2 & 0 & 0 & 0 & 0 & 0 \\ 0 & N_3 & 0 & 0 & 0 & N_4 & 0 & N_5 & 0 & 0 & 0 & N_6 \\ 0 & 0 & N_7 & 0 & N_8 & 0 & 0 & 0 & N_9 & 0 & N_{10} & 0 \\ 0 & 0 & 0 & N_1 & 0 & 0 & 0 & 0 & 0 & N_2 & 0 & 0 \\ 0 & 0 & N_{11} & 0 & N_{12} & 0 & 0 & 0 & N_{13} & 0 & N_{14} & 0 \\ 0 & N_{15} & 0 & 0 & 0 & N_{16} & 0 & N_{17} & 0 & 0 & 0 & N_{18} \end{bmatrix} \tag{4.4}$$

The shape functions calculated in Equation (4.4) are actually valid in the linear elastic range of response for the beam. When the element experiences material inelasticity, shape functions calculated for elastic case are used as an approximation.

The section force deformation relation is calculated as follows;

$$\mathbf{s} = \boldsymbol{k_s}\boldsymbol{e}(\mathrm{x}) \tag{4.5}$$

The section stiffness matrix, $\boldsymbol{k_s}$ in Equation (4.5) is calculated as follows;

$$\boldsymbol{k_s} = \begin{bmatrix} \int_A EdA & \int_A EzdA & \int_A -EydA & 0 & 0 & 0 \\ & \int_A Ey^2dA & \int_A -EyzdA & 0 & 0 & 0 \\ & & \int_A Ez^2dA & 0 & 0 & 0 \\ & & & k_y\int_A GdA & 0 & -k_y\int_A GzdA \\ & \text{symmetric} & & & k_z\int_A GdA & k_z\int_A GydA \\ & & & & & \int_A G\left(k_zy^2 + k_yz^2\right)dA \end{bmatrix} \tag{4.6}$$

4.3. VALIDATION OF MIXED ELEMENT IN 3D

Derivation of the 3d mixed element is presented in the third chapter. In this section, proposed 3d mixed element is validated under nonlinear conditions by comparing the proposed element with 3d displacement based elements that are available in the literature for various geometric, loading and support conditions. This is achieved by considering four different set of numerical examples where some of them also have several sub cases.

The first example in Section 4.3.1 includes comparison of the proposed 3d mixed element with the 3d displacement based Friedman and Kosmatka [12] element that is presented in Section 4.2 under monotonic loading for a uniform cantilever member that has a solid circular section.

The second set of examples in Section 4.3.2 includes three different sub cases where application of torsion to a cantilever member that has solid circular section along the span is common for all three sub cases. In the first sub case, proposed mixed element is compared with the exact solution under pure torsion. In the second sub case, proposed mixed element is validated under axial load and torsion by utilizing an analytical solution that exists in the literature. In the third sub case, proposed mixed element is compared again with the displacement based Friedman and Kosmatka [12] element. However in that sub case, the cantilever member is not uniform but tapered to its free end.

The effect of coupling of stresses and resulting forces on the nonlinear behavior of a cantilever member that has solid and hollow circular sections is investigated for different levels of axial and torsional loads considering 3d cyclic bending in the third set of examples of Section 4.3.3. The first sub case includes nonlinear analysis of

members with solid section and the second sub case includes nonlinear analysis of members with hollow sections having various inner and outer radii.

Fourth set of examples in Section 4.3.4, which are also last set of examples for the validation of the proposed mixed element under nonlinear conditions, refer to the results of the study by Nowzartash and Mohareb [55]. The nonlinear interaction of bending and torsion is investigated for a long pipe, and the influence of shear force on bending is investigated for a short fixed-fixed pipe where loading is applied at a node in the span for both sub cases.

4.3.1. Comparison of 3d Mixed and Displacement Based Elements

In this example, a uniform cantilever steel member that has the same solid circular cross-section throughout the span is displaced monotonically in the direction of global X (Figure 4.1) by imposing tip displacement at the free end of the member in order to compare proposed 3d mixed element with 3d displacement based Friedman and Kosmatka [12] element under nonlinear conditions for various cases.

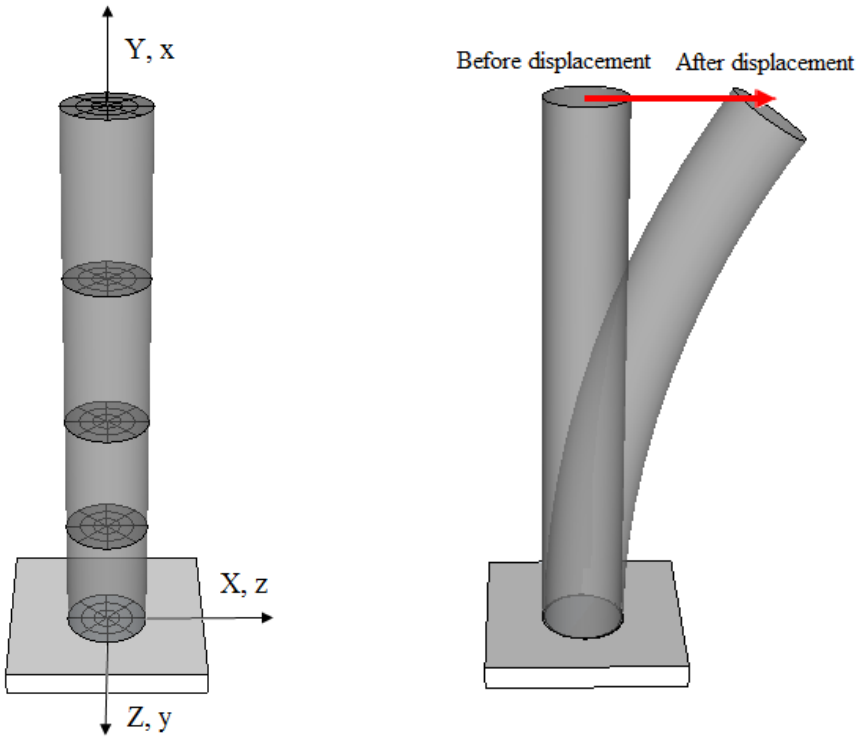

a. Orientation of axes b. Tip displacement in the global *X* direction

Figure 4.1. Orientation of global and local axes and tip displacement

The member is assumed to be perfectly fixed at one end and free at the other end having homogenous and isotropic steel material throughout the length, L of the element which is 180 units. Member has uniform solid circular cross-section with a diameter, d of 18 units, Young modulus, E of 29000 units, Poisson ratio, $\nu = 0.3$ and yield strength, f_y of 36 units. The geometric and material properties assumed in this example are also used in some of the following examples.

The assumed values of geometric and material properties are physically consistent. However, they are deliberately left unitless in order to concentrate on the effect of some parameters like the type of element, number of elements and integration points

on nonlinear behavior rather than the effect of physical quantities. Another assumption is the negligence of the self-weight of the member in the analysis. 3d J_2 plasticity model is utilized in the material model for the reponse of steel since that model is a good option for ductile materials. Kinematic and isotropic hardening values are both assumed to be zero.

Response of the circular cross-section is monitored by numerical integration of the parameters with the help of meshing of the section in both radial and circumferential directions as shown in Figure 4.2 and using mid-point integration rule. Sensitivity analysis are carried out in order to determine the adequate number of meshing in each direction and it is identified that odd numbers 11 for both radial and circumferential directions are suitable for reflecting the nonlinear response accurately.

Response of the whole member is also attained by numerical integration along the member. Although there are some other methods like Gauss-Lobatta for numerical integration, Gauss quadrature rule is utilized to model the aggregation of the response of the several sections along the beam length since the nonlinearity is expected to initiate at the fixed end of the member and Gauss quadrature is a good option to eliminate probable numerical errors due to location of quadrature points by its nature.

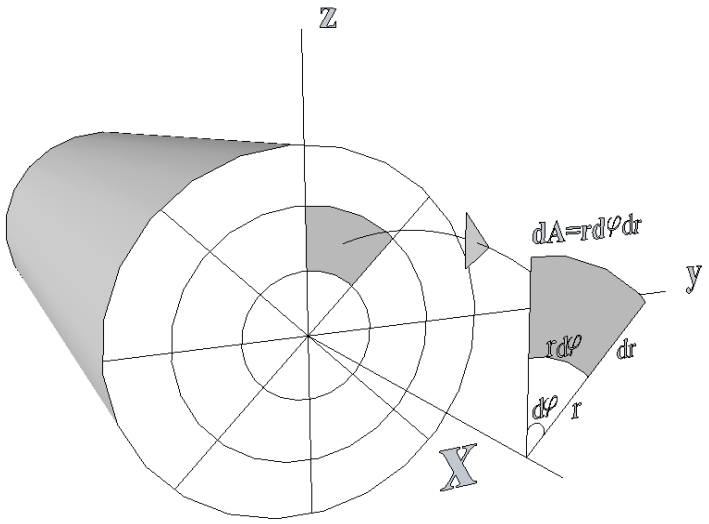

Figure 4.2. Discretization of circular section in radial and circumferential directions in local coordinates

The abbreviations "MF" and "DB" are used to denote proposed mixed formulation and Friedman and Kosmatka [12] displacement based elements, respectively in the following figures and discussions about resulting responses of the elements. Although it is not presented in this thesis, linear elastic responses of both MF and DB elements are investigated a priori to the investigation of their nonlinear responses. Consequently, it is observed that both elements are free from shear-locking especially for the case of short members and successful in simulating the linear elastic response by giving exact results when the member has uniform cross-section along the element length. However, due to the meaninglessness of depicting the same responses for both elements, reporting linear elastic responses of them are considered to be enough. But, it should also be noted that for the case of varying cross-sections as in the case of tapered members, MF is still capable of matching the exact element response but DB necessitates derivation of special shape functions as in the studies by Friedman and Kosmatka [56], Murín and Kutiš [57] and Shooshtari and Khajavi [58] or it should be paid attention to the discretization of the member by mesh refinement especially along the element span. This phenomenon is put forward by a

numerical comparison for a tapered member under pure torsion at its free end in the last sub case of the next example in Section 4.3.2.3.

Before comparison of MF and DB elements under nonlinear conditions, the effect of number of integration points, n_{IP} that is needed to perform numerical integration along the element is investigated in order to determine the convergence of it to an optimum value. With this regards, n_{IP} is varied to be 2, 5, 10, 15 and 20 by keeping number of elements, $n_e = 1$ constant per member for both MF and DB elements and Figure 4.3 and Figure 4.4 are plotted. It is inferred from these figures that increasing n_{IP} beyond 5 is not necessary because nonlinear load-displacement curves nearly coincide with each other after that limiting value. Another point that can be deduced from these figures is that for $n_{IP} = 2$, DB overestimates and MF underestimates the nonlinear response.

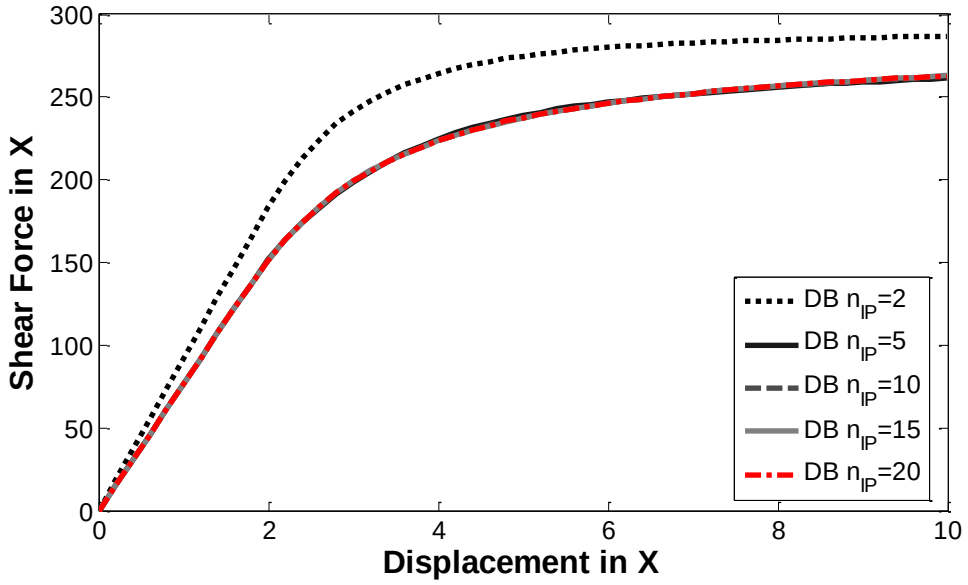

Figure 4.3. Comparison of the variation of number of integration points on DB

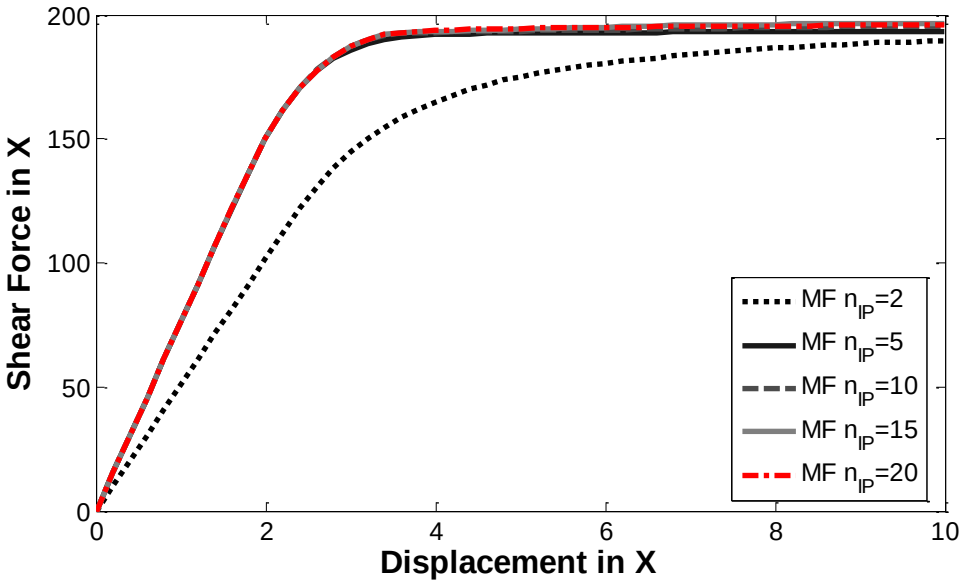

Figure 4.4. Comparison of the variation of number of integration points on MF

After investigation of the influence of the number of integration points on the nonlinear response, the effect of variation of the number of elements per span, n_e on the same response is investigated by keeping $n_{IP} = 5$ constant for each case and monitoring the shear value at the fixed end vs. tip displacement at the free end. According to the Figure 4.5, it can be concluded that increasing the number of elements per span for MF is insignificant for the nonlinear analysis because its behavior does not deviate or improve too much compared to the cases with higher number of elements per span. So, it can be inferred from the figure that MF is capable of modeling the nonlinear behavior correctly even with only one element per span. However, the effect of n_e for DB is realized prominently from Figure 4.6 that depicts comparison of DB and MF for different number of elements. According to that figure, even increasing n_e from 1 to 16 by doubling each time the number of elements used in the previous case is not enough to guarantee the accuracy ensured with only one element by MF.

There is also an important issue that would be better to clarify at this point. The duration needed to perform the nonlinear analysis with DB and MF is very close to each other if the analyses are carried out with the same number of elements per span in each case. Therefore, the superiority of MF to DB does not prevail in this regards. However, using MF offers an undeniable opportunity to perform nonlinear analysis with lesser number of elements and still obtain more accurate results than DB. This advantage of MF may not be perceptible if the nonlinear analysis of only a single member is considered but will be obvious if the nonlinear analysis of a frame structure that is exposed to strong ground motion is imagined. In this case, utilization of lesser number of elements for MF will decrease the solution time dramatically and still offer a high accuracy as compared to DB. Additionally, less storage capacity will be needed for the case of MF. That kind of a problem for larger structural systems was handled in 2d for a frame system [17] and it was concluded that the use of mixed formulation elements even for large systems reduces the computation time ensuring high accuracy of the results at the same time. This substantiates that proposed MF is superior to DB under nonlinear conditions.

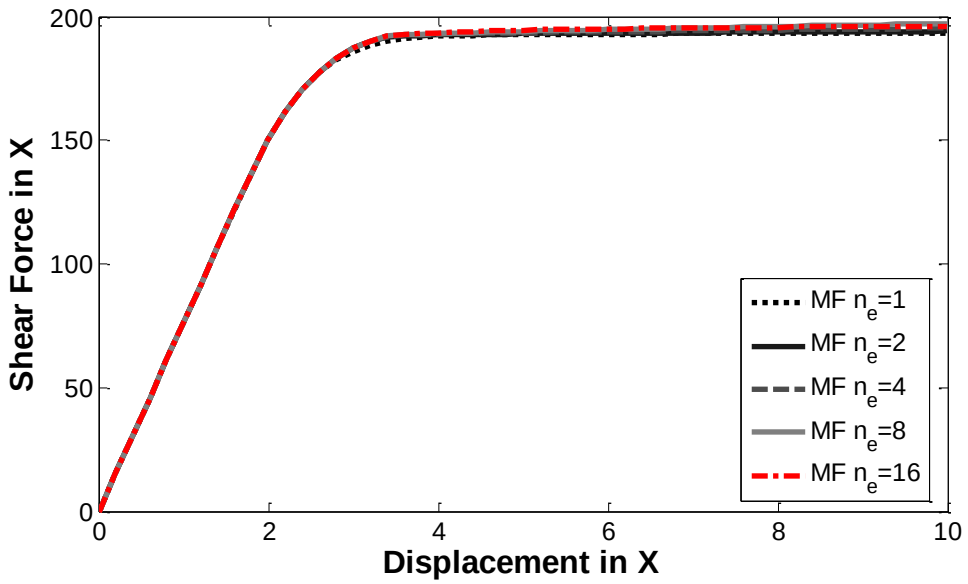

Figure 4.5. Effect of different number of elements on MF

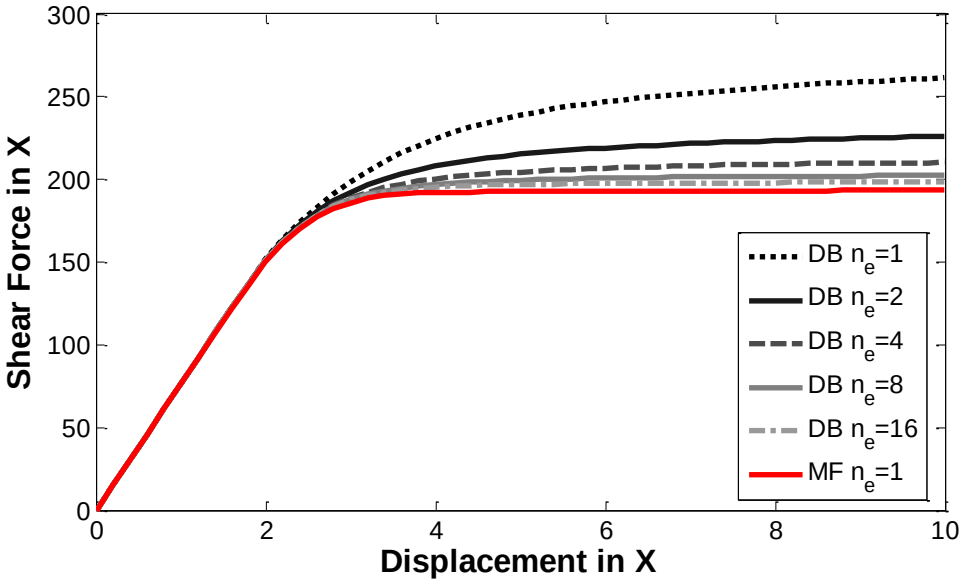

Figure 4.6. Comparison of the effect of number of elements on DB and MF

4.3.2. Nonlinear Performance of Mixed Element Under Torsion

4.3.2.1. Pure Torsion of a Uniform Cantilever Beam with Solid Circular Section

The expression that is used to obtain the torque, T applied around the element axis at the free end of a uniform cantilever beam with solid circular section that has elastoplastic material properties can be easily derived explicitly and one can refer to the text books for detailed derivation (Such as [59]) since it is out of the scope of this thesis. However, the final expression can be given as follows;

$$T = \left(\frac{2\pi b^3}{3}\right)\tau_y\left[1 - \frac{1}{4}\left(\frac{\phi_y}{\phi}\right)^3\right] \tag{4.7}$$

In Equation (4.7), b is the outer radius of the circular cross-section as defined previously in Equation (3.103), τ_y is the shear stress at yield and ϕ_y is the angle of twist at yield calculated as follows;

$$\phi_y = \frac{\tau_y L}{Gb} \tag{4.8}$$

In Equation (4.8), G is the shear modulus and L is the length of the member as already defined before. If ϕ is sufficiently large as a result of the plastic deformations, then ϕ_y/ϕ in the right hand side of the Equation (4.7) approaches to zero forcing the expression in the brackets to approach to one. Consequently, the torque on the section gives the plastic torque, T_p indicating that the entire section is in its plastic state as obtained by the following expression;

$$T_p = \left(\frac{2\pi b^3}{3}\right)\tau_y \tag{4.9}$$

It should also be noted that if ϕ is equal to ϕ_y then, ϕ_y/ϕ in the right hand side of the Equation (4.7) becomes one revealing the fact that the elastic limit is 75% of the plastic limit for the circular section.

Aforementioned theory is utilized to verify the proposed MF element by applying pure torsion around the element axis at the free end of the member and performing nonlinear analysis. Geometric and material properties such as length, diameter, modulus of elasticity and etc. of the member are assumed to be same with the properties of the member in the example in Section 4.3.1 and Figure 4.7 is plotted. According to the figure, the nonlinear curve obtained by MF under pure torsion with

only one element per member span matches successfully with the exact solution. Additionally, MF is capable of not only verifying the phenomenon that the torque at yield is 75% of the plastic torque but also capable of simulating correctly the initiation of plasticity.

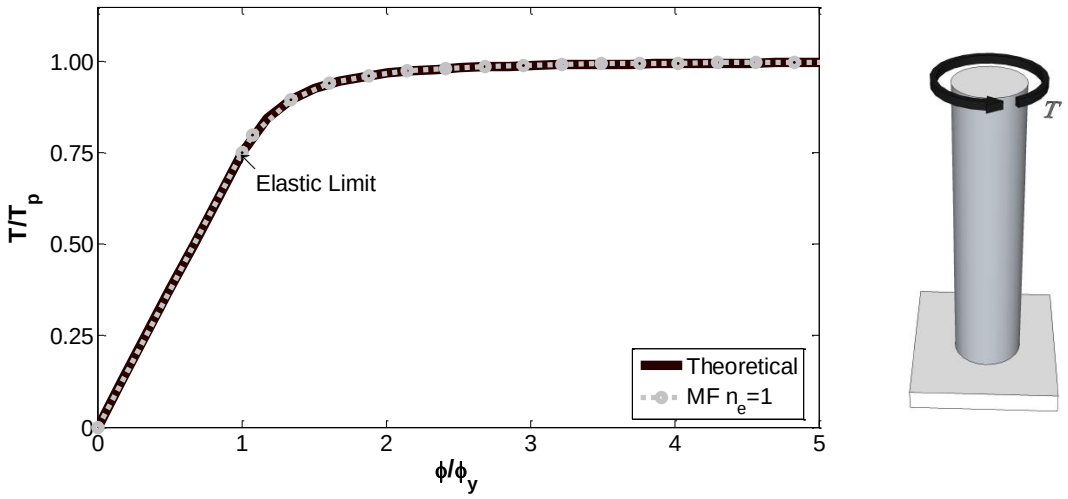

Figure 4.7. Exact solution vs. MF element under pure torsion for uniform cantilever member with solid circular section

4.3.2.2. Combined Axial Load and Torque on a Uniform Cantilever Beam with Solid Circular Section

After verification of the MF element under pure torsion in the previous example, the ability of the element to simulate the nonlinear behavior under torque that is accompanied by axial load is investigated in this example. Nonlinear analysis of a uniform cantilever beam with solid circular section that has same material and geometric properties with the element given in Section 4.3.1 is performed by applying the same load pattern described in the study of Gaydon [60]. This study

includes explicit expressions that are derived by integration of the Reuss equations to calculate shear stress and tension in the plastic material of a solid circular cylinder for various combinations of torque and tension. Similar loading to that case is frequently encountered in critical engineering components, such as bolted joints, couplings and rotating shafts [61] and utilized in experimental studies [62].

At the beginning of the nonlinear analysis, a single MF element per span is given a predetermined extension corresponding to a certain tension such that the element yields due to plastic deformations immediately after an additional loading is applied. At that instant there is not any shear stress on the member. Then, a gradually increasing torsion is applied around the axis of the element at the free end of the member while keeping the axial extension constant and nonlinear response of the MF element is monitored as given in Figure 4.8. That figure depicts the variation of normalized axial load by axial load at yield, N/N_y and normalized torque by a multiple of torque at yield, $T/1.5T_y$ similar to the presentation by Gaydon [60]. According to that figure, axial load carrying capacity of the member diminishes as quick as the torque is applied, reaching asymptotically to zero where the latter converges to 2/3 in a synchronized manner without being affected. This example shows that MF beam element is able to capture exactly the closed form expressions provided by Gaydon [60] with only single element per member span disclosing its capabilities on reflecting force coupling correctly.

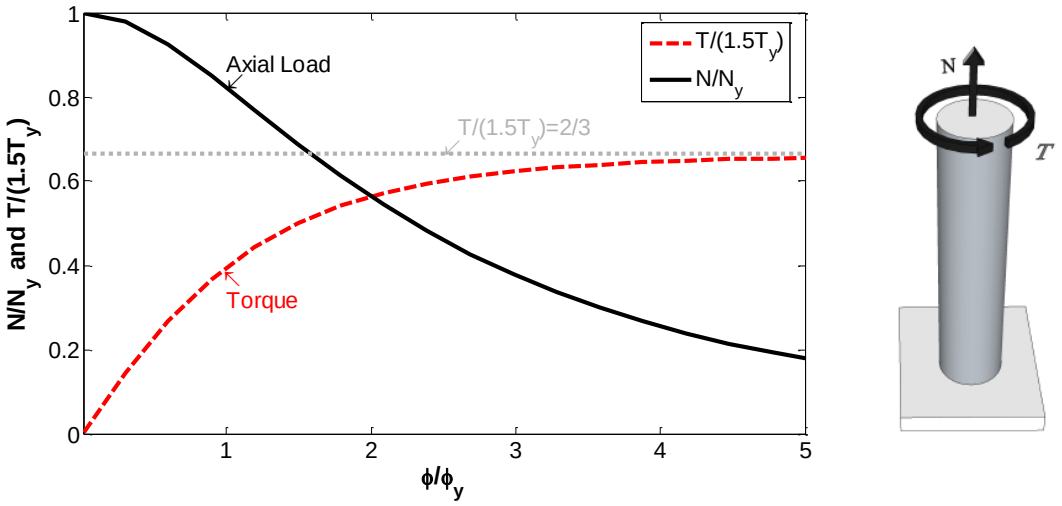

Figure 4.8. Variation of axial load and torque with angle of twist for solid circular section by holding extension constant after yield

4.3.2.3. Comparison of Tapered MF and DB Elements Under Torsion

Comparison of the MF and DB elements having circular cross sections are given in Section 4.3.1 and advantages of the former are presented for uniform cantilever member. In this example, nonlinear responses of MF and DB elements having same material and geometric properties presented in Section 4.3.1 are compared by applying pure torsion around the element axis at the free end of the member, but this time the geometry is tapered from fixed end to the free end of the member having diameter $d = 18$ at the fixed end and $d = 9$ units at the free end of the member, respectively. Superiority of the MF element compared to DB element is shown by performing the nonlinear analysis with using only one element per span for the case of MF but varying n_e as 2, 4 and 8 for the case of DB.

Although it is not displayed in this thesis, it should be reported that using DB element that is used in Section 4.3.1 in place of MF element analyzed in examples

given in Sections 4.3.2.1 and 4.3.2.2 will yield the similar results for the case of uniform member. But, DB element lacks accuracy for the case of nonlinear analysis of tapered members where MF has still favorable response as depicted in Figure 4.9. According to that figure, $n_e = 8$ is not good enough to model even linear portion of the total response and should be increased beyond that number in order to compete with the nonlinear response provided by MF with only one element per span.

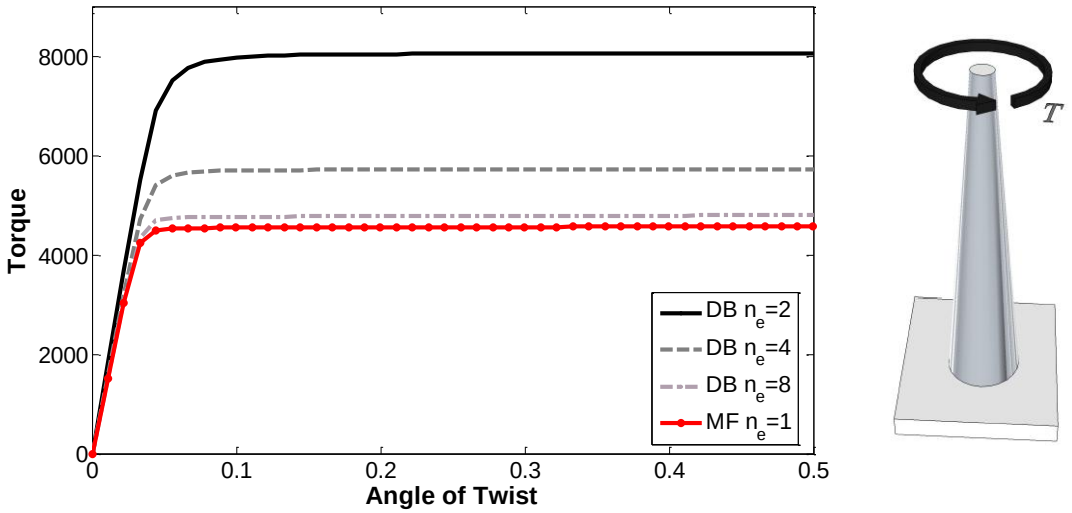

Figure 4.9. Comparison of the effect of number of elements for the analysis of tapered members with DB and MF frame elements

4.3.3. Nonlinear Analysis of Beams with Solid and Hollow Circular Sections

In this section, the ability of proposed MF element on modeling sound nonlinear coupling between internal forces is displayed by performing three dimensional nonlinear analysis of a uniform cantilever beam possessing solid and hollow circular sections. Since authentication of the proposed MF element is presented in the

previous sections with several examples, only MF element is used in the following numerical analysis. All of the nonlinear analyses are carried out with one MF element per member span with the similar discretization and same assumptions on geometric and material properties given in Section 4.3.1 except loading which is explained in the subsequent discussions and figures.

4.3.3.1. Nonlinear Analysis of Uniform MF for Solid Circular Section

Two different pseudo-load cases called as "Case A" and "Case B" are defined to perform nonlinear analysis. Since analysis with both loading cases are carried out in pseudo-time, loading is named as pseudo. The difference between loading cases originates from the application of axial load for Case A and torsion for Case B. Moreover, each load cases have four sub-cases that are indicated with number suffixes attached to the letters "A" and "B" depending on the level of the axial load or torsion applied on the member.

For Case A, at $t = 0$, the member is at rest and there is not any displacement in the axis of the member untill $t = 0.1$. But in between, the free end of the member is loaded axially in the negative global *Y*-direction (Force History in Figure 4.10), i.e. a compressive force is applied increasing gradually up to pseudo time, $t = 0.1$. That compresive load is kept constant from $t = 0.1$ to the instant $t = 2$ at when the analysis is terminated.

Besides application of the axial load, at the moment $t = 0.1$ displacement of the free end of the member linearly 6 units away from its original position in global *X*-direction (Disp. History X in Figure 4.10) until $t = 0.5$ is initiated. From $t = 0.5$ to $t = 1$, X coordinate of the member is kept constant. After that instant, linear

displacement of the member starts in the negative *X*-direction until $t = 1.5$ at when the *X* coordinate becomes zero until the end of the analysis, i.e. $t = 2$.

The member is displaced not only in the direction of global *X*-direction but also in the direction of global *Z*-direction but with a time shift that is equal to $t = 0.5$ being exposed to axial load at the same time. At $t = 0.5$ sec, free end of the member is started to be displaced linearly 6 units in global *Z*-direction (Disp. History Z in Figure 4.10) until $t = 1$ and *Z* coordinate is kept constant until $t = 1.5$. After that instant, free end of the member is displaced linearly in the negative *Z*-direction until $t = 2$ and the free end of the member returns back to its position at rest following a square path (Figure 4.11).

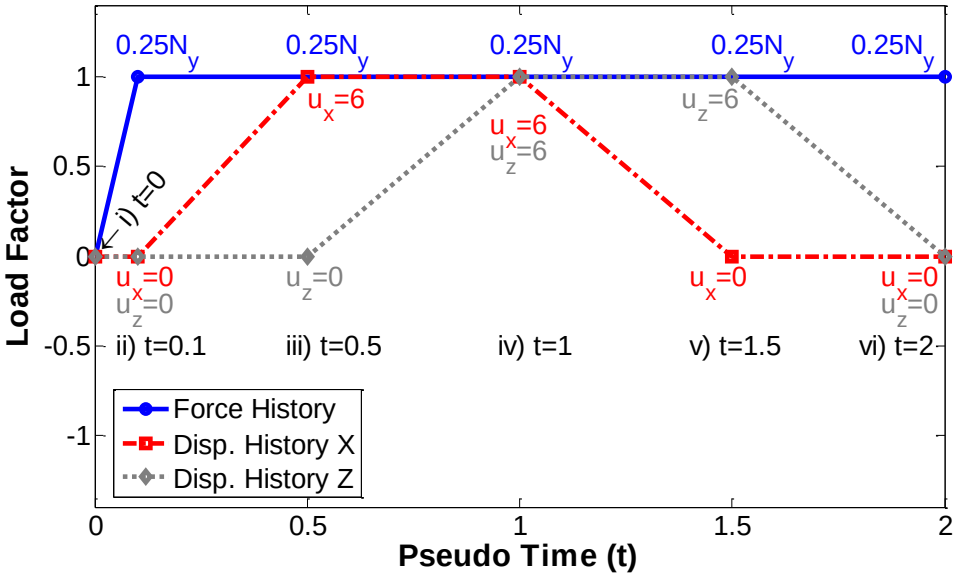

Figure 4.10. Force and displacement pseudo-time histories imposed on the element for Case A2 for $0.25N_y$.

Since there are four sub-cases of Case A, the loading scheme explained in the previous paragraphs are performed four times on the member for different levels of axial loading given as 0, $0.25N_y$, $0.50N_y$ and $0.75N_y$ that form four sub-cases A1, A2, A3 and A4, respectively. Axial force at yield, N_y is calculated as the area of the section times yield strength of the member. Figure 4.10 and Figure 4.11 try to illustrate that loading procedure for A2. However, those figures are also valid for other sub-cases except the level of axial loading that is interchangeable with 0, $0.50N_y$ and $0.75N_y$.

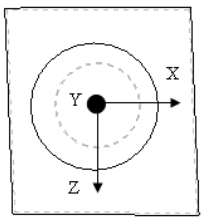	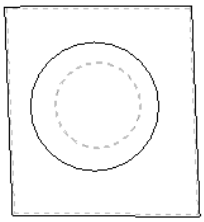	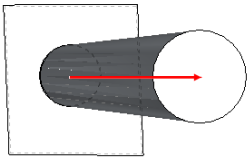
i) $t = 0$, No axial force, $u_x = 0, u_z = 0$	ii) $t = 0.1$, $0.25N_y$, $u_x = 0, u_z = 0$	iii) $t = 0.5$, $0.25N_y$, $u_x = 6, u_z = 0$
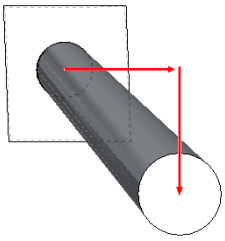	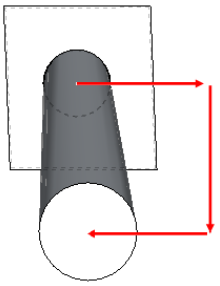	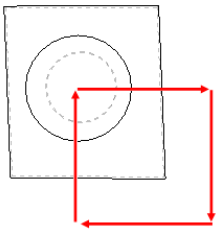
iv) $t = 1$, $0.25N_y$, $u_x = 6, u_z = 6$	v) $t = 1.5$, $0.25N_y$, $u_x = 0, u_z = 6$	vi) $t = 2$, $0.25N_y$, $u_x = 0, u_z = 0$

Figure 4.11. Illustration of loading history for Case A2 for $0.25N_y$

(View of the free end of the element in the negative global *Y*-direction).

In Figure 4.10, horizontal axis designates pseudo time and vertical axis called "Load Factor" shows the portion of the load or displacement imposed on the member at that pseudo time. Figure 4.11 is an alternative illustration of the loading sketched in Figure 4.10 and it depicts force and displacement history by looking free end of the member in the negative global *Y*-direction.

Application of the aforementioned force and displacement histories for each sub-cases of Case A will yield Figure 4.12 and Figure 4.13 that give shear force at the fixed end of the member vs. displacement of the free end of the member in *X* and *Z* directions, respectively. In these figures, nonlinearity arises from the inelasticity caused by combined effects of axial load and displacements in *X* and *Z* directions and capacity of the solid circular section decreases as the level of axial load increases.

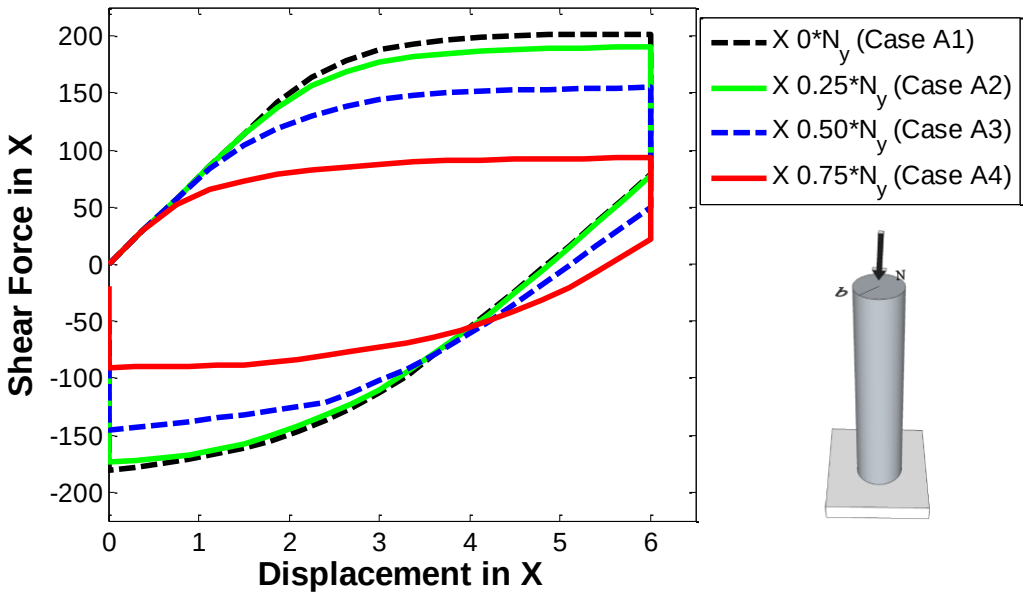

Figure 4.12. Base shear vs. tip displacement in global *X*-direction for Cases A1, A2, A3 and A4 for solid section.

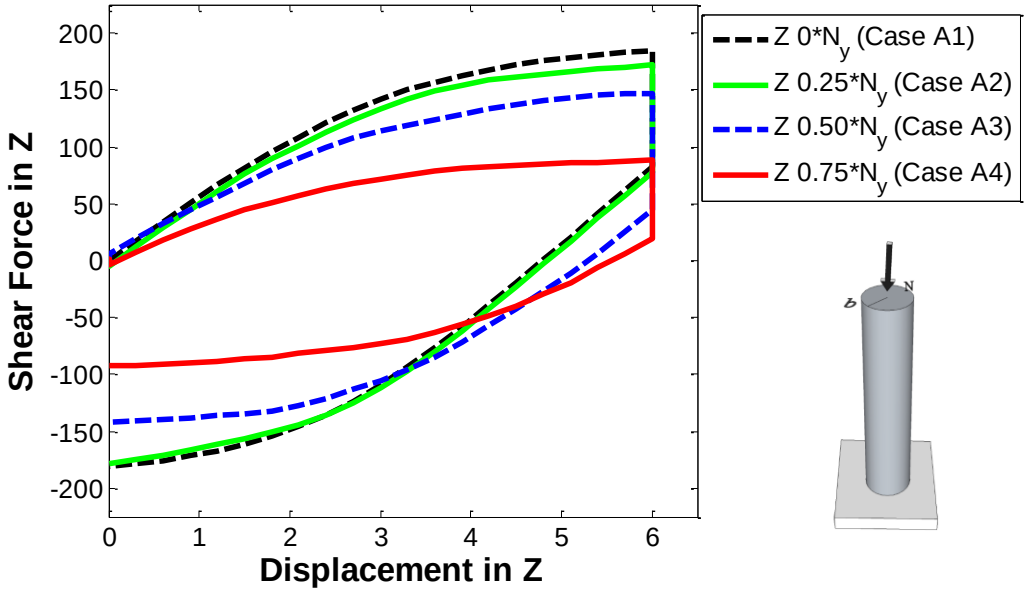

Figure 4.13. Base shear vs. tip displacement in global *Z*-direction for Cases A1, A2, A3 and A4 for solid section.

After nonlinear analyses are performed for Case A, same loading and displacement histories are applied for Case B to the same member by only changing the type of loading at the free end in that case. In Case B, torsion is applied around global *Y*-direction at the free end of the member instead of axial force applied in Case A. According to the experiments that are conducted for ductile materials verify that the yield stress obtained from a pure torsion test, τ_y is 0.5 to 0.6 times the yield stress, f_y that is obtained from a uniaxial tension test [8]. Therefore, utilization of the Von Mises yield criterion is ideal for estimation of the yield strength in shear accurately because τ_y is equal to $0.577f_y$ in octahedral shear stress theory. Consequently, torsion at yield, T_y is calculated to be $(2\pi/3)(b)^3(\tau_y)$ by assuming there is a constant shear stress in the section at yield $(\tau_y = 0.577f_y)$ and taking integral of this stress over the area of the section (Figure 4.14) in Case B.

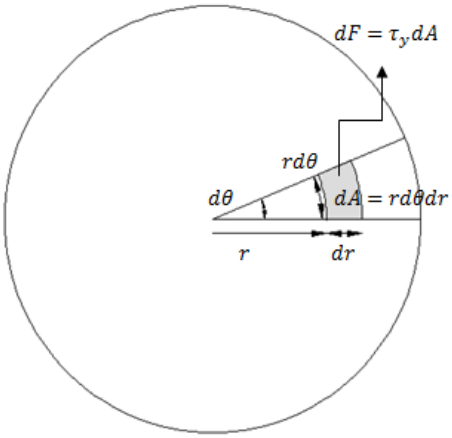

Figure 4.14. Calculation of the shear stress for circular section.

Similar to the Case A, Case B has also four sub-cases named as B1, B2, B3 and B4 according to the level of torque that is applied at the free end of the member. The loading and displacement histories that are defined in Figure 4.10 and Figure 4.11 are applied to the member by varying torque level as 0, $0.25T_y$, $0.50T_y$ and $0.75T_y$ in each sub-cases. As a result, nonlinear response of the member is obtained by monitoring shear force at the fixed end of the member vs. displacements of the free end of the member in X and Z directions, respectively as plotted for solid circular section in Figure 4.15 and Figure 4.16.

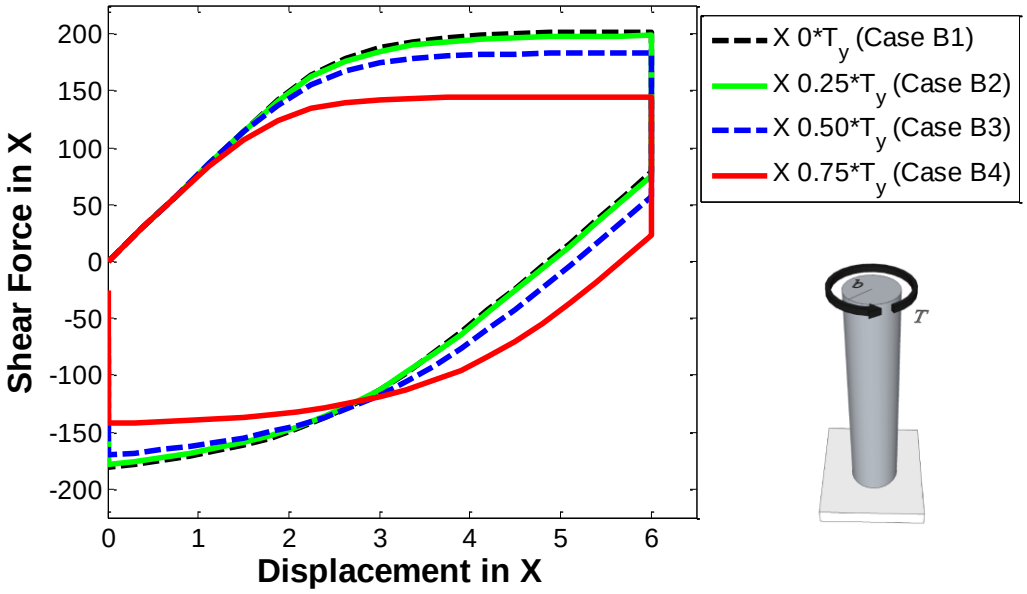

Figure 4.15. Base shear vs. tip displacement in global *X*-direction for Cases B1, B2, B3 and B4 for solid section.

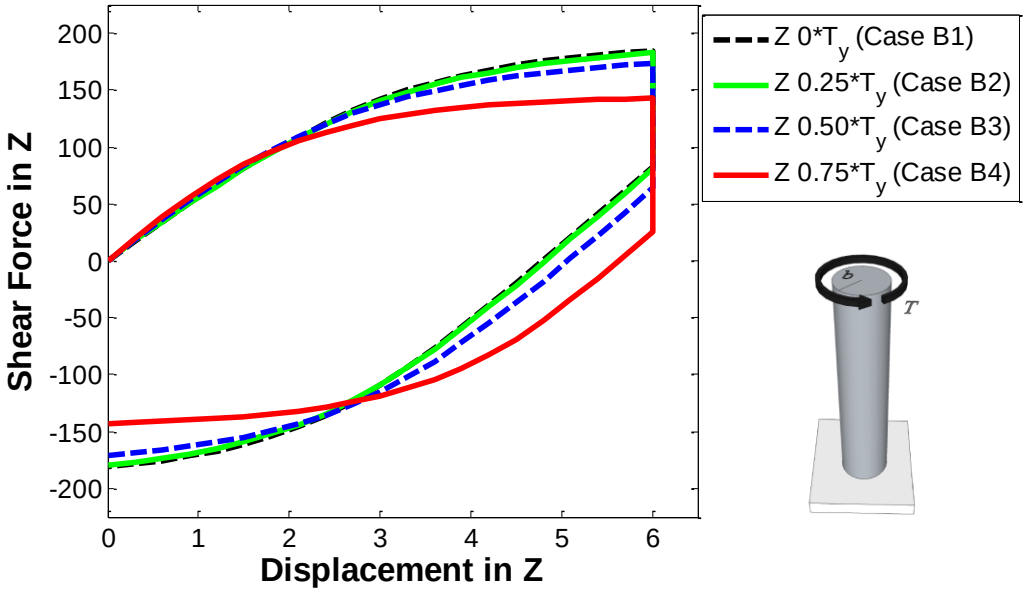

Figure 4.16. Base shear vs. tip displacement in global *Z*-direction for Cases B1, B2, B3 and B4 for solid section.

According to the Figure 4.15 and Figure 4.16, capacity of the solid circular section decreases as the level of torsion increases. However, when these figures are evaluated together with Figure 4.12 and Figure 4.13, the ifluence of axial load on nonlinear behavior is more prominent compared to the effect of torsion for the 3d solid member. These figures display also the ability of the proposed 3d mixed element to consider strong coupling between axial force, shear, bimoments and torsion. Moreover, figures reveal that the element is capable of reflecting the dependency of nonlinear behavior on direction of loading since nonlinear curves for X and Z directions are not identical for the same level of axial load or torsion in Cases A and B.

4.3.3.2. Nonlinear Analysis of Uniform MF for Hollow Circular Section

In the previous section, nonlinear response of the uniform cantilever beam with solid circular section is investigated under various loading and displacement histories. In this section, nonlinear analysis of the same member is carried out for the same loading and displacement histories with the only difference in the type of the circular section which is hollow circular section in this case.

The ratio, a/b of the inner radius a to outer radius b (Figure 4.17) of the hollow section is varied as 0.3, 0.7, 0.9, 0.95 and 0.99 in the analysis and Equation (3.103) is used for calculation of the shear correction factor in the element response. It should also be noted that nonlinear geometric effects such as local buckling especially for the thin-walled geometry are not considered in determination of the section response of the proposed element.

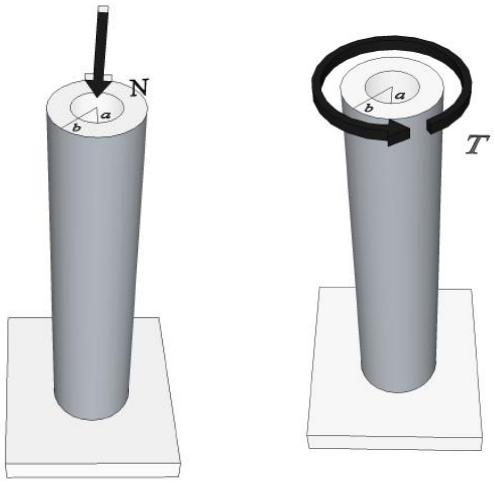

Case A Case B

Figure 4.17. Loading of hollow circular section for Cases A and B

Variation of the nonlinear response with different levels of axial load, N_y and torsion, T_y is obtained for each a/b ratio mentioned in the previous paragraph by applying the cyclic load and displacement histories defined as Case A and B and resulting outputs are plotted in Figure 4.18 to Figure 4.21 by adding the nonlinear curves for the ratio $a/b = 0$ that is already obtained in Section 4.3.3.1 and presenting the variation of base shear at the fixed end of the member vs. displacements in the *X* and *Z* directions, respectively.

If nonlinear geometric effects such as local buckling of especially thin-walled sections are neglected, the ability of the proposed 3d mixed element to model the nonlinear response correctly can be attested by numerical comparison of the base shear values for the case where zero axial load is applied on the member with the theoretical values that neglect also the nonlinear geometric effects.

In order to make such a comparison base shear values are calculated by dividing theoretical values of yield moment under zero axial load on member, $M_y = Sf_y$ and plastic moment, $M_p = Z_p f_y$ to the length of member that are obtained for both solid and hollow circular sections. In these equalities, S is the elastic section modulus which is given as $S = \pi(b^4 - a^4)/(4b)$ and Z_p is the plastic section modulus that is found as $Z_p = 4(b^3 - a^3)/3$. Results are tabulated in Table 4.1 for different a/b ratios.

If Table 4.1 and Figure 4.18 to Figure 4.21 are probed into, it will be appreciated that the proposed 3d mixed element is successful in modeling nonlinear behavior for solid and various hollow sections.

Table 4.1. Theoretical shear values calculated from moment at yield and plastic limit

a/b	S	M_y	M_y/L	Z_p	M_p	M_p/L
0	572.56	20611.99	114.51	972.00	34992.00	194.40
0.3	567.92	20445.03	113.58	945.76	34047.22	189.15
0.7	435.08	15663.05	87.02	638.60	22989.74	127.72
0.9	196.90	7088.46	39.38	263.41	9482.83	52.68
0.95	106.21	3823.40	21.24	138.63	4990.73	27.73
0.99	22.56	812.19	4.51	28.87	1039.30	5.77

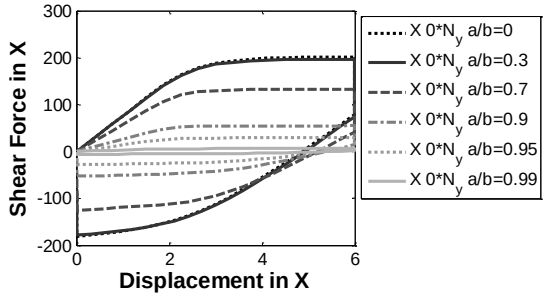

a. Case A1 in *X* for 0*N_y

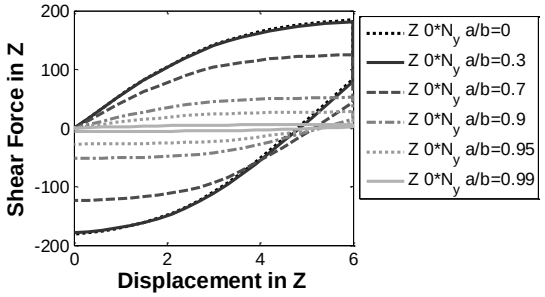

b. Case A1 in *Z* for 0*N_y

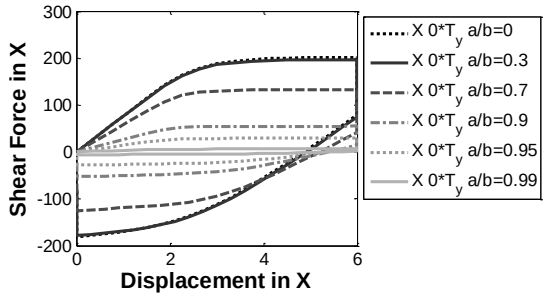

c. Case B1 in *X* for 0*T_y

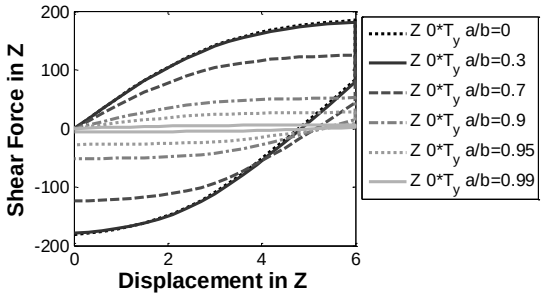

d. Case B1 in *Z* for 0*T_y

Figure 4.18. Cases A1 and B1 for *X* and *Z* directions for solid and hollow circular sections for different a/b ratio under cyclic loading.

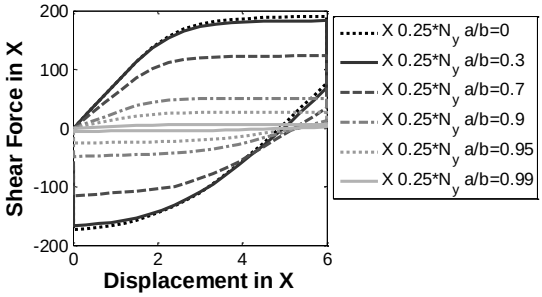

a. Case A2 in *X* for $0.25*N_y$

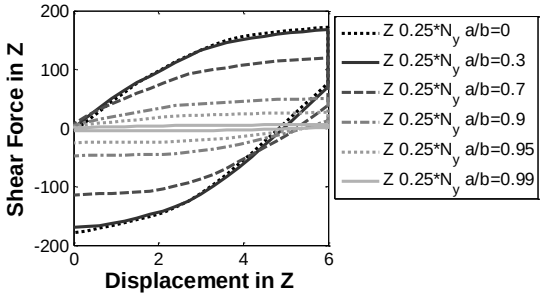

b. Case A2 in *Z* for $0.25*N_y$

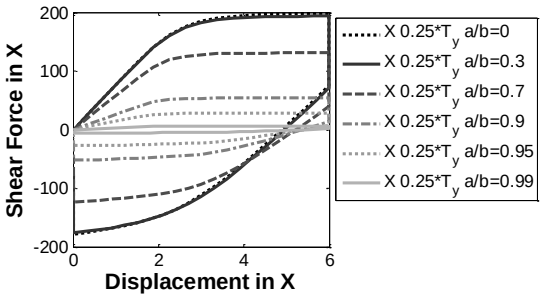

c. Case B2 in *X* for $0.25*T_y$

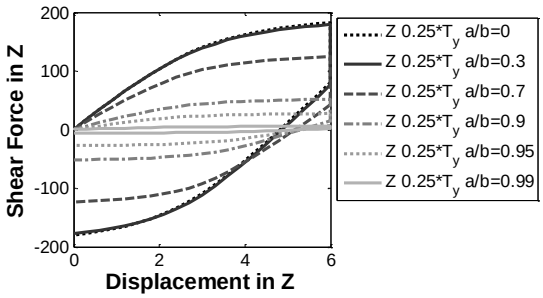

d. Case B2 in *Z* for $0.25*T_y$

Figure 4.19. Cases A2 and B2 for *X* and *Z* directions for solid and hollow circular sections for different a/b ratio under cyclic loading.

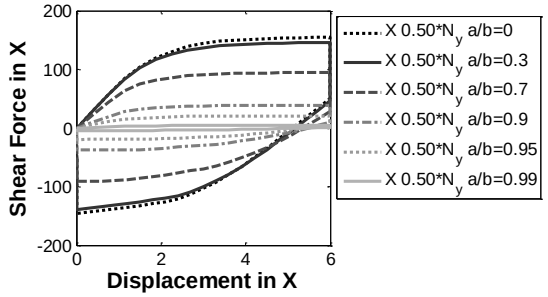

a. Case A3 in *X* for 0.50*N_y

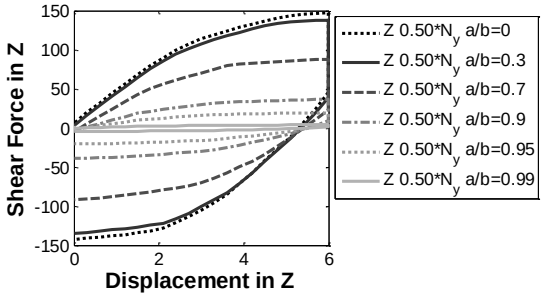

b. Case A3 in *Z* for 0.50*N_y

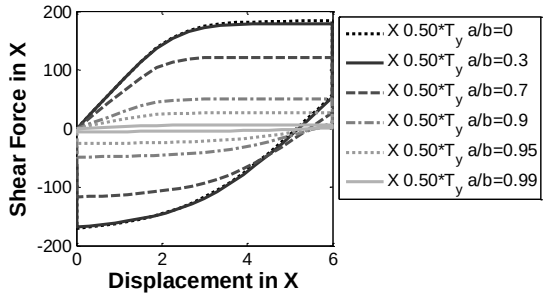

c. Case B3 in *X* for 0.50*T_y

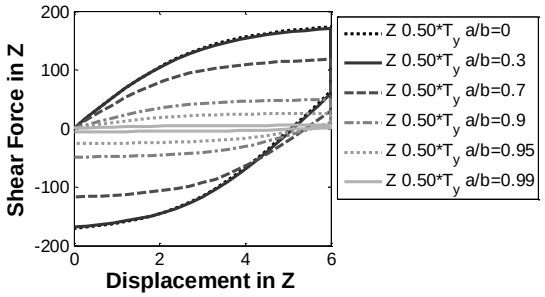

d. Case B3 in *Z* for 0.50*T_y

Figure 4.20. Cases A3 and B3 for *X* and *Z* directions for solid and hollow circular sections for different a/b ratio under cyclic loading.

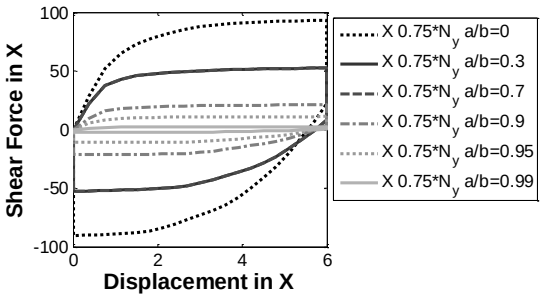

a. Case A4 in *X* for 0.75*N_y

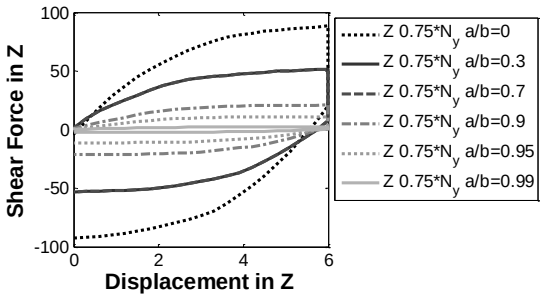

b. Case A4 in *Z* for 0.75*N_y

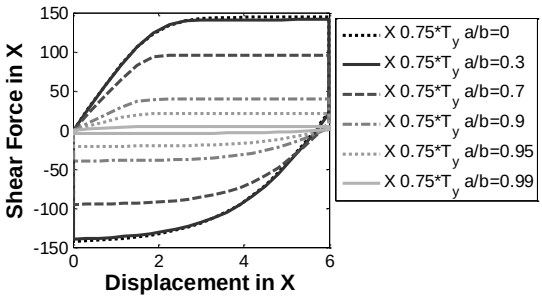

c. Case B4 in *X* for 0.75*T_y

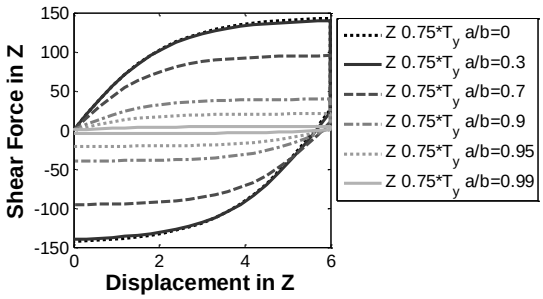

d. Case B4 in *Z* for 0.75*T_y

Figure 4.21. Cases A4 and B4 for *X* and *Z* directions for solid and hollow circular sections for different a/b ratio under cyclic loading.

Since capacity of the members with thin-walled sections is low compared to the sections with thick-walled sections in the above figures, an effort may be required to see values especially corresponding to $a/b = 0.99$. Therefore, responses of cyclically loaded members with thin-walled sections are plotted again with more consistent scale in terms of global *X* and *Z* directions for a/b ratio is equal to 0.9, 0.95 and 0.99 in Figure 4.22 to Figure 4.24. But this time, varitaion of nonlinear response with different level of loading is given in the same figure for each a/b ratio.

According to the Figure 4.22 to Figure 4.24, as axial load and torsion increase, capacity of the section decreases which is a reasonable situation as observed previously for member with solid section. However, for thin walled sections, the effect of axial load and torsion on nonlinear behavior is more pronounced than the effect of same parameters on solid circular section. Dependency of the nonlinear response on the direction of loading is more clear in the thin-walled circular sections and this can be also seen from the figures.

As mentioned previously, it is observed that the influence of torsion on nonlinear behavior is less important compared to the effect of axial load for solid circular sections. However, for thin walled sections, coupling of torsion has a worthy effect to be considered besides the importance of axial load on nonlinear response of members with hollow circular sections. The results of the nonlinear examples presented so far confirm that the proposed 3d mixed beam element have the ability of capturing this interaction providing a credit for reliable nonlinear analysis of members with various sections and under miscellaneous loading and boundary conditions.

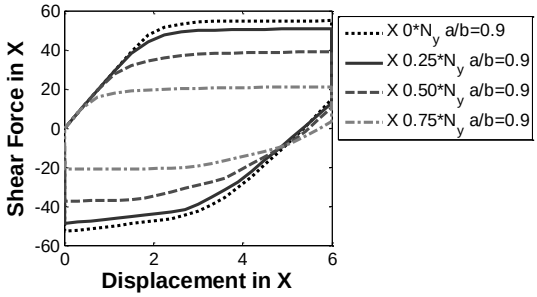

a. Base shear force vs. tip displacement in *X* for different level of N_y and a/b=0.9

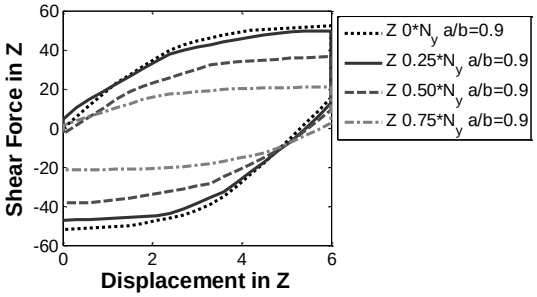

b. Base shear force vs. tip displacement in *Z* for different level of N_y and a/b=0.9

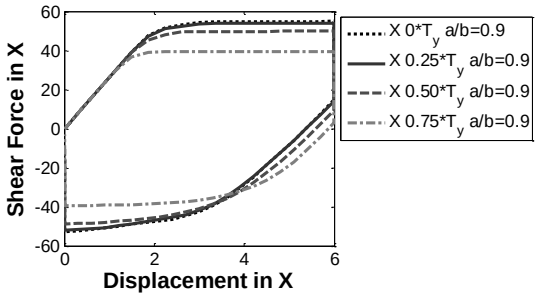

c. Base shear force vs. tip displacement in *X* for different level of T_y and a/b=0.9

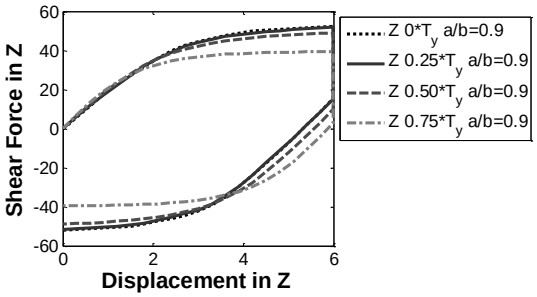

d. Base shear force vs. tip displacement in *Z* for different level of T_y and a/b=0.9

Figure 4.22. Base shear vs. tip displacement in global *X* and *Z* directions under cyclic loading for hollow circular sections for a/b ratio is equal to 0.90.

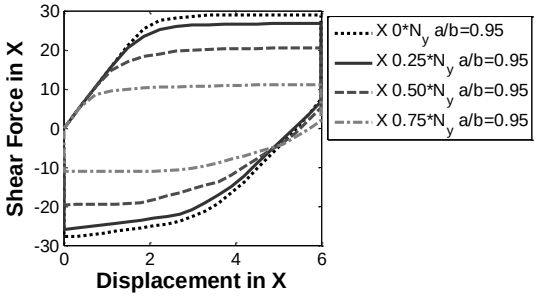

a. Base shear force vs. tip displacement in *X* for different level of N_y and a/b=0.95

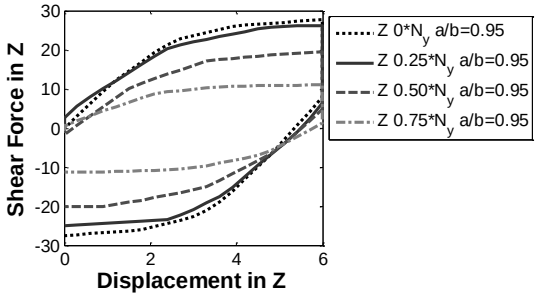

b. Base shear force vs. tip displacement in *Z* for different level of N_y and a/b=0.95

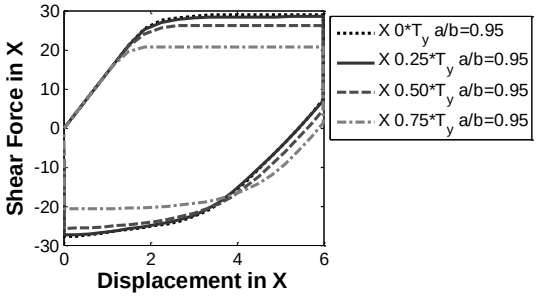

c. Base shear force vs. tip displacement in *X* for different level of T_y and a/b=0.95

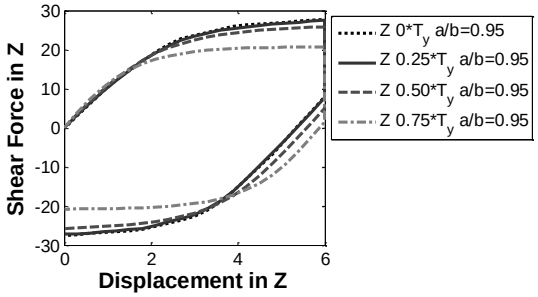

d. Base shear force vs. tip displacement in *Z* for different level of T_y and a/b=0.95

Figure 4.23. Base shear vs. tip displacement in global *X* and *Z* directions under cyclic loading for hollow circular sections for a/b ratio is equal to 0.95.

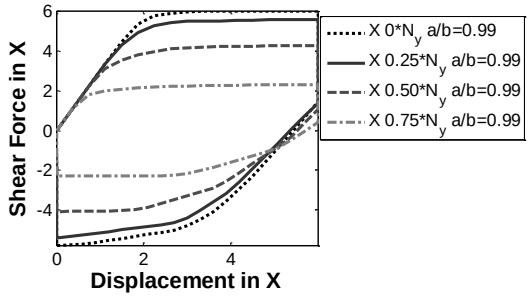

a. Base shear force vs. tip displacement in *X* for different level of N_y and a/b=0.99

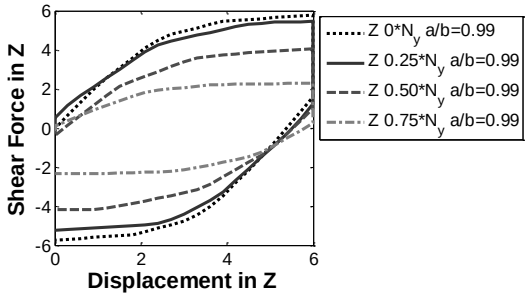

b. Base shear force vs. tip displacement in *Z* for different level of N_y and a/b=0.99

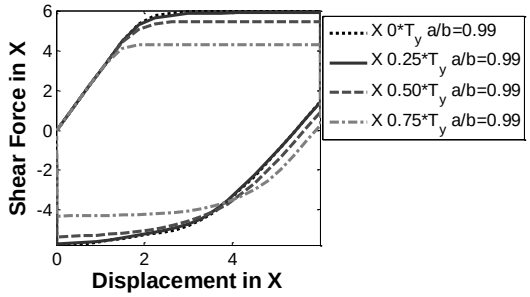

c. Base shear force vs. tip displacement in *X* for different level of T_y and a/b=0.99

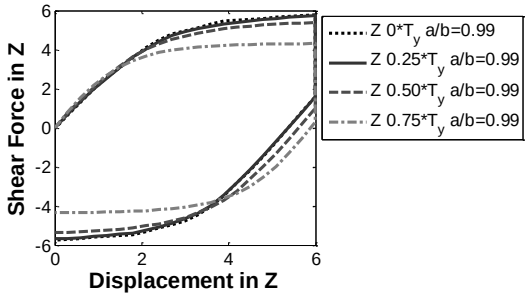

d. Base shear force vs. tip displacement in *Z* for different level of T_y and a/b=0.99

Figure 4.24. Base shear vs. tip displacement in global *X* and *Z* directions under cyclic loading for hollow circular sections for a/b ratio is equal to 0.99.

4.3.4. Nonlinear Analysis of Uniform Fixed-Fixed Pipe

In this section, nonlinear responses of the proposed 3d mixed beam element (abbreviated as proposed MF) and Euler-Bernoulli version of the current mixed formulation Timoshenko beam element (abbreviated as EB-MF) are compared with some of the examples presented in the study of Nowzartash and Mohareb [55] for the same loading, material, geometry and boundary conditions stated in those examples.

The properties of the proposed MF element are already explained in the previous parts. When the EB-MF element is considered, it should be noted that that element is capable of taking into account the existence of inelasticity due to material for normal stress oriented along element length. Moreover, the element assumes that the shear stresses on the section are elastic and caused by application of no loads other than torsion.

The element presented by Nowzartash and Mohareb [55] is abbreviated as P3D2HE in that study where the letter "P" stands for the pipe section that is used in the analysis of elevated and submerged steel pipes, "3D" stands for a 3d lumped plasticity beam element, "2H" denotes two probable plastic hinges at both nodes and "E" designates the yield surface. It is worth mentioning that the element by Nowzartash and Mohareb assumes that the response of the element is elastic perfectly plastic where the plasticity is lumped at plastic hinges at element end nodes having zero length. Hence, a priori calculation/estimation of sectional geometric parameters and yield and plastic capacities of section forces is needed due to deficiency of the formulation of the element. Therefore in some examples in the aforementioned study, only the fomation of first plastic hinge is taken into consideration not presenting parameters related with formation of other hinges. However, the proposed MF element does not have to cope with that kind of hindrances since its formulation is based on fiber discretization model for section

state determination and it uses distributed inelasticity formulation for element state determination.

The results of the nonlinear analyses which exist in the study of Nowzartash and Mohareb that are used to compare the P3D2HE element with the elements B33, PIPE31, FRAME3D and ELBOW31 that are readily available in the library of ABAQUS [63] are also made use of for the verification of the proposed MF element together with the EB-MF element.

It is tedious and needless to mention whole of the features of all elements that are used in the comparison of nonlinear response. Therefore, it is preferred only to summarize characteristic properties of elements in Table 4.2 and suggested referring to the study by Nowzartash and Mohareb [55] for more detailed discussion. Euler-Bernoulli and Timoshenko beam theories are abbreviated as "EBT" and "TBT", respectivelly as mentioned previously in Section 3.4.

Table 4.2. Features of elements used in comparison of nonlinear responses

Element Name	**Element Type**	**Beam Formulation**	**Number of nodes / element**	**Number of dofs**
B33	EBT	DB	2 end nodes	6 per node
PIPE31	TBT (shear elastic)	DB	2 end nodes	6 per node
FRAME3D	EBT (lumped plasticity)	DB	2 end nodes 1 intermediate node	6 per end nodes 3 for intermediate
ELBOW31	TBT	DB	2 end nodes	6 per node
P3D2HE	TBT (lumped plasticity)	DB	2 end nodes	6 per node
EB-MF	EBT	MF	2 end nodes	6 per node
Proposed MF	TBT	MF	2 end nodes	6 per node

Nowzartash and Mohareb dealt with a DN90 STD pipe section that has an outer diameter 101.6 mm, thickness 5.74 mm, elastic modulus 200 GPa, yield strength 350 MPa and Poisson's ratio 0.3 in their study. Following loading cases for the same pipe are presented for verification purposes in this thesis.

4.3.4.1. Combined Bending and Torsion of a Long Fixed-Fixed Pipe

In the first loading case, a vertical load, P (kN) directed towards beam axis perpendicularly and torque, $T = P$ (kN.m) surrounding the beam axis at the same point of application of the vertical load are exerted on a 6m fixed-fixed pipe. All the loads are applied to the second node which is 4m away from the fixed-end node 1 and 2m away from the other fixed-end node 3. Nonlinear response of the pipe under that loading is investigated by monitoring node 2 as depicted in Figure 4.25.

It can be deduced from the figure that proposed MF is able to appropriately reflect the influence of the combined effects of the vertical and torsion loads applied on the member with only two elements per span. However, 120 ELBOW31 and 48 B33 or PIPE31 displacement based elements are needed to catch similar nonlinear response for the case of long member.

Although EB-MF overestimates the nonlinear response, it is successful in modeling the elastic portion of the plastic curve with only two elements per member span. Main reason of this condition is the dominance of flexural effects rather than shear effects since the length of the member is long enough that shear effects do not come into prominence. Therefore, it can be used preferably for the elastic analysis of sufficiently long beams due to its computational efficiency.

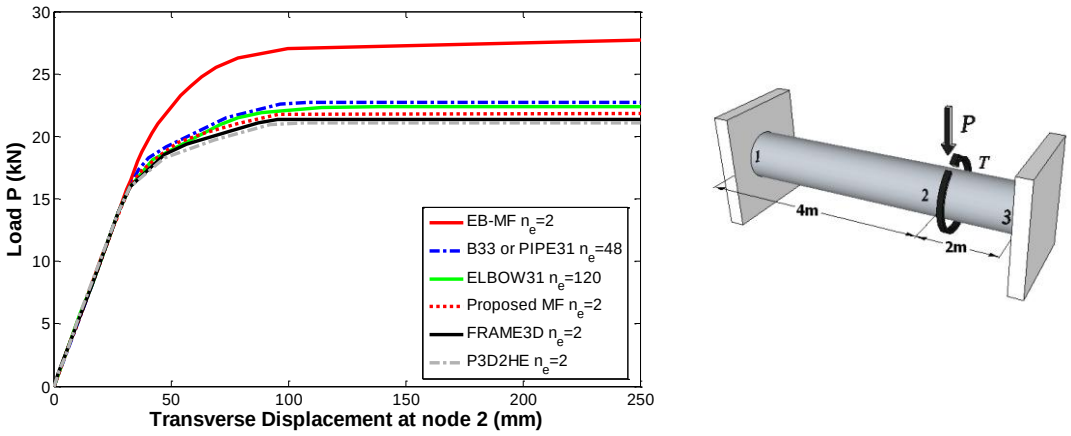

Figure 4.25. Comparison of load vs. transverse displacement at node 2 for long pipe.

4.3.4.2. Bending of a Short Fixed-Fixed Pipe

In the second loading case, the total length of the pipe is shortened to 1m and only a vertical load pointing perpendicularly towards beam axis is applied to the second node which is 0.8m from fixed-end node 1 as shown in Figure 4.26.

In this case proposed MF element is the most successful element that captures the nonlinear behavior with only two elements per member span by converging the theoretical value 189.5 kN-m obtained with upper bound theorem as given by Nowzartash and Mohareb [55]. That condition gives evidence that the proposed MF element is good at modeling nonlinear behavior not only for long beams but also for short beams without any shear locking.

FRAME3D, EB-MF and PIPE31 are incapable of modeling even elastic portion of the entire response since the member is short and those elements neglect shear deformation effects due to EBT assumption although FRAME3D was successful for

the case of long beam in the previous comparison. ELBOW31 elements and P3D2HE elements coincide for the elastic portion of the entire response whereas the former overestimates even with 100 elements and the latter underestimates with two elements per member span the nonlinear response.

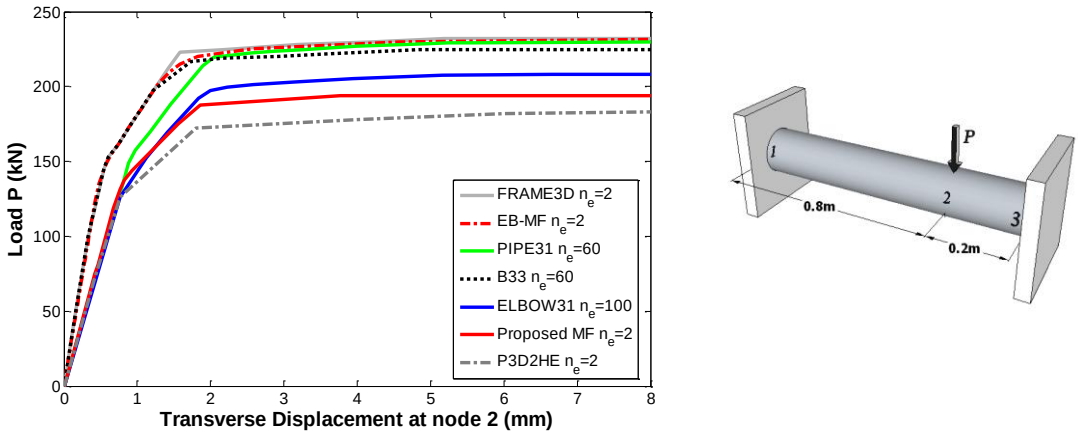

Figure 4.26. Comparison of load vs. transverse displacement at node 2 for short pipe.

CHAPTER 5

FREE VIBRATION OF MIXED ELEMENT

5.1. INTRODUCTION

It is important to consider rotatory inertia and shear effects in determination of the free vibration response of special types of structures like, chimneys, pier of a deck, tower of wind turbines, etc. Therefore, computation of consistent mass and stiffness matrices accurately are also important for especially determination of higher order vibration modes of structures.

In this chapter, derivation of 3d displacement based and flexibility based consistent mass matrices are presented and the advantages of the latter are displayed in the subsequent chapter by carrying out linear elastic free vibration analysis of the proposed 3d mixed beam element and comparing its several higher order vibration frequencies with the closed form solutions and frequencies that are obtained from a finite element software.

5.2. DISPLACEMENT BASED MASS MATRIX

Dynamic response of an element can be modeled using displacement based approach by requiring the work done by external forces is equal to the work done by inertial, viscous and internal forces for small displacements as follows [31];

$$\int_{\Omega} \delta\mathbf{u}^{\mathrm{T}}\mathbf{b}d\Omega + \int_{\Gamma} \delta\mathbf{u}^{\mathrm{T}}\mathbf{t}d\Gamma + \sum_{i=1}^{n} \delta\mathbf{u}_i^{\mathrm{T}}\,\mathbf{p}_i = \int_{\Omega} (\delta\boldsymbol{\varepsilon}^{\mathrm{T}}\boldsymbol{\sigma} + \delta\mathbf{u}^{\mathrm{T}}\rho\ddot{\mathbf{u}} + \delta\mathbf{u}^{\mathrm{T}}\kappa_{\mathrm{d}}\dot{\mathbf{u}})\, d\Omega \qquad (5.1)$$

In Equation (5.1), $\mathbf{p}_i$ denotes the concentrated loads acting on "n" different points of the member which are usually nodal points, ρ is the mass density of the material, κ_{d} is a parameter that deals with the material-damping, and other parameters are defined in the previous sections. The displacement field, $\mathbf{u}$ and its first two derivatives with respect to time denoted with dotted accent sign can be shown as follows;

$$\mathbf{u} = \mathbf{N}\bar{\boldsymbol{u}} \qquad \dot{\mathbf{u}} = \mathbf{N}(\dot{\bar{\boldsymbol{u}}}) \qquad \ddot{\mathbf{u}} = \mathbf{N}(\ddot{\bar{\boldsymbol{u}}}) \qquad (5.2)$$

In Equation (5.2), $\mathbf{N}$ denotes the shape functions components of which are given in the previous sections for 3d version of the displacement based element of Friedman and Kosmatka [12]. If Equation (5.2) is substituted into Equation (5.1) and necessary arrangements are done, then following expression is obtained.

$$\delta\bar{\mathbf{u}}^{\mathrm{T}}\left[\int_{\Omega} \mathbf{B}^{\mathrm{T}}\boldsymbol{\sigma}d\Omega + \int_{\Omega} \rho\mathbf{N}^{\mathrm{T}}\mathbf{N}d\Omega\,(\ddot{\bar{\boldsymbol{u}}}) + \int_{\Omega} \kappa_{\mathrm{d}}\mathbf{N}^{\mathrm{T}}\mathbf{N}d\Omega\,(\dot{\bar{\boldsymbol{u}}}) - \int_{\Omega} \mathbf{N}^{\mathrm{T}}\mathbf{b}d\Omega - \int_{\Gamma} \mathbf{N}^{\mathrm{T}}\mathbf{t}d\Gamma - \sum_{i=1}^{n} \mathbf{p}_i\right] = 0 \qquad (5.3)$$

In Equation (5.3), element mass, $\boldsymbol{m}$ and damping, $\boldsymbol{c}$ matrices are defined as follows;

$$\boldsymbol{m} = \int_{\Omega} \rho \mathbf{N}^{\mathrm{T}} \mathbf{N} d\Omega \tag{5.4}$$

$$\boldsymbol{c} = \int_{\Omega} \kappa_{\mathrm{d}} \mathbf{N}^{\mathrm{T}} \mathbf{N} d\Omega \tag{5.5}$$

If Equations (5.4) and (5.5) are substituted into Equation (5.3);

$$\boldsymbol{m}(\ddot{\bar{\boldsymbol{u}}}) + \boldsymbol{c}(\dot{\bar{\boldsymbol{u}}}) + \boldsymbol{r}_{int} = \boldsymbol{r}_{ext} \tag{5.6}$$

where element internal and external load vectors are $\boldsymbol{r}_{int}$ and $\boldsymbol{r}_{ext}$, respectively and given as follows;

$$\boldsymbol{r}_{int} = \int_{\Omega} \mathbf{B}^{\mathrm{T}} \boldsymbol{\sigma} d\Omega \tag{5.7}$$

$$\boldsymbol{r}_{ext} = \int_{\Omega} \mathbf{N}^{\mathrm{T}} \mathbf{b} d\Omega + \int_{\Gamma} \mathbf{N}^{\mathrm{T}} \mathbf{t} d\Gamma + \sum_{\mathrm{i}=1}^{\mathrm{n}} \mathbf{p}_{\mathrm{i}} \tag{5.8}$$

No matter the material is linear or nonlinear, Equation (5.6) can be utilized for dynamic analysis. If stresses on the element are linear function of strains, then internal load vector can be obtained by using the stiffness matrix, $\boldsymbol{k}$ and Equation (5.6) becomes;

$$\boldsymbol{m}(\ddot{\bar{\boldsymbol{u}}}) + \boldsymbol{c}(\dot{\bar{\boldsymbol{u}}}) + \boldsymbol{k}(\bar{\boldsymbol{u}}) = \boldsymbol{r}_{ext} \tag{5.9}$$

If it is assumed that there is no external load acting on the system that is analyzed and damping is negligible, then free vibration analysis of the assembled structure can be carried out by using the following expression;

$$\mathbf{M\ddot{U}} + \mathbf{KU} = \mathbf{0} \tag{5.10}$$

The mass matrix obtained by using the procedure presented above will be "consistent mass matrix" because the shape functions used for determining the mass matrix are the same with the shape functions used for determination of the stiffness matrix. Moreover the mass matrix will be capable of incorporating the effects of shear deformations and rotary inertia since shape functions include those effects in the formulation. Lumped mass matrix that lumps some portion of the mass to the nodes of the element is also an alternative in the dynamic analysis but lumping neglects shear deformations and rotary inertia although it is possible to include the latter for the rotational dofs.

Consistent mass matrix considers effects that lumped mass matrix does not and they can be used interchangeably depending on the analysis case. Lumped mass matrix necessitates lower computational effort since it is a diagonal matrix. Although, the rotational dofs can be eliminated from a lumped mass matrix by static condensation, it is not possible to discard rotational and translational dofs from a consistent mass matrix [64]. However, for some types of structures like bridges, chimneys, dams, nuclear facilities, and etc., lumped-mass idealization is not preferred much [32].

Although it is not shown separately in this thesis, it is found that the consistent mass matrix obtained by using displacement based approach and shape functions of

Friedman and Kosmatka [12] is the same with the consistent mass matrix obtained by using flexibility based approach for a uniform member. However, special shape functions are needed to obtain accurate consistent mass matrices by using displacement based approach for a member which is not uniform or homogeneous whereas flexibility based approach does not necessitate such kind of an additional effort since it is possible to obtain accurate consistent mass matrices for members with any nonuniformity in geometry or heterogeneity in material with this approach due to its nature as explained in the subsequent section.

5.3. FLEXIBILITY BASED MASS MATRIX

Flexibility-based approach by Molins et al. [44] is utilized and presented in this part in order to derive 3d consistent mass matrix. The procedure enables obtaining not only consistent mass matrices of members having uniform sections but also mass matrices of members having non-uniform sections by taking into account the actual distribution of mass within the member without any need for interpolation of the displacement field.

The novelty of this thesis is the utilization of the flexibility based consistent mass matrix that is offered by Molins et al. [44] and the stiffness matrix of the proposed mixed formulation element to compare the first several free vibration frequencies of various cantilever beams having different cross sections and uniformity in the next chapter. Therefore, in order to provide integrity and consistency throughout the thesis the derivation of the flexibility based consistent mass matrix is presented in accordance with the symbolic expressions used in this thesis.

5.3.1. Equilibrium of the Element

In the formulation, instead of the simply supported basic system that is explained in Section 3.2.1, a cantilever basic system is adapted for formulation, where this beam is fixed at node i and free at node j. Therefore, Equation (3.53) remains nearly the same with the expression given as Equation (5.11) but the force interpolation matrix for the cantilever beam, $\boldsymbol{b_c}(x, L)$ and forces due to distributed loads, $\boldsymbol{s_p}^*(x)$ are introduced as follows;

$$\boldsymbol{s}(x) = \boldsymbol{b_c}(x, L)\boldsymbol{q_L} + \boldsymbol{s_p}^*(x) \tag{5.11}$$

where

$$\boldsymbol{b_c}(x, L) = \begin{bmatrix} 1 & 0 & 0 & 0 & 0 & 0 \\ 0 & 1 & 0 & 0 & 0 & 0 \\ 0 & 0 & 1 & 0 & 0 & 0 \\ 0 & 0 & 0 & 1 & 0 & 0 \\ 0 & 0 & (x-L) & 0 & 1 & 0 \\ 0 & (L-x) & 0 & 0 & 0 & 1 \end{bmatrix} \tag{5.12}$$

$$\boldsymbol{s_p}^*(x) = \int_{\boldsymbol{x}}^{\boldsymbol{L}} \boldsymbol{b_c}(x, \xi)\, \boldsymbol{w} d\xi \tag{5.13}$$

Equation (5.11) relates the basic end forces at the free end, $\boldsymbol{q_L}$ to the internal section forces $\boldsymbol{s}(x)$ by the help of force interpolation matrix $\boldsymbol{b_c}(x, L)$ that gives the exact equilibrium of forces between sections that are x units and L units away from the fixed end of the member, respectively. To sum up, the equation relates the forces at free end to the forces at any section of the member. In Equation (5.13), $\boldsymbol{w}$ stands for the distributed loads on the member. In the following equations, expressions with

subscript " 0" and "L" denote parameters at fixed and free ends of the member, respectively.

5.3.2. Element Displacements and Deformations

The beam element in complete system has displacements at node i, as well. Displacements at free end of the member, $\boldsymbol{u_L}$ can be related to the displacements at the fixed end of the member, $\boldsymbol{u_0}$ as follows by using the basic system of cantilever beam;

$$\boldsymbol{u_L} = \boldsymbol{b_c}^{\mathrm{T}}(0, L)\boldsymbol{u_0} + \int_0^L \boldsymbol{b_c}^{\mathrm{T}}(x, L)\boldsymbol{e}(\mathrm{x})dx \tag{5.14}$$

The term with the integral sign in Equation (5.14) corresponds to the movement of the free end caused by the deformation, $\mathbf{v}$ of the cantilever beam element that is similar to the expression given in Equation (3.9).

$$\mathbf{v} = \boldsymbol{u_L} - \boldsymbol{b_c}^{\mathrm{T}}(0, L)\boldsymbol{u_0} = \int_0^L \boldsymbol{b_c}^{\mathrm{T}}(x, L)\boldsymbol{e}(\mathrm{x})dx \tag{5.15}$$

5.3.3. Response of the Element

It is possible to relate sectional forces to sectional deformations as given in Equation (4.5) through section stiffness matrix under linear elastic material response as follows;

$$\boldsymbol{k}_{\mathrm{S}} = \begin{bmatrix} \int_A EdA & 0 & 0 & 0 & \int_A EzdA & -\int_A EydA \\ & GA_{s_y} & 0 & 0 & 0 & 0 \\ & & GA_{s_z} & 0 & 0 & 0 \\ & & & GJ & 0 & 0 \\ & & & & \int_A Ez^2dA & -\int_A EyzdA \\ & sym. & & & & \int_A Ey^2dA \end{bmatrix} \tag{5.16}$$

Where E is the modulus of eleasticity of a material point, G is the shear modulus, J is the torsional inertia, A_{s_y} and A_{s_z} are the shear corrected areas.

Equation (4.5) can be rearranged as follows;

$$\boldsymbol{e}(x) = \boldsymbol{k_s}^{-1}(x)\boldsymbol{s}(x) \tag{5.17}$$

If Equation (5.17) is substituted into Equation (5.15), following expression is obtained;

$$\mathbf{v} = \boldsymbol{u_L} - \boldsymbol{b_c}^{\mathrm{T}}(0, L)\boldsymbol{u_0} = \int_0^L \boldsymbol{b_c}^{\mathrm{T}}(x, L)\boldsymbol{k_s}^{-1}(x)\boldsymbol{s}(x)dx \tag{5.18}$$

Basic end forces at the fixed end, $\boldsymbol{q_0}$ and free end $\boldsymbol{q_L}$ can be associated with the internal section forces at any point along the element with the help of Equation (5.11). If Equation (5.11) is substituted into Equation (5.18), following expression is obtained;

$$\mathbf{v} = \int_0^L \left(\boldsymbol{b_c}^{\mathrm{T}}(x, L)\boldsymbol{k_s}^{-1}(x)\boldsymbol{b_c}(x, L)\boldsymbol{q_L} + \boldsymbol{b_c}^{\mathrm{T}}(x, L)\boldsymbol{k_s}^{-1}(x)\boldsymbol{s_p}^{*}(x)\right)dx \tag{5.19}$$

Equation (5.19) can be given in more compact form as follows;

$$\mathbf{v} = \mathbf{F}\boldsymbol{q_L} + \mathbf{v}^* \tag{5.20}$$

where element flexibility matrix of the member, $\mathbf{F}$ and vector of deformations at free end due to the distributed loads in its isostatic case, $\mathbf{v}^*$ is defined as;

$$\mathbf{F} = \int_0^L \boldsymbol{b_c}^{\mathrm{T}}(x, L)\boldsymbol{k_s}^{-1}(x)\boldsymbol{b_c}(x, L)dx \tag{5.21}$$

$$\mathbf{v}^* = \int_0^L \boldsymbol{b_c}^{\mathrm{T}}(x, L)\boldsymbol{k_s}^{-1}(x)\boldsymbol{s_p}^*(x)\,dx \tag{5.22}$$

Stiffness matrix of an element can be obtained by relating forces and end node displacements of free end of the element by combining Equation (5.20) and left side of Equation (5.15) as follows;

$$\boldsymbol{q_L} = -\mathbf{F}^{-1}\boldsymbol{b_c}^{\mathrm{T}}(0, L)\boldsymbol{u_0} + \mathbf{F}^{-1}\boldsymbol{u_L} - \mathbf{F}^{-1}\mathbf{v}^* \tag{5.23}$$

Similar expression is obtained for the fixed end of the element by combining Equations (5.11) and (5.23) as follows;

$$\boldsymbol{q_0} = \boldsymbol{b_c}^{\mathrm{T}}(0, L)\left(-\mathbf{F}^{-1}\boldsymbol{b_c}^{\mathrm{T}}(0, L)\boldsymbol{u_0} + \mathbf{F}^{-1}\boldsymbol{u_L} - \mathbf{F}^{-1}\mathbf{v}^*\right) + \boldsymbol{q_0}^* \tag{5.24}$$

It is possible to express Equations (5.23) and (5.24) in matrix form as follows;

$$\begin{bmatrix}\boldsymbol{q_0}\\ \boldsymbol{q_L}\end{bmatrix} = \begin{bmatrix}-\boldsymbol{b_c}^{\mathrm{T}}(0, L)\mathbf{F}^{-1}\boldsymbol{b_c}^{\mathrm{T}}(0, L) & \boldsymbol{b_c}^{\mathrm{T}}(0, L)\mathbf{F}^{-1}\\ -\mathbf{F}^{-1}\boldsymbol{b_c}^{\mathrm{T}}(0, L) & \mathbf{F}^{-1}\end{bmatrix}\begin{bmatrix}\boldsymbol{u_0}\\ \boldsymbol{u_L}\end{bmatrix} - \begin{bmatrix}\boldsymbol{b_c}^{\mathrm{T}}(0, L)\mathbf{F}^{-1}\mathbf{v}^* - \boldsymbol{q_0}^*\\ \mathbf{F}^{-1}\mathbf{v}^*\end{bmatrix} \tag{5.25}$$

Equation (5.25) can be given in a more simpler form as follows;

$$\mathbf{P} = \mathbf{K}\mathbf{U} + \mathbf{P}^* \tag{5.26}$$

where **P** is the vector of end forces, **K** is the stiffness matrix of the element, **U** is the vector of end displacements and $\mathbf{P}^*$ is the vector of reactions caused by fixed end of the element.

5.3.4. Mass Matrix Based on Flexibility Method

Inertia forces that act on a section, $\boldsymbol{f_I}(x)$ can be calculated by the following expression by assuming that cross-sections in the member move as rigid bodies in their own plane.

$$\boldsymbol{f_I}(x) = \mathbf{M_s}(x)\ddot{\boldsymbol{u}}(x) \tag{5.27}$$

where

Sectional mass matrix, $\mathbf{M_s}(x)$ and vector of accelaration of a point on the axis, $\ddot{\boldsymbol{u}}(x)$ are given as follows;

$$\mathbf{M_s}(x) = \int_A \begin{bmatrix} \rho & 0 & 0 & 0 & \rho z & -\rho y \\ 0 & \rho & 0 & -\rho z & 0 & 0 \\ 0 & 0 & \rho & \rho y & 0 & 0 \\ 0 & -\rho z & \rho y & \rho(y^2+z^2) & 0 & 0 \\ \rho z & 0 & 0 & 0 & \rho z^2 & -\rho yz \\ -\rho y & 0 & 0 & 0 & -\rho yz & \rho y^2 \end{bmatrix} dA \tag{5.28}$$

$$\ddot{\boldsymbol{u}}(x) = \begin{bmatrix} \ddot{u}_x(x) & \ddot{u}_y(x) & \ddot{u}_z(x) & \ddot{\theta}_x(x) & \ddot{\theta}_y(x) & \ddot{\theta}_z(x) \end{bmatrix}^{\mathrm{T}} \tag{5.29}$$

If it is assumed that there is not any distributed loads on the element and Equations (5.14), (5.17) and (5.23) are rearranged, following expression is obtained;

$$\boldsymbol{e}(x) = \boldsymbol{k_s}^{-1}(x)\boldsymbol{b_c}(x,L)\left(-\mathbf{F}^{-1}\boldsymbol{b_c}^{\mathrm{T}}(0,L)\boldsymbol{u_0} + \mathbf{F}^{-1}\boldsymbol{u_L}\right) \tag{5.30}$$

If Equation (5.30) is substituted into Equation (5.14), following expression is obtained;

$$\boldsymbol{u}(x) = \boldsymbol{G}(x)\begin{bmatrix}\boldsymbol{u_0}\\ \boldsymbol{u_L}\end{bmatrix} \tag{5.31}$$

Equation (5.31) relates exactly displacements of any point in the axis of the member to the nodal displacmenets if the deformation of the member is only due to the end node displacements. However, if there are also distributed loads acting on the element, then the equation is approximate. The matrix that relates nodal displacements to the displacements on the section, $\boldsymbol{G}(x)$ has the following form;

$$\boldsymbol{G}(x) = \left[\boldsymbol{b_c}^{\mathrm{T}}(0,x) - \mathbf{F_s}(x)\mathbf{F}^{-1}\boldsymbol{b_c}^{\mathrm{T}}(0,L) \quad \mathbf{F_s}(x)\mathbf{F}^{-1}\right] \tag{5.32}$$

$$\mathbf{F_s}(x) = \int_0^x \boldsymbol{b_c}^{\mathrm{T}}(\xi,x)\boldsymbol{k_s}^{-1}(x)\boldsymbol{b_c}(\xi,L)d\xi \tag{5.33}$$

It is possible to adapt and use the same logic in Equation (5.13) that is valid for static condition and use d'Alembert's principle to obtain the inertia forces caused by loads distributed on the basic isostatic configuration by replacing $\boldsymbol{w}$ with $\boldsymbol{f_I}(\xi)$ as follows;

$$\boldsymbol{s_p}^*(x) = \int_x^L \boldsymbol{b_c}(x,\xi)\,\boldsymbol{f_I}(\xi)d\xi \tag{5.34}$$

Equations (5.27) and (5.31) can be combined to obtain inertia forces as follows;

$$\boldsymbol{f_I}(\xi) = \mathbf{M_s}\boldsymbol{G}(\xi)\begin{bmatrix}\ddot{\boldsymbol{u}}_{\boldsymbol{0}}\\ \ddot{\boldsymbol{u}}_{\mathbf{L}}\end{bmatrix} \tag{5.35}$$

Equation (5.34) can be substituted into Equation (5.22) and following expression is obtained;

$$\mathbf{v}^* = \int_0^L \boldsymbol{b_c}^{\mathrm{T}}(x,L)\boldsymbol{k_s}^{-1}(x)\int_x^L \boldsymbol{b_c}(x,\xi)\,\boldsymbol{f_I}(\xi)d\xi dx \tag{5.36}$$

If Equations (5.35) and (5.36) are substituted into Equation (5.25), mass matrix, **M** of the whole element can be obtained with the realization of the fact that $\mathbf{P}^*$ is the product of the mass matrix by the node accelerations.

$$\mathbf{M} = \begin{bmatrix} \mathbf{m_{11}} & \mathbf{m_{12}} \\ \mathbf{m_{21}} & \mathbf{m_{22}} \end{bmatrix} \tag{5.37}$$

$$\mathbf{m_{22}} = \mathbf{F}^{-1} \int_0^L \boldsymbol{b_c}^{\mathrm{T}}(x, L) \boldsymbol{k_s}^{-1}(x) \left(\int_x^L \boldsymbol{b_c}(x, \xi)\, \mathbf{M_s}(\xi) \mathbf{F_s}(\xi) \mathbf{F}^{-1} d\xi \right) dx \tag{5.38}$$

$$\begin{aligned} \mathbf{m_{21}} = \mathbf{F}^{-1} \int_0^L \boldsymbol{b_c}^{\mathrm{T}}(x, L) \boldsymbol{k_s}^{-1}(x) \Bigg(\int_x^L \boldsymbol{b_c}(x, \xi)\, \mathbf{M_s}(\xi) \Big(\boldsymbol{b_c}^{\mathrm{T}}(0, \xi) \\ - \mathbf{F_s}(\xi) \mathbf{F}^{-1} \boldsymbol{b_c}^{\mathrm{T}}(0, L) \Big) d\xi \Bigg) dx \end{aligned} \tag{5.39}$$

$$\mathbf{m_{12}} = \mathbf{m_{21}}^{\mathrm{T}} = -\boldsymbol{b_c}(0, L) \mathbf{m_{22}} + \int_0^L \boldsymbol{b_c}(0, x)\, \mathbf{M_s}(x) \mathbf{F_s}(x) \mathbf{F}^{-1} dx \tag{5.40}$$

$$\begin{aligned} \mathbf{m_{11}} = -\boldsymbol{b_c}(0, L) \mathbf{m_{21}} \\ + \int_0^L \boldsymbol{b_c}(0, x)\, \mathbf{M_s}(x) \Big(\boldsymbol{b_c}^{\mathrm{T}}(0, x) - \mathbf{F_s}(x) \mathbf{F}^{-1} \boldsymbol{b_c}^{\mathrm{T}}(0, L) \Big) dx \end{aligned} \tag{5.41}$$

Contrary to the derivation given in this thesis, the derivation by Molins et al. [44] necessitates taking transpose of the first term after integral sign, $\boldsymbol{b_c}(0, x)$ in Equations (5.40) and (5.41). However, a step by step derivation reveals that there is no need to take transpose. The study by Molins et al. is so neat and straightforward that the probability of misprint in that document is higher than a mistake in the

formulation. The work presented by Molins et al. by the way did not provide elaborate comparisons of the numerical accuracy of the presented consistent mass matrix via exact solutions, but only provided numerical analysis on historical bridges under seismic action. In that regards, the strength of their formulation remained relatively unnoticed in the literature.

There are numerous advantages of the flexibility based mass matrix obtained by the above procedure. With this approach, it is possible to obtain accurate mass matrices for elements with nonuniform sections such as tapered beams. It is also possible to obtain reasonable mass matrices for members that have functionally graded and composite materials without any additional effort to derive mass matrices for each individual case.

Since, numerical examples and closed form solutions are generally available for the linear elastic case in the literature, the mass matrix derivation of which is presented above is also obtained under linear elastic conditions for making numerical comparisons more effectively in the following chapter. However, it should be noted that, the mass matrix obtained by the procedure explained above can also be used in nonlinear analysis.

CHAPTER 6

VALIDATION OF VIBRATION OF MF ELEMENT

6.1. INTRODUCTION

In this chapter, validation of the proposed MF element for free vibration analysis is presented by including higher order vibration frequencies considering modes that originate from three dimensional behavior of a steel cantilever beam with different cross-sections and having various uniformity conditions. The mass and stiffness matrices that are used in the analyses are both force based and derivation of them are presented in the previous chapters.

Numerical analyses are performed for various length over depth ratios (L/d) of uniform and tapered cantilever members with circular and rectangular cross-sections by monitoring first five free vibration frequencies in 3d by using different n_e per member span. Similar analyses are performed also with Abaqus [65] by using solid elements and resulting vibration frequencies are plotted for the modes obtained from analyses. Vibration freqencies obtained from both analysis with MF element and Abaqus are compared with explicit results available in the literature.

It should be noted that nonlinear vibration properties of the proposed mixed element could not be investigated due to the lack of explicit or exact solutions in the literature that can be used for comparison of the results. Therefore, analyses are performed only for linear elastic conditions.

6.2. UNIFORM MEMBER WITH CIRCULAR SECTION

In this section, first five free vibration frequencies of the proposed 3d MF element are investigated by performing free vibration analysis of a uniform cantilever beam that has circular cross section and same material and geometric properties with the member that is presented in Section 4.3.1. However, length over depth ratios are varied as L/d is equal to 1, 1.5, 2, 3 or 5 by keeping the diameter of the section, $d = 18$ units constant and varying the length of the member in the analysis. Then, resulting frequencies are compared with the theoretical frequencies obtained by explicit methods that exist in two complementary studies of Leissa and So [41, 66].

In the first study of Leissa and So [41], a method of three dimensional analysis for the free vibration freqencies of solid circular cylinders of elastic material was developed by assuming displacements as polynomials in the radial and axial directions and considering various types of boundary conditions and L/d ratios. Constants that can be used to obtain frequency values were given for the free-free and fixed-free boundary conditions and it was stated in the study that frequencies were exact to five or six figures for the former case and three or four figures for the latter case, respectively. These frequencies were compared with the frequencies that were obtained from elementary (Euler-Bernoulli) and improved 1-D theories for longitudinal, torsional and bending modes for a variety range of L/d in that study.

In their complementary study, Leissa and So [66] presented additional data for the 3d frequencies of solid circular sections for the same length over depth ratio utilized in the analyses with MF element. In that study, it was stated that there was not any published results for the 3d vibrations of cantilever beams by emphasizing that this problem was more difficult to be dealt compared to the free-free case since stress singularities in the corner at the fixed end result in a reduction of convergence of

solutions. Moreover, the paper concluded with the statement that the frequency data in that work can be used to compare the results obtained by other methods like finite element or finite difference. Therefore, Table V in that study which gives the constants that can be used to obtain 3d frequencies of a cantilever cylinder is used to compare the frequencies obtained by the proposed MF element.

The computer software, Abaqus 6.12, which enables performing finite element analysis is also used to determine mode shapes and free vibration frequencies of the uniform cantilever member with circular cross-section. Solid elements, named as C3D8R that exist in the library of the software are used for modeling the cantilever member. Mesh refinement for the member is applied until first five freqencies converge to a certain value which does not result in exceedance of the capacity of the computer to continue processing analyses. Consequently free vibration frequencies and mode shapes of the member are obtained for various L/d ratios and plotted through Figure 6.1 to Figure 6.5 for the first five vibration frequencies by not replotting one of the symmetrical modes in the perpendicular direction of the member axis due to symmetry in section geometry for each bending mode.

Figure 6.1 that depicts vibration modes for $L/d = 1$ includes one more mode totalling to six as compared to other figures. Because, for that case, fifth frequency of the member is warping mode that is combination of axial and bending which is not possible to obtain by the proposed MF element due to the assumption of Timoshenko beam theory unless a special warping function is assumed for the section of MF element. Therefore only this mode is neglected in comparison of the resulsts obtained by the proposed MF element, Abaqus and Leissa and So [66] where latter also includes constants for warping modes. However, proposed MF element is able to capture accurately the modes that do not include warping for all L/d ratios.

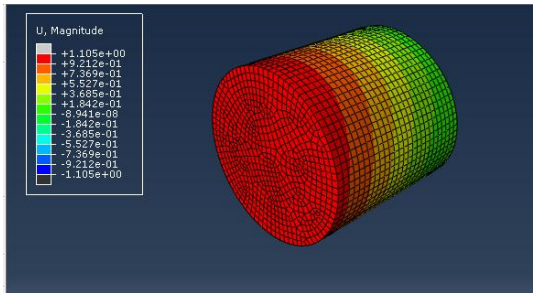

a. 1st Mode (1st bending mode)

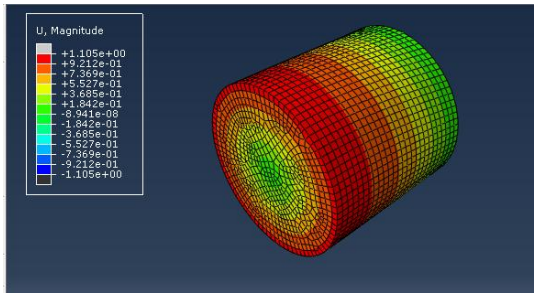

b. 2nd Mode (1st torsion mode)

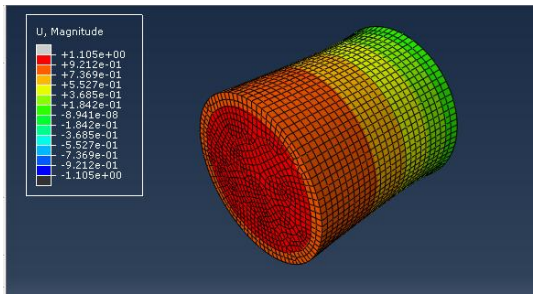

c. 3rd Mode (1st axial mode)

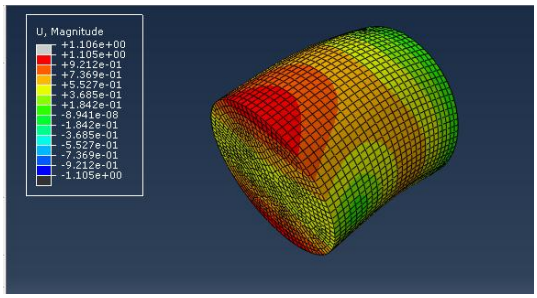

d. 4th Mode (2nd bending mode)

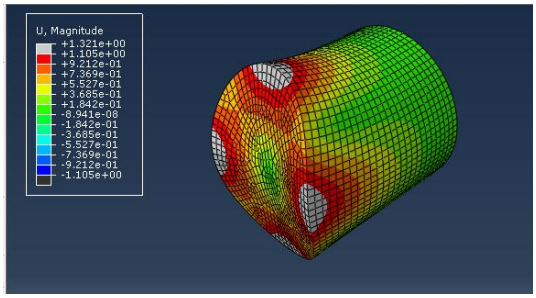

e. 5th Mode (1st warping mode)

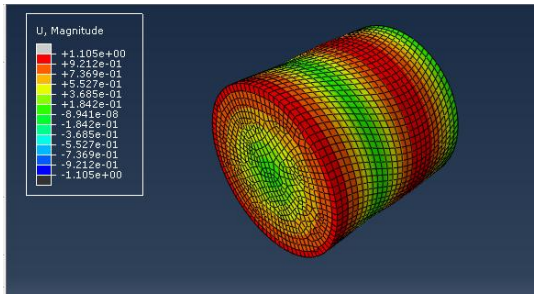

f. 6th Mode (2nd torsion mode)

Figure 6.1. Free vibration modes obtained by Abaqus for L/d=1

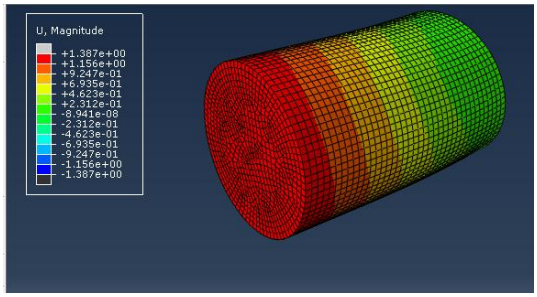

a. 1st Mode (1st bending mode)

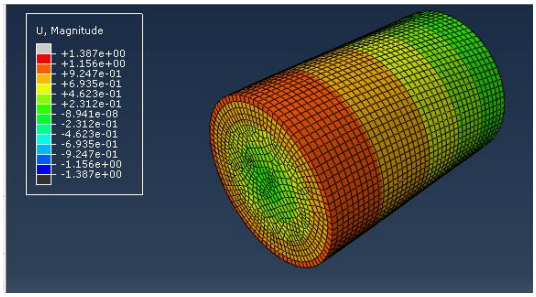

b. 2nd Mode (1st torsion mode)

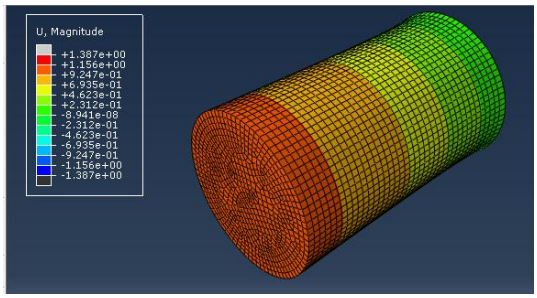

c. 3rd Mode (1st axial mode)

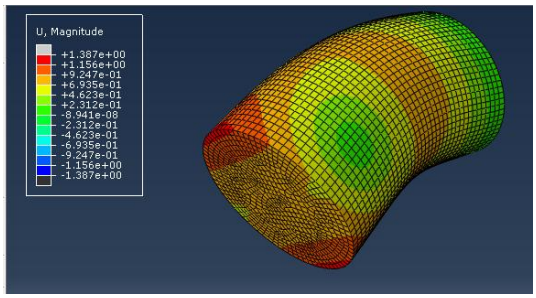

d. 4th Mode (2nd bending mode)

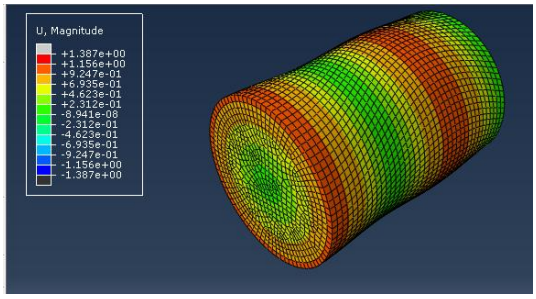

e. 5th Mode (2nd torsion mode)

Figure 6.2. Free vibration modes obtained by Abaqus for *L/d*=1.5

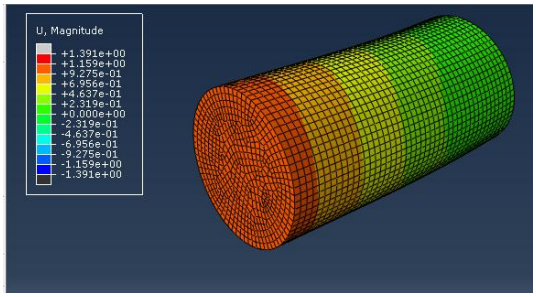

a. 1st Mode (1st bending mode)

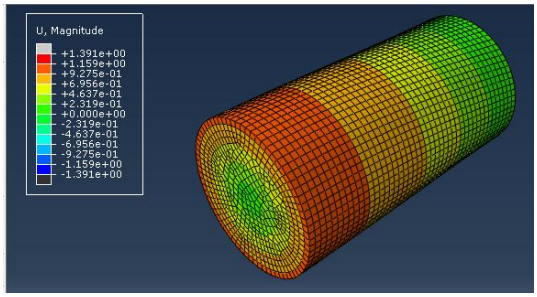

b. 2nd Mode (1st torsion mode)

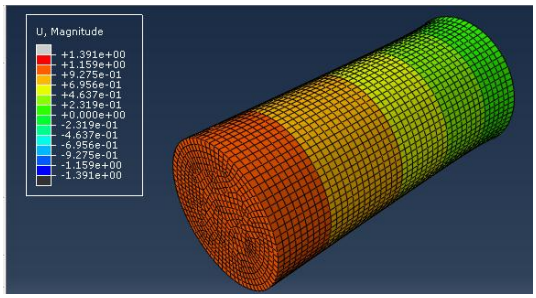

c. 3rd Mode (1st axial mode)

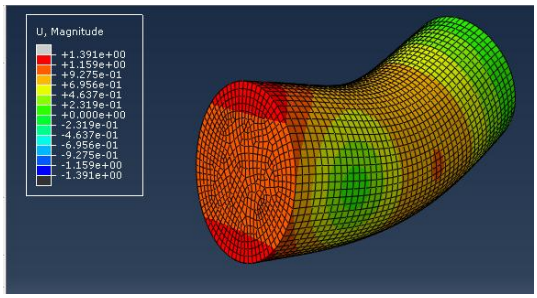

d. 4th Mode (2nd bending mode)

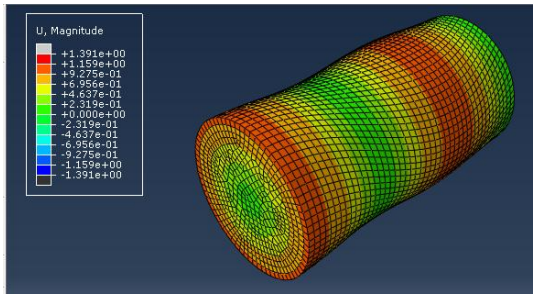

e. 5th Mode (2nd torsion mode)

Figure 6.3. Free vibration modes obtained by Abaqus for L/d=2

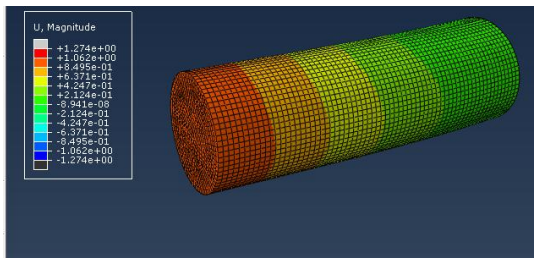

a. 1st Mode (1st bending mode)

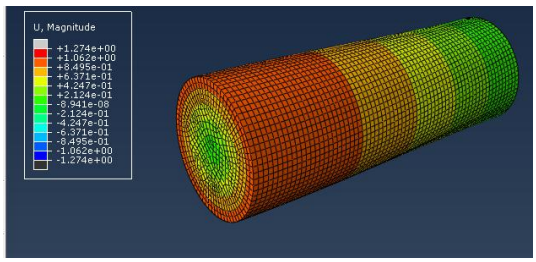

b. 2nd Mode (1st torsion mode)

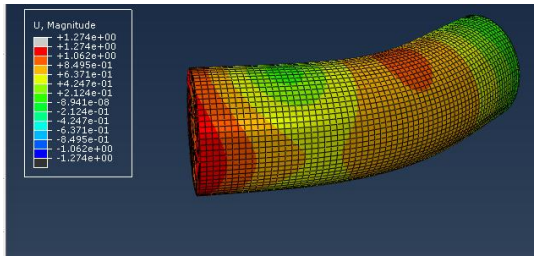

c. 3rd Mode (2nd bending mode)

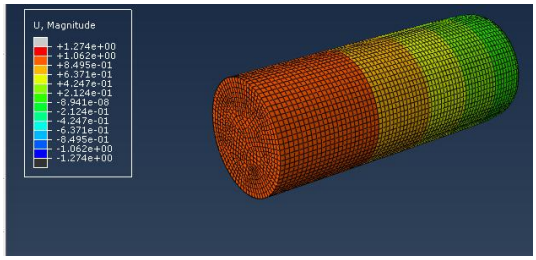

d. 4th Mode (1st axial mode)

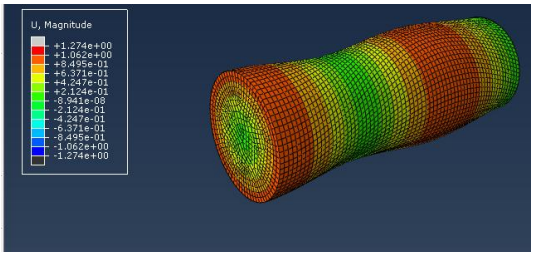

e. 5th Mode (2nd torsion mode)

Figure 6.4. Free vibration modes obtained by Abaqus for *L/d*=3

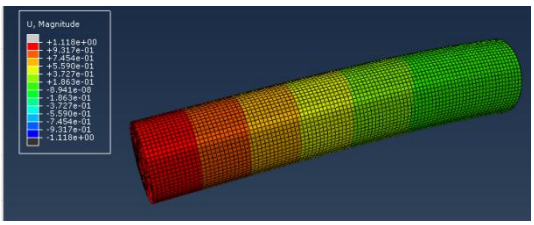

a. 1st Mode (1st bending mode)

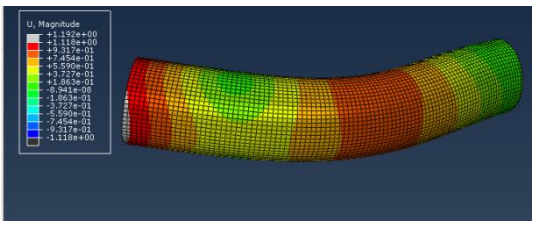

b. 2nd Mode (2nd bending mode)

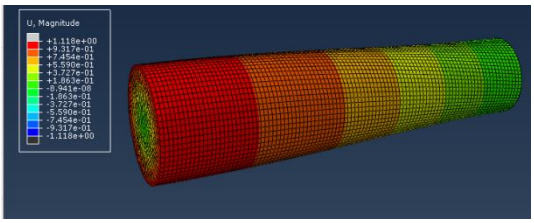

c. 3rd Mode (1st torsion mode)

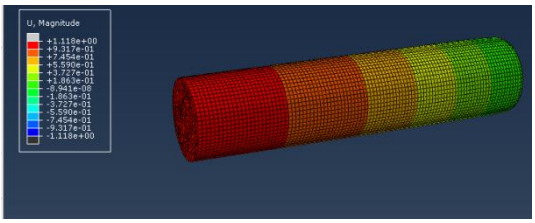

d. 4th Mode (1st axial mode)

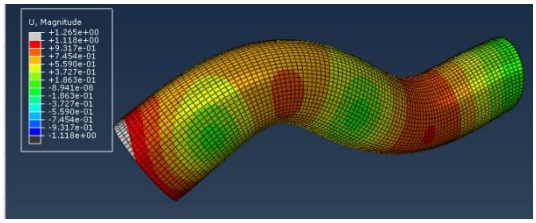

e. 5th Mode (3rd bending mode)

Figure 6.5. Free vibration modes obtained by Abaqus for *L/d*=5

According to Figure 6.1 to Figure 6.5, for $1 \leq L/d \leq 5$, the fundamental mode of the uniform cantilever member with solid circular section is bending. This fact is stated also by Leissa and So [66]. Moreover, for $1 \leq L/d \leq 3$, first five modes are in the order of 1st bending, 1st torsion, 1st axial, 2nd bending and 2nd torsion. This situation is tabulated in Table 6.1 by neglecting warping mode (Figure 6.1.e) for the case of $L/d = 1$.

Table 6.1. Mode shapes for various *L/d* ratios for uniform cantilever beam with solid circular section

	Mode number				
L/d	**1**	**2**	**3**	**4**	**5**
1	1st bending	1st torsion	1st axial	2nd bending	2nd torsion
1.5	1st bending	1st torsion	1st axial	2nd bending	2nd torsion
2	1st bending	1st torsion	1st axial	2nd bending	2nd torsion
3	1st bending	1st torsion	2nd bending	1st axial	2nd torsion
5	1st bending	2nd bending	1st torsion	1st axial	3rd bending

First five frequency values obtained by the proposed MF element are compared with the first five frequencies obtained by frequency constants in the study of Leissa and So (abbreviated as LS hereafter) [66] by computing ratio of frequency values $\omega_{\mathrm{MF}}/\omega_{\mathrm{LS}}$ for $\mathrm{n_e}$ is equal to 1, 2, 4, 8, 16 and 32 for aforementioned L/d ratios where ω_{MF} and ω_{LS} denote the frequency values obtained by the proposed mixed element and study of Leissa and So, respectively. In those comparisons, only one of the symmetric modes around an axis is considered. Results are plotted in Figure 6.6 to Figure 6.10. All of these plots have logarithmic horizontal and linear vertical axes, i.e. they are semilog plots. It should be noted that in those figures fifth vibration mode for $\mathrm{n_e} = 1$ is missing because, with only one element per member span, MF element can only capture first four vibration frequencies.

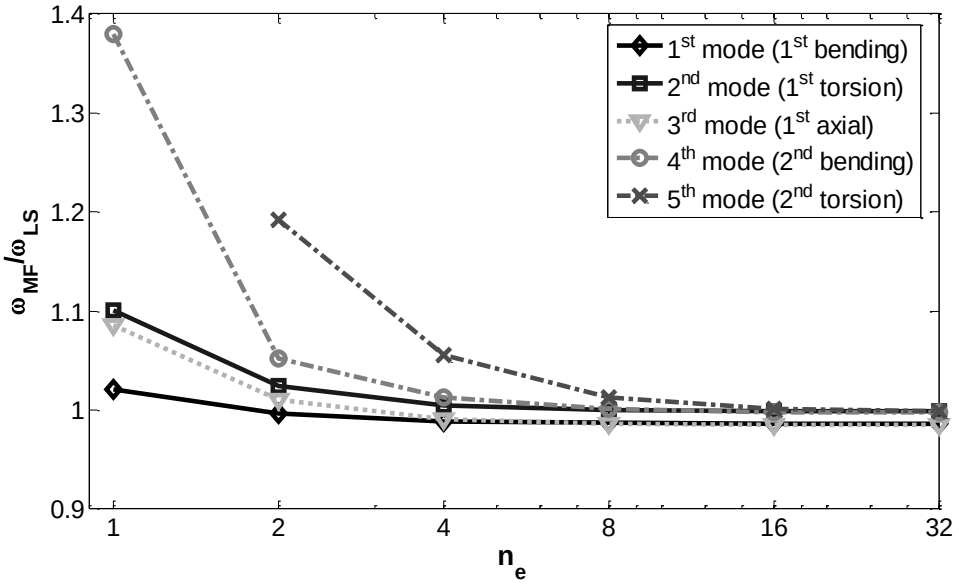

Figure 6.6. Comparison of vibration frequencies between MF and LS for L/d=1 (Uniform cantilever beam with solid circular section)

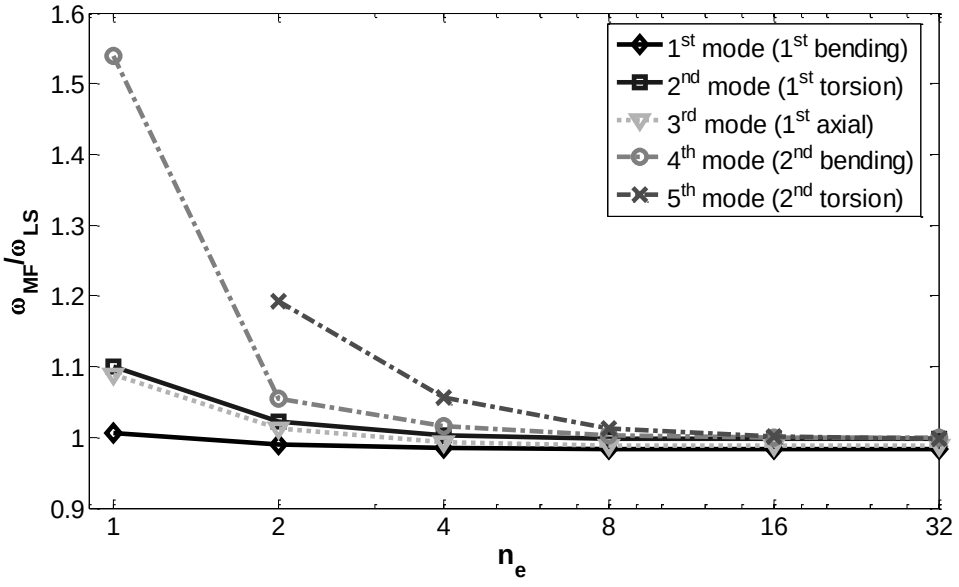

Figure 6.7. Comparison of vibration frequencies between MF and LS for L/d=1.5 (Uniform cantilever beam with solid circular section)

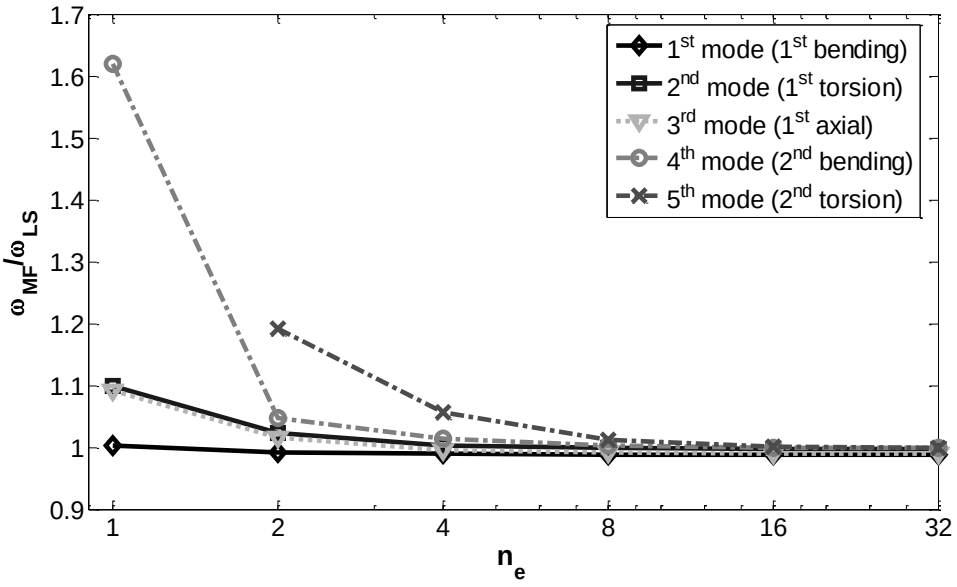

Figure 6.8. Comparison of vibration frequencies between MF and LS for L/d=2 (Uniform cantilever beam with solid circular section)

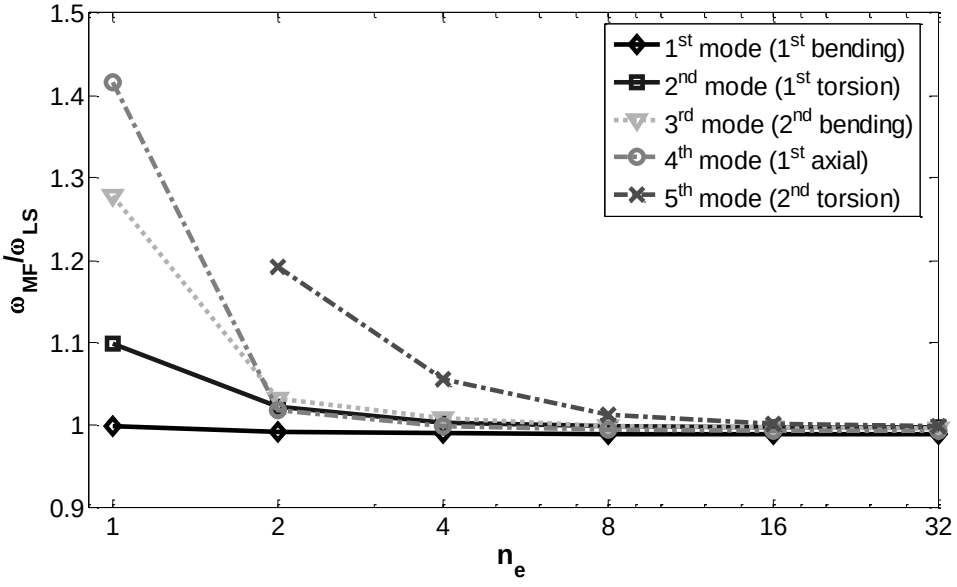

Figure 6.9. Comparison of vibration frequencies between MF and LS for L/d=3 (Uniform cantilever beam with solid circular section)

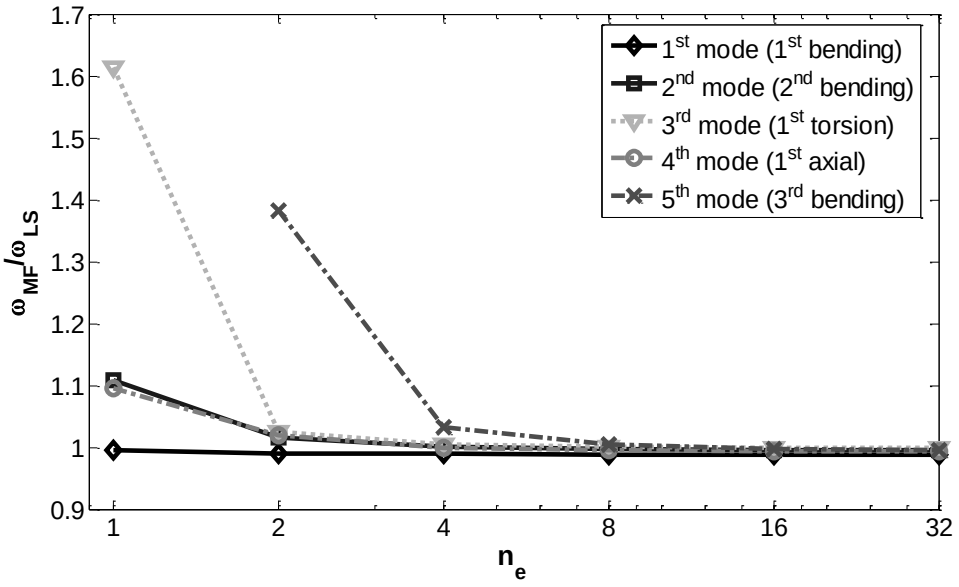

Figure 6.10. Comparison of vibration frequencies between MF and LS for *L/d*=5 (Uniform cantilever beam with solid circular section)

According to the Figure 6.6 to Figure 6.10, as n_e increases, then ω_{MF}/ω_{LS} converges to the value 1 asymptotically for all *L/d* which is an expected result. In these figures, if 1 is subtracted from ratio of frequency values ω_{MF}/ω_{LS} that are given in the vertical axis and the expression is multiplied by 100, then the percent difference of MF element from LS results can be obtained. Moreover, if the value of ω_{MF}/ω_{LS} is greater than 1, then the percent difference is positive, i.e. values of frequencies obtained by MF element are greater than LS results and if the ratio is smaller than 1, then the percent difference is negative indicating that frequency values obtained by MF element are smaller than LS results.

Another point to be emphasized is the ability of MF element to compute fundamental frequency accurately with only one element with a difference from LS results less than 2% for all *L/d* and first three frequencies with a difference less than 10% for all *L/d* except *L/d=3*. Additionally, first four frequencies are computed with a difference

less than 6% from LS results by using only two elements per span. First five frequencies are also computed with a difference less than 6% from LS results but this time by using four elements per span. Actually, percent differences of MF element results from LS results decrease as *L/d* increases, i.e. the difference is more pronounced for a short beam.

Similar comparison is made with the freqeuency values obtained by calculating ratio of first five frequency values calculated by LS and Abaqus, $\omega_{\mathrm{LS}}/\omega_{\mathrm{Abaqus}}$ for previously stated L/d ratios and results are plotted in Figure 6.11. Although, $\omega_{\mathrm{LS}}/\omega_{\mathrm{Abaqus}} = 1.005$ for the warping mode given in Figure 6.1.e for $L/d = 1$, it is neglected in Figure 6.11 and the next mode is assumed to be the fifth mode as stated previously in order to provide consistency with the results obtained by MF element.

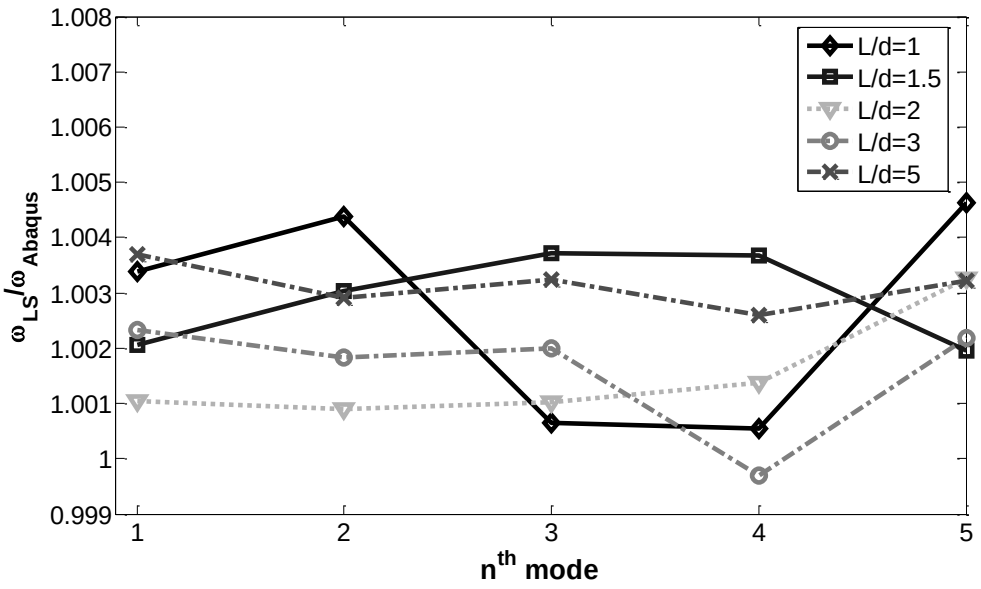

Figure 6.11. Comparison of vibration frequencies between LS and Abaqus for various *L/d*

According to the Figure 6.11, maximum percent differences of LS and Abaqus results are less than 0.5% percent in the positive side and %0.1 in the negative side. But, the constants which are given in the study of Leissa and So that are used to obtain first five frequnecies are given correct to three figures after decimal. Although the percent differences of LS and Abaqus results are very low, the difference may be originated from both the numerical computation by using those constants and the size of the meshing used in Abaqus. The chaotic nature of the curves that connect values of ratios rather than a trend line in the figure strenghens this idea. Therefore, it is thought that those differences can be tolerated in the comparisons given in Figure 6.6 to Figure 6.10. It should also be noted that, if $\omega_{\mathrm{MF}}/\omega_{\mathrm{LS}}$ ratios in Figure 6.6 to Figure 6.10 are multiplied with the corresponding $\omega_{\mathrm{LS}}/\omega_{\mathrm{Abaqus}}$ values in Figure 6.11, then ratio of MF element and Abaqus results, $\omega_{\mathrm{MF}}/\omega_{\mathrm{Abaqus}}$ can be obtained. So, there is no need to present $\omega_{\mathrm{MF}}/\omega_{\mathrm{Abaqus}}$ in a plot in addition to the comparisons of MF element results with LS results.

6.3. TAPERED MEMBER WITH CIRCULAR SECTION

In this section, first five free vibration frequencies of the proposed 3d MF element are investigated by performing free vibration analysis of a tapered cantilever beam that has solid circular cross section and same material properties with the member that is presented in Section 4.3.1. However, since the member is tapered linearly to the free end of the member, the geometry of the member is defined as in Figure 6.12. Ratio of the length of the member to the depth of fixed end, d_0 is varied as L/d_0 is equal to 1 and 3 by keeping the diameter of the section at the fixed end, $d_0 = 18$ units constant and varying the length and diameter of the member in the analysis. Another parameter that is kept constant in the anlysis is the ratio of the diameter of the free end of the member, d_1 to the diameter of the fixed end of the member, d_1/d_0

which is equal to 0.5. Then, resulting frequencies obtained by MF element are compared with the frequencies obtained by Abaqus.

Although there exists studies related with determination of free vibration frequencies of 3d tapered members with solid circular sections [67, 68], these studies do not include the boundary conditions for the cantilever beam analyzed in this thesis. There exists several studies giving tables for vibration frequencies of tapered cantilever members with solid circular sections but, these studies are in 2d [69-71]. Therefore, Abaqus results are thought to be enough for numerical comparison.

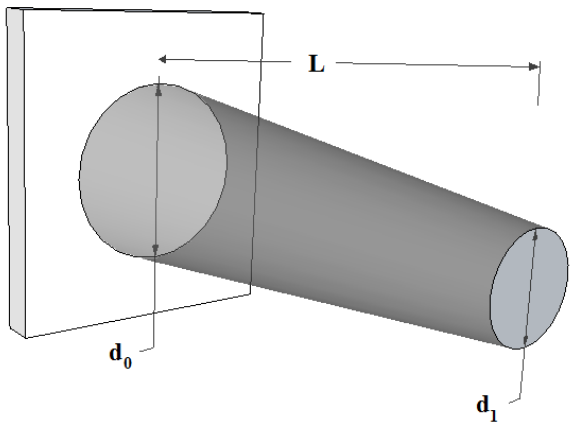

Figure 6.12. Tapered cantilever beam with circular cross section

Mode shapes obtained by Abaqus are plotted in Figure 6.13 and Figure 6.14 for L/d_0=1 and 3 where d_1/d_0=0.5 for both cases. Symmetrical modes, like bending around two perpendicular axes are considered only once in plotting mode shapes and counting mode numbers.

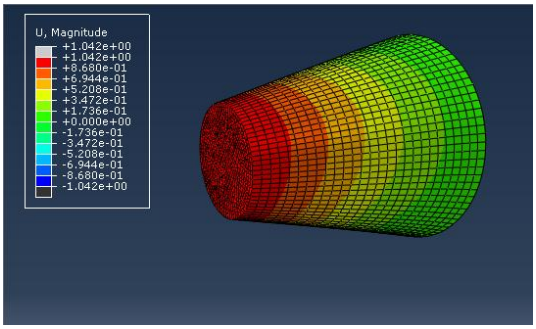

a. 1st Mode (1st bending mode)

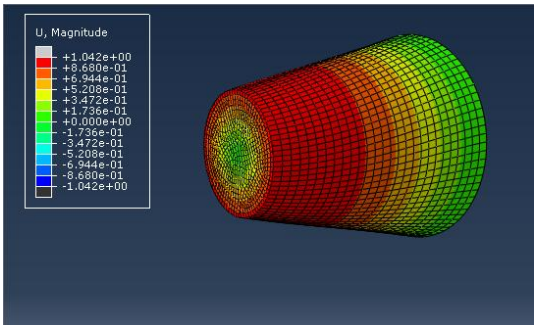

b. 2nd Mode (1st torsion mode)

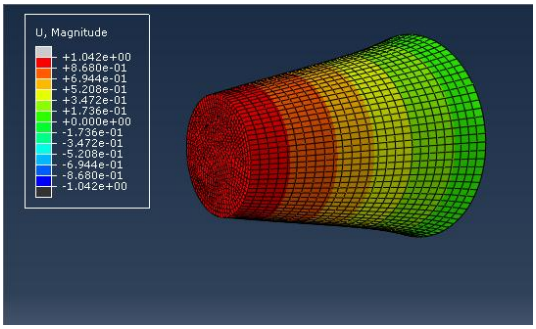

c. 3rd Mode (1st axial mode)

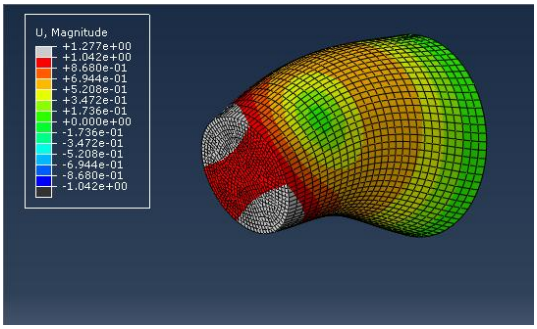

d. 4th Mode (2nd bending mode)

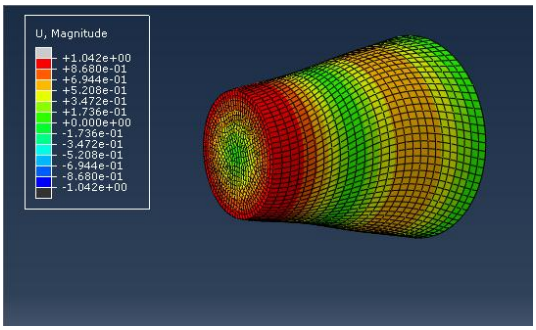

e. 5th Mode (2nd torsion mode)

Figure 6.13. Free vibration modes obtained by Abaqus for L/d_0=1 and d_1/d_0=0.5

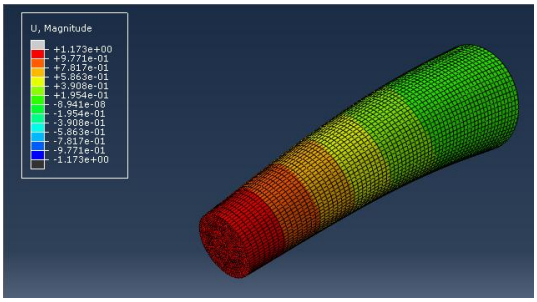

a. 1st Mode (1st bending mode)

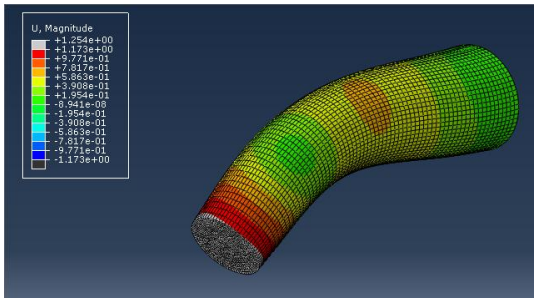

b. 2nd Mode (2nd bending mode)

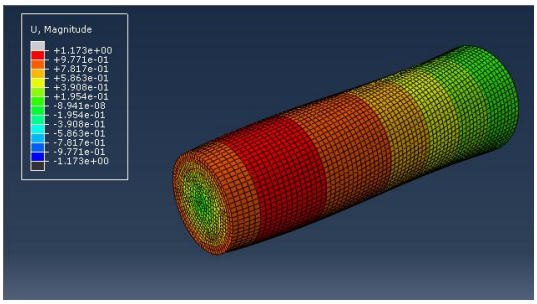

c. 3rd Mode (1st torsion mode)

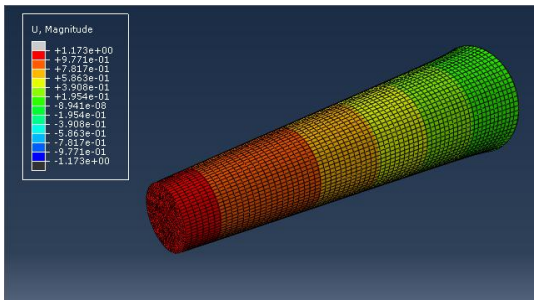

d. 4th Mode (1st axial mode)

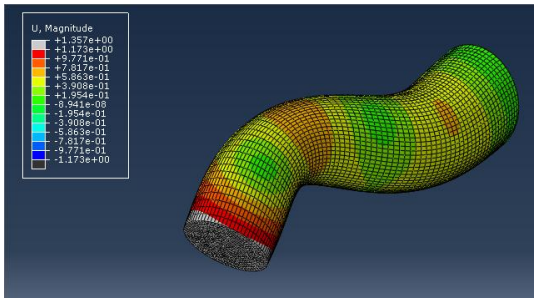

e. 5th Mode (3rd bending mode)

Figure 6.14. Free vibration modes obtained by Abaqus for L/d_0=3 and d_1/d_0=0.5

First five frequency values obtained by the proposed MF element are compared with the first five frequencies obtained by Abaqus by computing ratio of frequency values $\omega_{\mathrm{MF}}/\omega_{\mathrm{Abaqus}}$ for $\mathrm{n_e}$ is equal to 1, 2, 4, 8, 16 and 32 for aforementioned L/d_0 ratio is equal to 1 and 3, respectively. Symmetric modes are counted only once in those comparisons and results are depicted in Figure 6.15 and Figure 6.16 in semilog plots. Frequency values are missing in the plots for the fifth in Figure 6.15 and for the second mode in Figure 6.16 for $\mathrm{n_e} = 1$, because MF element can not capture those modes with only one element per span.

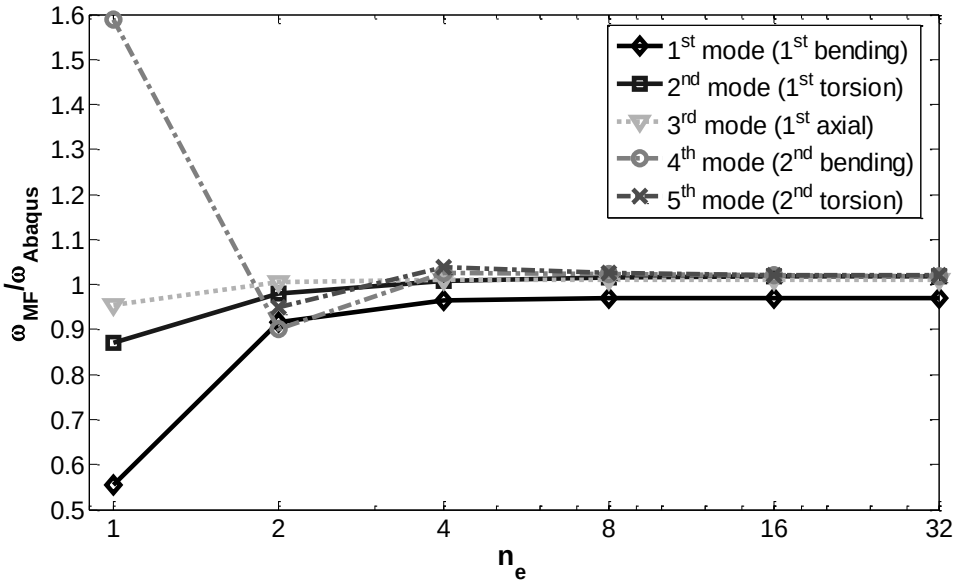

Figure 6.15. Comparison of vibration frequencies between MF and Abaqus for L/d_0=1 and d_1/d_0=0.5 (Tapered cantilever beam with solid circular section)

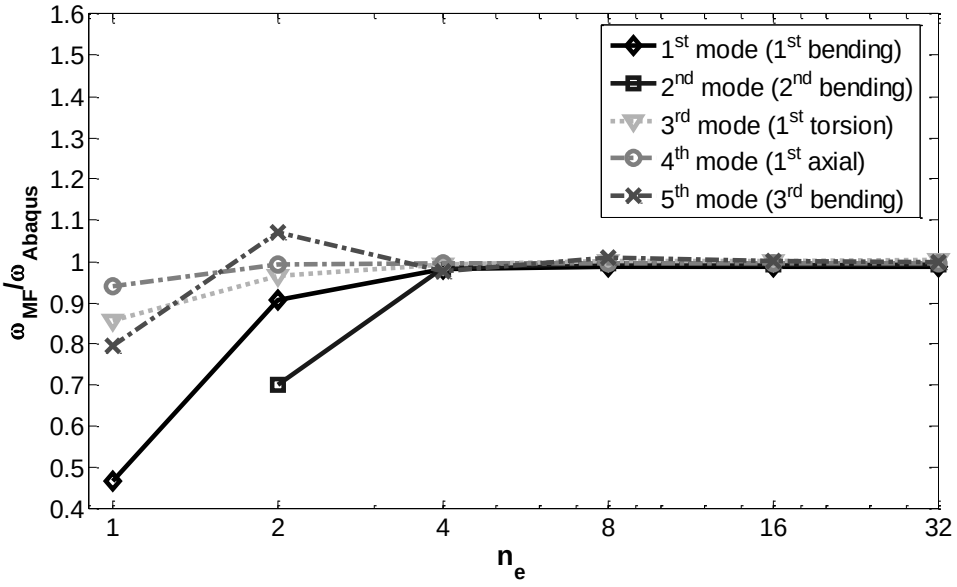

Figure 6.16. Comparison of vibration frequencies between MF and Abaqus for L/d_0=3 and d_1/d_0=0.5 (Tapered cantilever beam with solid circular section)

According to Figure 6.15 and Figure 6.16, as n_e increases, then $\omega_{MF}/\omega_{Abaqus}$ converges to the value 1 asymptotically for both L/d_0 values, but more rapidly for L/d_0=3 compared to the case for L/d_0=1 for the first mode.

It can be deduced from figures that, $n_e = 4$ is suitable for capturing first five frequencies with less than 4% difference from Abaqus results for the short beam case which is L/d_0=1 and less than 2.5% for L/d_0=3. Therefore it can be concluded that the proposed MF element is suitable for determination of free vibration frequencies of tapered cantilever member with circular solid section.

6.4. UNIFORM MEMBER WITH RECTANGULAR SECTION

First four or five free vibration frequencies of the proposed 3d MF element are investigated by performing free vibration analysis of a uniform cantilever beam that has solid rectangular cross section and same material properties with the member that is presented in Section 4.3.1. However, since the member has rectangular section, the geometry of the member is defined as in Figure 6.17. Three different cases are analyzed by varying dimensions of the member. Width and height of the section are kept constant to be $b = c = 18$ units in all analyses, whereas the ratio of lenght of the member, a to the height of the member, a/c is varied as 1, 2 and 5. Then, resulting frequencies obtained by MF element are compared with the frequencies obtained by using the frequency constants in Leissa and Zhang [72] and Abaqus for a/c is equal to 1 and 2. However, there is not any constant for the case of long beam in the study of Leissa and Zhang, therefore comparsion of the MF element for a/c = 5 is made only with results of Abaqus.

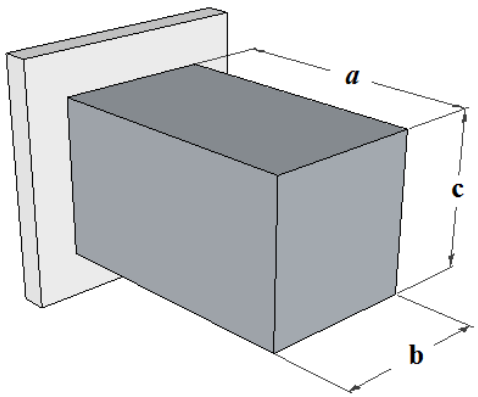

Figure 6.17. Uniform cantilever beam with rectangular cross section

Leissa and Zhang (abbreviated as LZ hereafter) [72] used Ritz method in their study where the displacements were assumed in the form of polynomials and presented a solution for the three-dimensional problem of determining the free vibration frequencies and mode shapes for a uniform cantilever beam with various rectangular sections where they called that kind of an element as parallelepiped. However, Leissa and So [66] noted that for this configuration, all three rectangular coordinates remained coupled preventing determination of the 3d frequencies not as accurate as for the case of circular sections analyzed in their study.

Free vibration analyses are carried out by Abaqus as defined in Section 6.2 and mode shapes that are obtained are plotted in Figure 6.18 to Figure 6.20 for a/c is equal to 1, 2 and 5, respectively. Symmetrical modes, like bending around two perpendicular axes are considered only once in plotting mode shapes and counting mode numbers as in the previous sections.

Fifth vibration frequencies for a/c is equal to 1 and 2 are warping modes and can not be captured with the proposed MF element. Therefore, comparisons of the frequencies of the MF element with LZ and Abaqus results are made for only first four vibration frequencies for these a/c ratios. But, MF element is able to capture all other modes that do not contain warping of the section for a/c is equal to 1, 2 and 5. Thus, comparison of the frequency values obtained by MF element with Abaqus results are made up to fifth vibration frequency for the case of a/c is equal to 5.

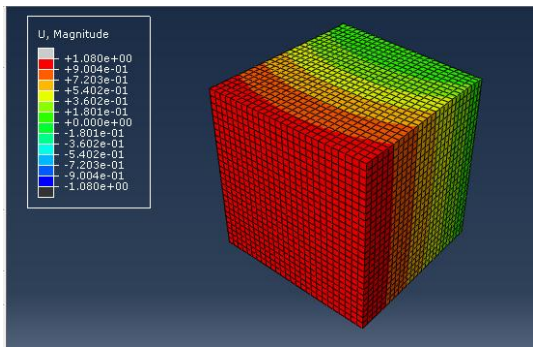

a. 1st Mode (1st bending mode)

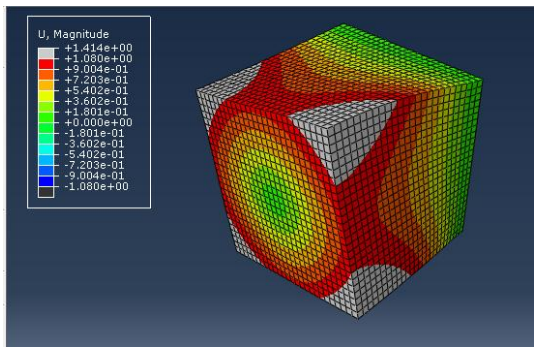

b. 2nd Mode (1st torsion mode)

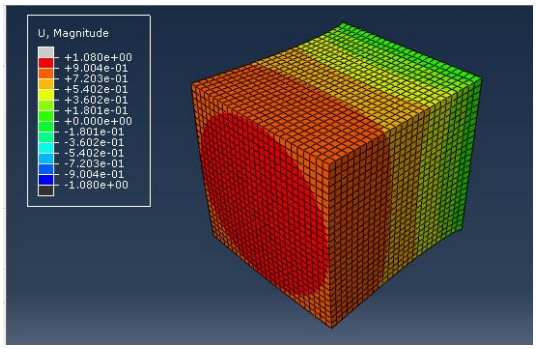

c. 3rd Mode (1st axial mode)

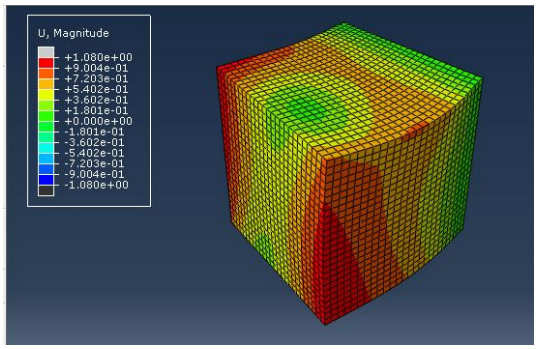

d. 4th Mode (2nd bending mode)

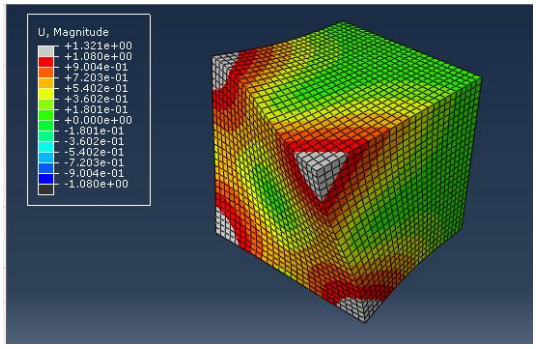

e. 5th Mode (1st warping mode)

Figure 6.18. Free vibration modes obtained by Abaqus for *a/c*=1

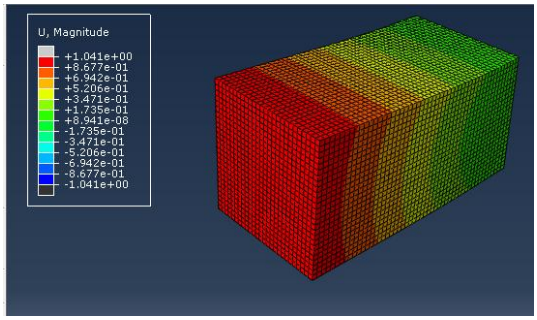

a. 1st Mode (1st bending mode)

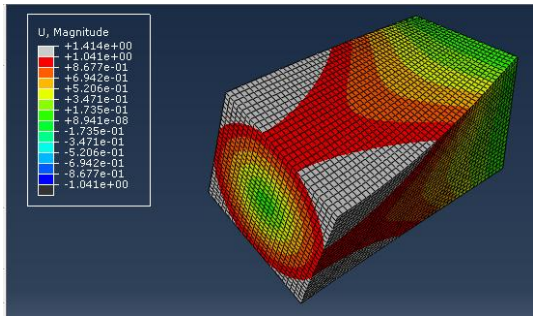

b. 2nd Mode (1st torsion mode)

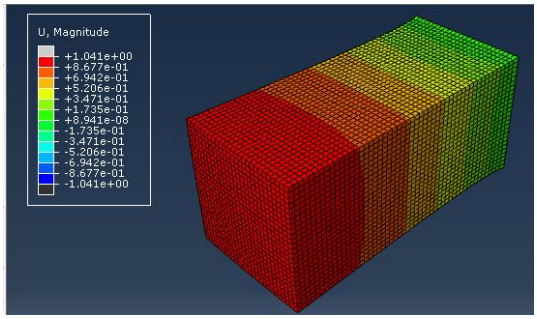

c. 3rd Mode (1st axial mode)

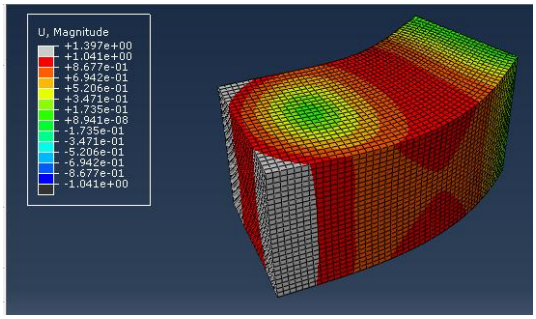

d. 4th Mode (2nd bending mode)

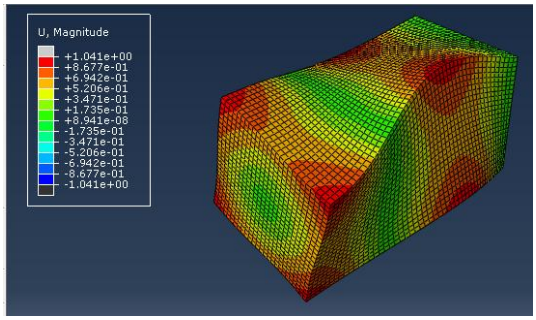

e. 5th Mode (1st warping mode)

Figure 6.19. Free vibration modes obtained by Abaqus for a/c=2

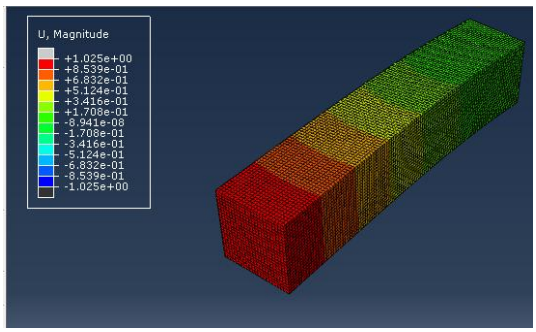

a. 1st Mode (1st bending mode)

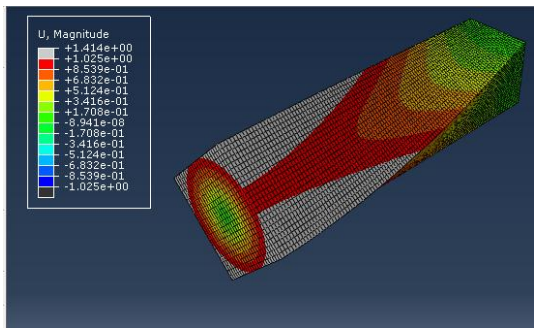

b. 2nd Mode (1st torsion mode)

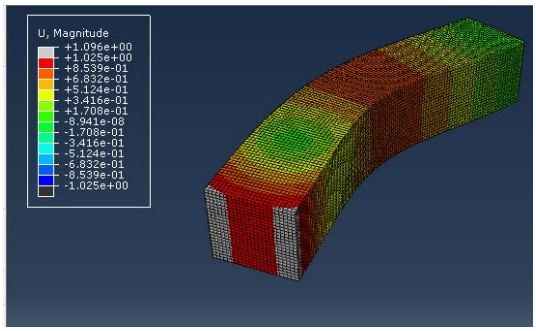

c. 3rd Mode (2nd bending mode)

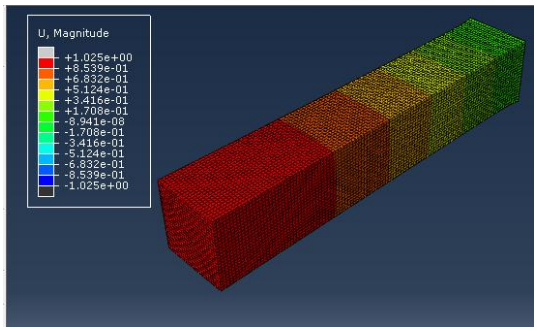

d. 4th Mode (1st axial mode)

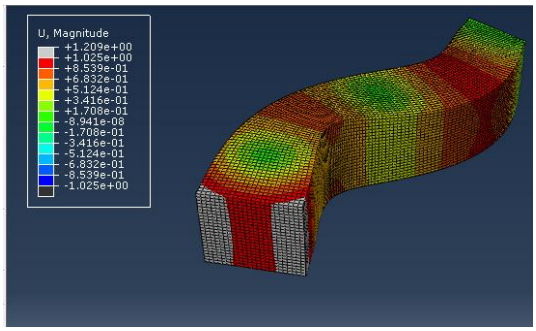

e. 5th Mode (3rd bending mode)

Figure 6.20. Free vibration modes obtained by Abaqus for *a/c*=5

First four frequency values obtained by proposed MF element are compared with the first four frequencies obtained by LZ by computing ratio of frequency values $\omega_{\mathrm{MF}}/\omega_{\mathrm{LZ}}$ for $\mathrm{n_e}$ is equal to 1, 2, 4, 8, 16 and 32 for aforementioned a/c ratio is equal to 1 and 2, respectively and by computing the ratio $\omega_{\mathrm{MF}}/\omega_{\mathrm{Abaqus}}$ for the same number of elements, but this time for $a/c = 5$. Symmetric modes are counted only once in those comparisons and results are depicted in Figure 6.21 to Figure 6.23 in semilog plots. Frequency values are missing in the plots for the fifth mode in Figure 6.23 for $\mathrm{n_e} = 1$, because MF element can not capture those modes with only one element per span.

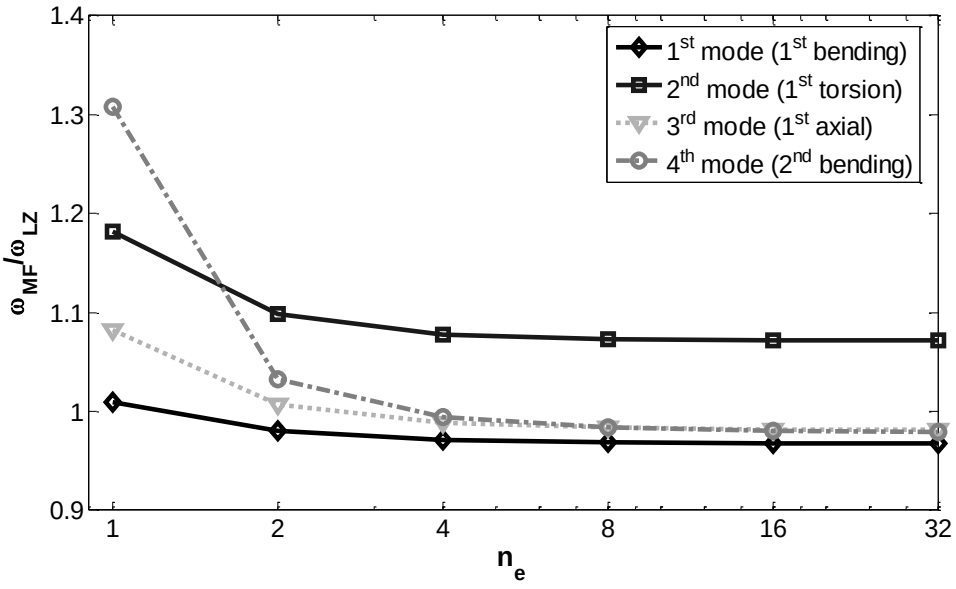

Figure 6.21. Comparison of vibration frequencies between MF and LZ for *a/c*=1 (Uniform cantilever beam with solid rectangular section)

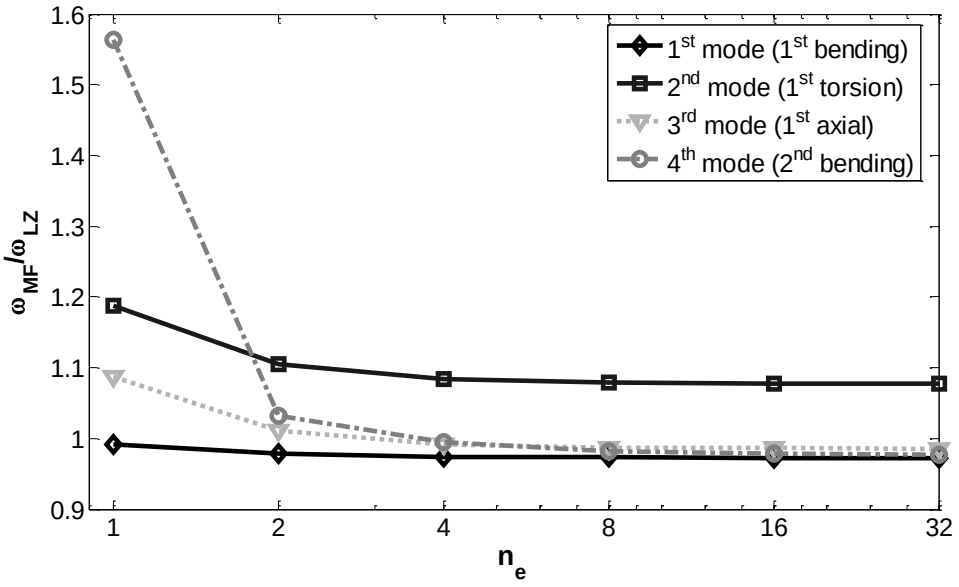

Figure 6.22. Comparison of vibration frequencies between MF and LZ for *a/c*=2 (Uniform cantilever beam with solid rectangular section)

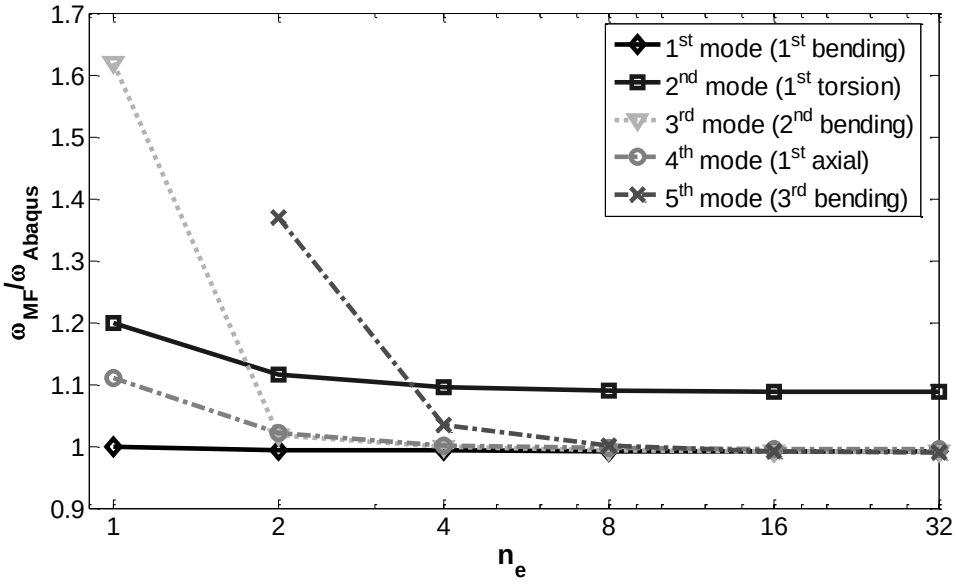

Figure 6.23. Comparison of vibration frequencies between MF and Abaqus for *a/c*=5 (Uniform cantilever beam with solid rectangular section)

According to Figure 6.21 to Figure 6.23, as n_e increases, then ω_{MF}/ω_{LZ} and $\omega_{MF}/\omega_{Abaqus}$ converges to the value 1 asymptotically for all *a/c* values, but modes other than second mode which is also the first torsion mode converges more rapidly.

It can be deduced from figures that, $n_e = 4$ is suitable for capturing first three frequencies except first torsion mode with less than 3% difference from LZ results for the short beam case which is *a/c*=1 and less than 10% difference for the first torsion mode. The same number of elements can be used to capture first three frequencies except first torsion mode with less than 2.5% difference from LZ results for *a/c*=2 and less than 10% difference for the first torsion mode. By the way, MF element presented in this thesis did not consider warping effects present in rectangular sections, thus the first torsion mode was estimated with 10% error due to this assumption in the formulation. In order to reduce this error, warping functions should be incorporated to get better estimation for rectangular sections.

Similar situation is valid in the comparison of MF element and Abaqus results. In that case first five frequencies except first torsion mode can be captured with MF element with less than 3.5% difference from Abaqus results and less than 10% difference for the first torsion mode.

Therefore it can be concluded that proposed MF element is suitable for determination of free vibration frequencies of uniform cantilever member with rectangular section with lesser accuracy in torsion mode. However, if it is paid attention to implement warping function in the derivation of the MF element, then it is possible to obtain torsion frequencies as accurate as other modes for the case of rectangular section.

Similar comparison is made with the freqeuency values obtained by calculating ratio of first five frequency values calculated by LZ and Abaqus, $\omega_{LZ}/\omega_{Abaqus}$ for a/c is

equal to 1 and 2 and results are plotted in Figure 6.24. According to the figure, LZ and Abaqus results do not deviate too much where the maximum difference is less than 1.5% and LZ results can capture the warping mode. The deviation may be due to the number of figures after decimals in constants used in the study of LZ and meshing size used in the analyses with Abaqus.

One can easily obtain the ratio of $\omega_{\mathrm{MF}}/\omega_{\mathrm{Abaqus}}$ by multiplying $\omega_{\mathrm{MF}}/\omega_{\mathrm{LZ}}$ ratios in Figure 6.21 and Figure 6.22 with $\omega_{\mathrm{LZ}}/\omega_{\mathrm{Abaqus}}$ ratios in Figure 6.24.

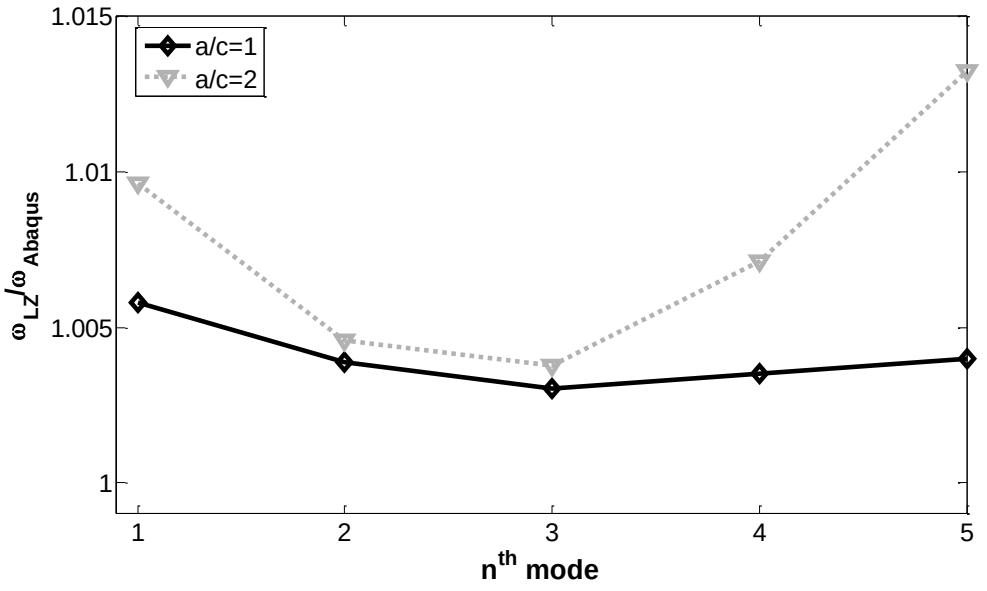

Figure 6.24. Comparison of vibration frequencies between LZ and Abaqus for various *a/c*

6.5. TAPERED MEMBER WITH RECTANGULAR SECTION

First five free vibration frequencies of the proposed 3d MF element are investigated by performing free vibration analysis of a tapered cantilever beam which is actually a truncated wedge that has solid rectangular cross section and same material properties with the member that is presented in Section 4.3.1. The geometry of the member is defined as in Figure 6.25 and it is linearly tapered only in the direction of its axis. Two different cases are analyzed by varying dimensions of the member. Width, b and the ratio of the height of the free end, h_1 to the height of the fixed end, h_0 of the member are kept constant to be $b = 18$ units and $h_1/\,h_0 = 0.5$ in all analyses, whereas the ratio of lenght of the member, L to the height at fixed end, h_0 of the member, L/h_0 is varied as 1 and 3 by assuming $h_0 = 18$ units in each cases. Then, resulting frequencies obtained by MF element are compared with the frequencies obtained by Abaqus for L/h_0 is equal to 1 and 3.

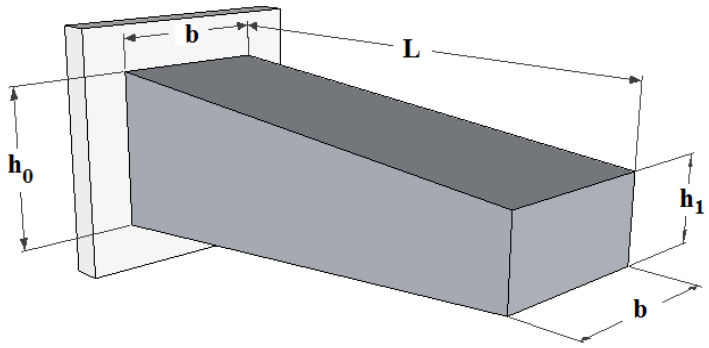

Figure 6.25. Tapered cantilever beam with rectangular cross section

There exists numerous studies and great effort related with determination of free vibration frequencies of tapered members with solid or hollow rectangular sections in 2d in the literature [40, 73-80]. These studies consider different types of boundary conditions and present various solution methods to deal with the free vibration problem. However, there is not any available study in the literature that can be taken as reference to compare the free vibration frequencies for 3d. Therefore, Abaqus results are thought to be a good option and enough for numerical comparison of vibration frequencies in 3d.

Mode shapes obtained by Abaqus are plotted in Figure 6.26 and Figure 6.27 for L/h_0=1 and 3 where h_1/h_0=0.5 for both cases. Since the member is tapered to the free end and dimensions of the section at the free end are not the same in two perpendicular directions, there is not any symmetrical mode in the plots. Because of that reason, bending modes are excessive in number compared to other modes in the analyses.

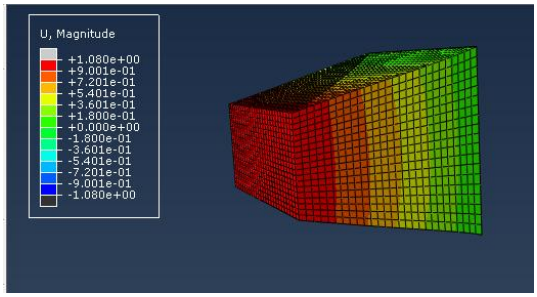

a. 1st Mode (1st bending mode)

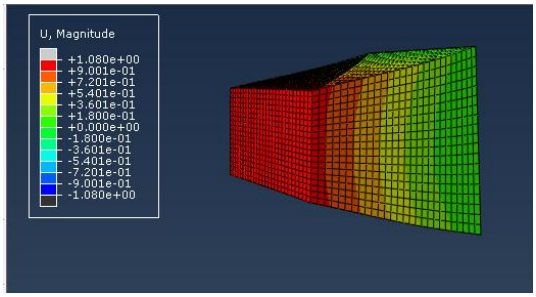

b. 2nd Mode (2nd bending mode)

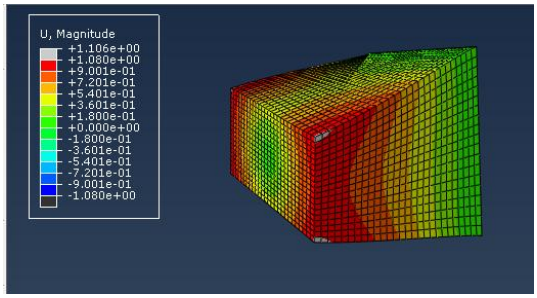

c. 3rd Mode (1st torsion mode)

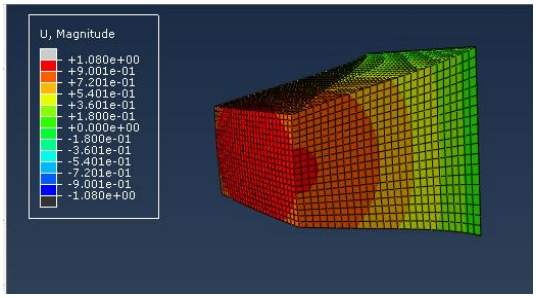

d. 4th Mode (1st axial mode)

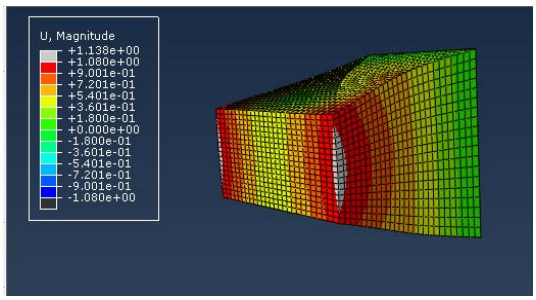

e. 5th Mode (3rd bending mode)

Figure 6.26. Free vibration modes obtained by Abaqus for L/h_0=1 and h_1/h_0=0.5

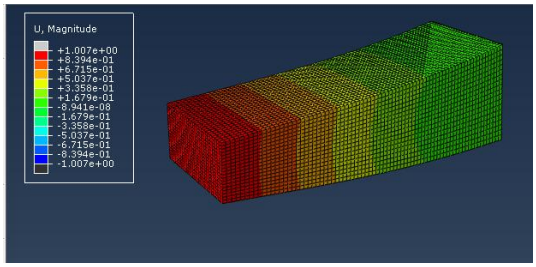

a. 1st Mode (1st bending mode)

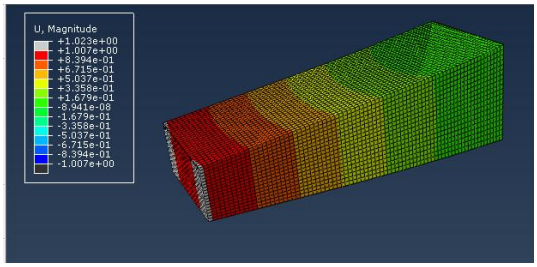

b. 2nd Mode (2nd bending mode)

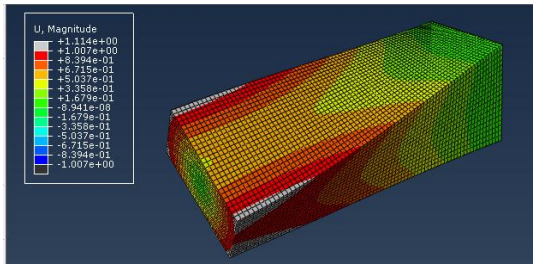

c. 3rd Mode (1st torsion mode)

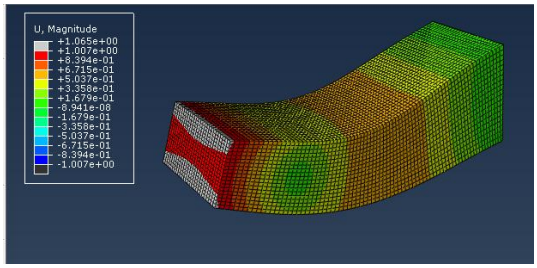

d. 4th Mode (3rd bending mode)

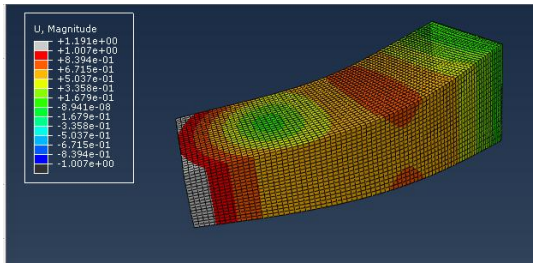

e. 5th Mode (4th bending mode)

Figure 6.27. Free vibration modes obtained by Abaqus for L/h_0=3 and h_1/h_0=0.5

First five frequency values obtained by the proposed MF element are compared with the first five frequencies obtained by Abaqus by computing ratio of frequency values $\omega_{\mathrm{MF}}/\omega_{\mathrm{Abaqus}}$ for $\mathrm{n_e}$ is equal to 1, 2, 4, 8, 16 and 32 for aforementioned L/h_0 ratio is equal to 1 and 3, respectively. Results are depicted in Figure 6.28 and Figure 6.29 in semilog plots by considering each bending mode in two perpendicular directions as separately. It should be noted that, although its accuracy is low except for axial and torsion modes, MF element is able to capture first five frequencies even for $\mathrm{n_e} = 1$ which is not the case in the previous sections of that section.

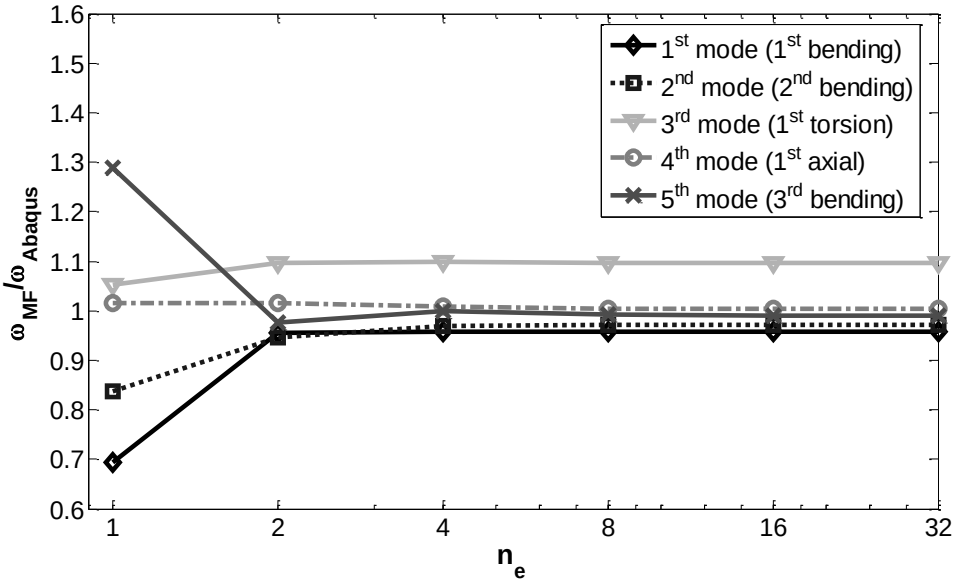

Figure 6.28. Comparison of vibration frequencies between MF and Abaqus for L/h_0=1 and h_1/h_0=0.5 (Tapered cantilever beam with rectangular section)

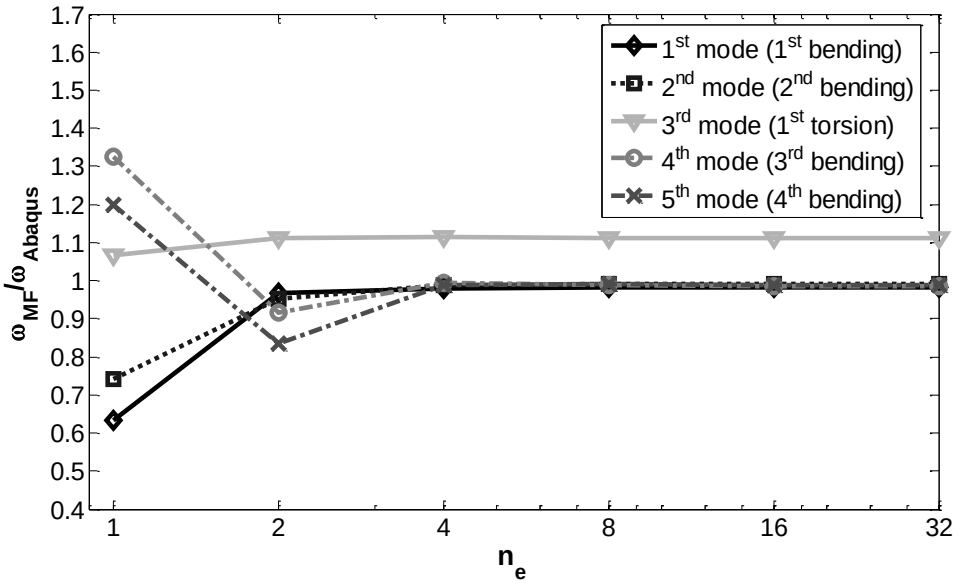

Figure 6.29. Comparison of vibration frequencies between MF and Abaqus for L/h_0=3 and h_1/h_0=0.5 (Tapered cantilever beam with rectangular section)

According to Figure 6.28 and Figure 6.29, as n_e increases, then $\omega_{MF}/\omega_{Abaqus}$ converges to the value 1 asymptotically for both L/h_0 values, but more rapidly for L/h_0=3 compared to the case for L/h_0=1.

It can be concluded from figures that, $n_e = 4$ is suitable for capturing first five frequencies with less than 4% difference from Abaqus results for the short beam case which is L/h_0=1 and less than 2% for L/h_0=3 except for the first torsion mode whose difference is less than 10% for both L/h_0 ratios. Therefore, it can be concluded that the proposed MF element is suitable for determination of free vibration frequencies of tapered cantilever member with rectangular section with a high accuracy for the modes except torsion. However, it is also possible to capture the effect of torsion more accurately than the present case by defining warping function in the derivation of MF element.

At this point it should be noted that free vibration analyses with MF element provide considerable reduction in analyses duration as compared to the analyses with Abaqus for the numerical validation studies given in Section 6.2 to 6.5. Because, for both uniform and tapered members with low and high length over depth ratios, $n_e = 2$ for member span is enough to capture fundamental mode with an accuracy that can be tolerated in the vibration analyses of structural systems. Moreover, $n_e = 4$ is sufficient for most of the cases analyzed for determination of the first five frequencies with a considerable accuracy.

CHAPTER 7

CONCLUSIONS

7.1. SUMMARY

In this thesis, the derivation of an accurate 3d mixed formulation nonlinear frame finite element that is based on three field Hu-Washizu functional was presented. The accuracy of the element stemmed from the utilization of force interpolation functions in the predetermined control sections instead of using displacement interpolation functions along the span of the beam element. Displacement values that were needed to perform analyses were only the displacements of the end nodes that existed at each end of the member rather than inter element displacements.

The accuracy of the proposed 3d mixed element was validated by carrying out nonlinear analyses of members with solid and hollow circular sections under various types of loading, boundary and uniformity conditions. Comparison of the results of nonlinear analyses of the 3d mixed element with exact solutions and 3d displacement based elements that are already available in the literature corroborated the superiority and ability of the mixed element to consider the 3d interaction of axial force, bending moment, shear force and torsion accurately.

The capability of the proposed 3d mixed element to determine linear elastic vibration modes with a considerable accuracy was also pointed out by performing free vibration analyses of uniform and tapered cantilever beams with circular and rectangular sections for various length over depth ratios. Mass and stiffness matrices that were used in the free vibration analyses were derived by employing flexibility

based approach as presented in this thesis. Comparison of the vibration frequencies obtained by using the proposed 3d mixed element with the frequencies obtained from closed-form solutions in the literature and the frequencies obtained by a finite element software established the ability of the proposed mixed element to determine first five vibration frequencies of a beam element accurately provided that warping was neglected in the analyses.

7.2. CONCLUSIONS

Conclusions that were extracted from the studies performed throughout the thesis were discussed by summarizing the main findings as follows;

- A 3d nonlinear mixed beam element based on the Hu-Washizu functional that is free from shear locking and capable of incorporating 3d interaction of stresses caused by axial force, shear force, bending moments and torsion accurately was developed.
- The mixed element was tested under nonlinear conditions for various types of loading configurations and it was concluded that behavior of the element under nonlinear conditions matched quite well with the exact solutions that are available in the literature even with only one element per member span.
- It was also shown that the 3d mixed element is superior to its 3d displacement based counterpart and some elements available in the library of a finite element software in nonlinear analyses through numerical comparisons by means of reflecting nonlinear behavior with lesser number of elements as compared to other displacement based elements.
- It was emphasized that both the effect of axial load and torsion is important in nonlinear behavior of members with solid and hollow circular sections. However, the effect of torsion was more pronounced and seemed to be more

important for members with hollow circular sections as compared to members with solid circular sections under nonlinear conditions.

- It was pointed out that increasing number of integration points on the section beyond some limiting value was unnecessary in nonlinear analyses since it did not provide any further accuracy other than increase in solution time and storage of data.
- A 3d flexibility based consistent mass matrix was derived referring to an article available in the literature and it was highlighted that consistent mass matrix was the same as the consistent mass matrix obtained from displacement based approach for a uniform element. However, it was explained that flexibility based mass matrix was superior to displacement based mass matrix for cases such as elements with nonuniform section or nonhomogenous material since displacement based mass matrix necessitates special shape functions in order to obtain reasonable mass matrices for such cases. But, flexibility based mass matrix did not need special attention for interpolation of section forces because it considered distribution of mass inside the element during derivation of the matrix and used force interpolation functions that were actually exact under small deformations.
- The 3d mixed element was used to evaluate first five linear elastic free vibration frequencies of uniform and tapered members with solid circular and rectangular sections by neglecting vibration modes that contain warping. It was concluded that the mixed element was capable of calculating those frequencies with a high accuracy by using two or four elements per span depending on the member type as compared with the frequencies obtained by using solid elements of a finite element program and using frequency constants that exist in the literature.

7.3. RECOMMENDATIONS FOR FUTURE STUDY

The proposed 3d mixed element, derivation of which was presented in this thesis was tested for nonlinear analyses of uniform and tapered members with some type of sections and boundary conditions. Authentication of the proposed element might be further made for different types of sections and boundary conditions other than the ones examined in this thesis.

Verification studies were carried out by considering material nonlinearity of only one type of material by neglecting nonlinear geometric effects. Other material types and nonlinear effects caused by geometry can also be incorporated to the proposed element in the subsequent studies.

Comparison of the proposed element with other displacement based elements and explicit solutions that exist in the literature for both nonlinear static and free vibration analyses were performed at element level in 3d. However, it is also possible to display the superiority of the proposed mixed element for 3d for these cases at structural level but this time it will be difficult to find explicit solutions that can be used as benchmark studies in comparisons.

Last but not the least, the proposed mixed element neglected warping modes in free vibration analysis. But, implementing warping function in the derivation of the element will solve this issue. Such an effort will provide valuable contribution in obtaining accurate response of wide-flange, channel or any other type of irregular sections as a part of finite element analysis of structural systems in 3d.

REFERENCES

1. Clough, R.W., *The Finite Element Method in Plane Stress Analysis*, in *Second ASCE Conference on Electronic Computation*1960: Pittsburgh: PA. p. 345-378.

2. Bathe, C.J., *Finite Element Procedures*. 1996, New Jersey: Prentice Hall.

3. Reddy, J.N., *An Introduction to the Finite Element Method*. 1993, New York: McGraw-Hill.

4. Reddy, J.N., *An Introduction to Nonlinear Finite Element Analysis*. 2004, New York: Oxford University Press.

5. Zienkiewicz, O.C., R.L. Taylor, and J.Z. Zhu, *The Finite Element Method: Its Basis and Fundamentals*. 2005, Oxford: Elsevier Butterworth-Heinemann.

6. Zienkiewicz, O.C. and R.L. Taylor, *The Finite Element Method for Solid and Structural Mechanics*. 2005, Oxford: Elsevier Butterworth-Heinemann.

7. Timoshenko, S.P. and J.N. Goodier, *Theory of Elasticity*. 1970, Singapore: McGraw-Hill.

8. Ugural, A.C. and S.K. Fenster, *Advanced strength and applied elasticity*. 2003, New Jersey: Prentice Hall.

9. Washizu, K., *Variational Methods in Elasticity and Plasticity*. 1968, London: Pergamon Press.

10. Hughes, T.J.R., R.L. Taylor, and W. Kanoknukulchai, *A simple and efficient finite-element for plate bending.* International Journal for Numerical Methods in Engineering, 1977. **11**: p. 1529-1543.

11. Yokoyama, T., *A reduced integration Timoshenko beam element.* Journal of Sound and Vibration, 1994. **169**(3): p. 411-418.

12. Friedman, Z. and J.B. Kosmatka, *An Improved Two-Node Timoshenko Beam Finite Element.* Computers & Structures, 1993. **47**(3): p. 473-481

13. Przemieniecki, J.S., *Theory of Matrix Structural Analysis*. 1968, New York: Dover Publications, Inc.

14. Mazars, J., et al., *Using multifiber beams to account for shear and torsion applications to concrete structural elements.* Comput. Methods Appl. Mech. Engrg., 2006. **195**: p. 7264-7281.

15. Triantafyllou, S.P. and V.K. Koumousis, *An inelastic Timoshenko beam element with axial–shear–flexural interaction.* Comput. Mech., 2011. **48**: p. 713-727.

16. Taylor, R.L., et al., *A mixed finite element method for beam and frame problems.* Computational Mechanics, 2003. **31**: p. 192-203.

17. Saritas, A. and O. Soydas, *Variational Base and Solution Strategies for Nonlinear Force-Based Beam Finite Elements.* International Journal of Non-Linear Mechanics, 2012. **47**(3): p. 54-64.

18. Spacone, E., F.C. Filippou, and F.F. Taucer, *Fibre beam-column model for non-linear analysis of R/C frames: Part I. Formulation.* Earthquake Engineering and Structural Dynamics, 1996. **25**: p. 711-725.

19. Souza, R.M., *Force-Based Finite Element for Large Displacement Inelastic Analysis of Frames*. 2000, University of California, Berkeley: PhD Thesis Dissertation.

20. Crisfield, M.A., *A consistent co-rotational formulation for non-linear, three dimensional, beam elements.* Computer methods in applied mechanics and engineering, 1990. **81**: p. 131-150.

21. Nukala, P.K.V.V. and D.W. White, *A mixed finite element for three-dimensional nonlinear analysis of steel frames.* Comput. Methods Appl. Mech. Engrg., 2004. **193**: p. 2507-2545.

22. Saritas, A. and F.C. Filippou, *Inelastic axial-flexure-shear coupling in a mixed formulation beam finite element.* International Journal of Non-Linear Mechanics, 2009. **44**: p. 913-922.

23. Saritas, A. and F.C. Filippou, *Frame Element for Metallic Shear-Yielding Members under Cyclic Loading.* Journal of Structural Engineering, 2009. **135**(9): p. 1115-1123.

24. Saritas, A. and F.C. Filippou, *Numerical integration of a class of 3d plastic-damage concrete models and condensation of 3d stress-strain relations for use in beam finite elements.* Engineering Structures, 2009. **31**: p. 2327-2336.

25. Papachristidis, A., M. Fragiadakis, and M. Papadrakakis, *A 3D Fibre Beam-Column Element with Shear Modelling.* Comput Mech, 2010. **45**: p. 553–572.

26. Argyris, J., L. Tenek, and A. Mattsson, *BEC: A 2-node fast converging shear-deformable isotropic and composite beam element based on 6 rigid-body and 6 straining modes.* Comput. Methods Appl. Mech. Engrg., 1998. **152**: p. 281-336.

27. Wackerfuss, J. and F.A. Gruttmann, *A Nonlinear Hu-Washizu Variational Formulation and Related Finite-Element Implementation for Spatial Beams with Arbitrary Moderate Thick Cross Sections.* Comput. Meth. Appl. Mech. Eng., 2011. **200**: p. 1671-1690.

28. Soydas, O. and A. Saritas, *An accurate nonlinear 3d Timoshenko beam element based on Hu-Washizu functional.* International Journal of Mechanical Sciences, 2013. **74**: p. 1-14.

29. Timoshenko, S.P., *On the correction for shear of the differential equation for transverse vibrations of prismatic bars.* Philos. Mag., 1921. **41**: p. 744-746.

30. Timoshenko, S.P., *On the transverse vibrations of bars of uniform cross sections.* Philos. Mag., 1922. **43**: p. 125-131.

31. Cook, R.D., D.S. Malkus, and P.M. E., *Concepts and Applications of Finite Element Analysis*. 1989, United States of America: John Wiley & Sons.

32. Chopra, A.K., *Dynamics of Structures : theory and applications to earthquake engineering*. Second ed. 2000, USA: Prentice-Hall, Inc.

33. Huang, T.C., *The Effect of Rotatory Inertia and of Shear Deformation on the Frequency and Normal Mode Equations of Uniform Beams With Simple End Conditions.* Journal of Applied Mechanics, 1961. **28**(4): p. 579-584.

34. Huang, T.C. and C.S. Kung, *New Tables of Eigenfunctions Representing Normal Modes of Vibration of Timoshenko Beams.* Developments in Theoretical and Applied Mechanics I, 1963. **1**: p. 59-71.

35. Cheng, F.Y., *Vibrations of Timoshenko Beams and Frameworks.* Journal of the Structural Division Proceedings of the American Society of Civil Engineers, 1970: p. 551-571.

36. Tessler, A. and S.B. Dong, *On a Hierarchy of Conforming Timoshenko Beam Elements.* Computers & Structures, 1981. **14**: p. 335-344.

37. Grant, D.A., *The Effect of Rotary Inertia and Shear Deformation on the Frequency and Normal Mode Equations of Uniform Beams Carrying a concentrated Mass.* Journal of Sound and Vibration, 1978. **57**(3): p. 357-365.

38. Swaminadham, M. and A. Michael, *A note on frequencies of a beam with a heavy tip mass.* Journal of Sound and Vibration, 1979. **66**(1): p. 144-147.

39. To, C.W.S., *Vibration of a Cantilever Beam with a Base Excitation and Tip Mass.* Journal of Sound and Vibration, 1982. **83**(4): p. 445-460.

40. Rossi, R.E., P.A.A. Laura, and R.H. Gutierrez, *A note on Transverse Vibrations of a Timoshenko Beam of Non-Uniform Thickness Clamped at one End and Carrying a Concentrated mass at the other.* Journal of Sound and vibration, 1990. **143**(3): p. 491-502.

41. Leissa, A.W. and J. So, *Comparisons of vibration frequencies for rods and beams from one-dimensional and three-dimensional analyses.* J. Acoust. Soc. Am., 1995. **98**(4): p. 2122-2135.

42. Archer, J.S., *Consistent Matrix Formulations for Structural Analysis Using Finite-Element Techniques.* AIAA Journal, 1965. **3**(10): p. 1910-1918.

43. Thomas, D.L., J.M. Wilson, and R.R. Wilson, *Timoshenko Beam Finite Elements.* Journal of Sound and Vibration, 1973. **31**(3): p. 315-330.

44. Molins, C., P. Roca, and A.H. Barbat, *Flexibility-based linear dynamic analyses of complex structures with curved-3d members.* Earthquake Engineering and Structural Dynamics, 1998. **27**: p. 731-747.

45. Popov, E.P., *Engineering Mechanics of Solids*. 1998: Prentice-Hall.

46. Cowper, G.R., *The Shear Coefficient Timoshenko's Beam Theory.* Journal of Applied Mechanics, 1966. **33**: p. 335-340.

47. Reddy, J.N., *On locking-free shear deformable beam finite elements.* Comput. Methods Appl. Mech. Engrg., 1997. **149**: p. 113-132.

48. Saritas, A., *Mixed Formulation Frame Element for Shear Critical Steel and Reinforced Concrete Members*, 2006, University of California, Berkeley.

49. Kaneko, T., *On Timoshenko's correction for shear in vibrating beams.* J. Phys. D: Appl. Phys., 1975. **8**: p. 1927-1936.

50. Chan, K.T., et al., *A new method to determine the shear coefficient of Timoshenko beam theory.* Journal of Sound and Vibration, 2011. **330**: p. 3488-3497.

51. Hutchinson, J.R., *Shear Coefficients for Timoshenko Beam Theory.* Journal of Applied Mechanics, 2001. **68**: p. 87-92.

52. Stephen, N.G., *On the Variation of Timoshenko's Shear Coefficient with Frequency.* Journal of Applied Mechanics, 1978. **45**: p. 695-697.

53. Zhang, P. and Y. Fu, *A Higher-order Beam Model for Tubes.* European Journal of Mechanics / A Solids, 2012. **38**: p. 12-19.

54. Luo, Y., *An Efficient 3d Timoshenko Beam Element with Consistent Shape Functions.* Adv. Theor. Appl. Mech. , 2008. **1**(3): p. 95-106.

55. Nowzartash, F. and M. Mohareb, *An elasto-plastic finite element for steel pipelines.* International Journal of Pressure Vessels and Piping, 2004. **81**: p. 919-930.

56. Friedman, Z. and J.B. Kosmatka, *Exact Stiffness Matrix Of A Nonuniform Beam-II. Bending Of A Timoshenko Beam.* Computers and Structures, 1993. **49**: p. 545-555.

57. Murín, J. and V. Kutiš, *3D-beam element with continous varitaion of the cross-sectional area.* Computers and Structures, 2002. **80**: p. 329-338.

58. Shooshtari, A. and R. Khajavi, *An efficient procedure to find shape functions and stiffness matrices of nonprismatic Euler-Bernoulli and Timoshenko beam elements.* European Journal of Mechanics A/Solids, 2010. **29**: p. 826-836.

59. Case, J., A.H. Chilver, and C.T.F. Ross, *Strength of Materials and Structures*. fourth ed. 1999, New York: John Wiley & Sons Inc.

60. Gaydon, F.A., *On the Combined Torsion and Tension of a Partly Plastic Circular Cylinder.* The Quarterly Journal of Mechanics & Applied Mathematics, 1951. **V**(1).

61. Ali, A.R.M. and M.S.J. Hashmi, *Theoretical and experimental results of the elastic–plastic response of a circular rod subjected to non-proportional combined torque and tension loadings.* Proceedings of the Institution of Mechanical Engineers, Part C: Journal of Mechanical Engineering Science, 1999. **213**(3): p. 251-261.

62. Zarroug, N.M., et al., *Mild steel (En8) rod tests under combined tension-torsion loading*. Journal of Materials Processing Technology, 2003. **143-144**: p. 807-813.

63. *ABAQUS theory manual. Version 6.2*. 2001, Pawtucket, RI, USA: Hibbit Karlsson and Sorensen, Inc.

64. Clough, R.W. and J. Penzien, *Dynamics of Structures*. Third ed. 2003, USA: Computers & Structures, Inc.

65. *Abaqus 6.12 Documentation*. [cited 2013; Available from: http://www.tu-chemnitz.de/projekt/abq_hilfe/docs/v6.12/.

66. Leissa, A.W. and J. So, *Accurate vibration frequencies of circular cylinders from three-dimensional analysis.* J. Acoust. Soc. Am., 1995. **98**(4): p. 2136-2141.

67. Kang, J.-H. and A.W. Leissa, *Three-dimensional vibrations of solid cones with and without an axial circular cylindrical hole* Internatiaonl Journal of Solids and Structures, 2004. **41**: p. 3735-3746.

68. Kang, J.-H. and A.W. Leissa, *Three-dimensioanl vibration analysis of thick, tapered rods and beams with circular cross-section.* International Journal of Mechanical Sciences, 2004. **46**: p. 929-944.

69. Gaines, J.H. and E. Volterra, *Transverse vibrations of cantilever bars of variable cross section.* Ther Journal of the Acoustical Society of America, 1966. **39**(4): p. 674-679.

70. Downs, B., *Reference frequencies for the validation of numerical solutions of transverse vibrations of non-uniform beams.* Journal of Sound and Vibration, 1978. **61**(1): p. 71-78.

71. Zhou, D. and Y.K. Cheung, *Vibrations of Tapered Timoshenko Beams in Terms of Static Timoshenko Beam Functions.* Journal of Applied Mechanics, 2001. **68**: p. 596-602.

72. Leissa, A.W. and Z. Zhang, *On the three-dimensional vibrations of the cantilevered rectangular parallelepiped.* J. Acoust. Soc. Am., 1983. **73**(6): p. 2013-2021.

73. Mabie, H.H. and C.B. Rogers, *Transverse Vibrations of Tapered Cantilever Beams with End Support.* The Journal of the Acoustical Society of America, 1968. **44**(6): p. 1739-1741.

74. To, C.W.S., *A Linearly Tapered Beam Finite Element Incorporating Shear Deformation and Rotary Inertia for Vibration Analysis.* Journal of Sound and Vibration, 1981. **78**(4): p. 475-484.

75. Jategaonkar, R. and D.S. Chehil, *Natural Frequencies of a Beam with Varying Section Properties.* Journal of Sound and Vibration, 1989. **133**(2): p. 303-322.

76. Gutierrez, R.H., P.A.A. Laura, and R.E. Rossi, *Fundamental Frequency of Vibration of a Timoshenko Beam of Non-uniform Thickness.* Journal of Sound and Vibration, 1991. **145**(2): p. 341-344.

77. Cleghorn, W.L. and B. Tabarrok, *Finite Element Formulation of a Tapered Timoshenko Beam for Free Lateral Vibration Analysis.* Journal of Sound and Vibration, 1992. **152**(3): p. 461-470.

78. Tong, X., B. Tabarrok, and K.Y. Yeh, *Vibration Analysis of Timoshenko Beams with Non-homogeneity and Varying Cross-section.* Journal of Sound and Vibration, 1995. **186**(5): p. 821-835.

79. Cheung, Y.K. and D. Zhou, *The Free Vibrations of Tapered Rectangular Plates Using a New Set of Beam Functions with the Rayleigh-Ritz Method.* Journal of Sound and Vibration, 1999. **223**(5): p. 703-722.

80. Zhou, D. and Y.K. Cheung, *The Free Vibration of a Type of Tapered Beams.* Comput. Methods Appl. Engrg., 2000. **188**: p. 203-216.

CURRICULUM VITAE

PERSONAL INFORMATION

Name, Surname: Ozan Soydaş
Date and Place of Birth: 1983, Zonguldak, Turkey
E-mail: ozansoydas@gmail.com

EDUCATION

Degree	Institution	Year of Graduation
MS	METU Civil Engineering	February 2009
BS	METU Civil Engineering	June 2006

WORK EXPERIENCE

Worked as an engineer for three years and took part in project approval and commissioning of power plants like wind, hydroelectric and thermal that have total installed capacity of approximately 5000MW and has been working as an energy and natural resources specialist since 2012 at Ministry of Energy and Natural Resources of Turkish Republic.

FOREIGN LANGUAGES

Advanced English, Beginner French

PUBLICATIONS

- O. Soydas, A. Saritas, An Accurate Nonlinear 3d Timoshenko Beam Element Based on Hu-Washizu Functional, International Journal of Mechanical Sciences 74 (2013) 1-14 (dx.doi.org/10.1016/j.ijmecsci.2013.04.002)
- A. Saritas, O. Soydas, Variational base and solution strategies for nonlinear force-based beam finite elements, Int. Journal of Non-Linear Mechanics 47 (3) (2012) 54-64 (dx.doi.org/10.1016/j.ijnonlinmec.2012.01.003)
- O. Soydaş, A. Sarıtaş, Yapısal Elemanların Titreşim Frekanslarının Analizi için Üç Boyutlu Timoshenko Kiriş Elemanı, 2. Türkiye Deprem Mühendisliği ve Sismoloji Konferansı, Hatay, Türkiye, (2013)
- O. Soydaş, A. Sarıtaş, Nonlinear Analysis Of A Three Dimensional Mixed Formulation Frame Finite Element Based On Hu-Washizu Functional, 10th International Congress on Advances in Civil Engineering, Ankara, Turkey, (2012)

- O. Soydaş, A. Sarıtaş, Deplasman Temelli ve Karma Formülasyon Kiriş Sonlu Elemanlarının Karşılaştırılması, 17. Ulusal Mekanik Kongresi, Elazığ, Türkiye, (2011)
- A. Yakut, O. Soydaş, Evaluation of Shear Wall Indexes for RC Buildings, 9th US and 10th Canadian Joint Earthquake Engineering Conference, Toronto, Canada, (2010)
- O. Soydaş, Evaluation of Shear Wall Indexes for Reinforced Concrete Buildings, MS Thesis, Middle East Technical University (2009)